EMPLOYING DOUBLE-STRANDED DNA PROBES ON COLLOIDAL SUBSTRATES FOR COMPETITIVE HYBRIDIZATON EVENTS

A Dissertation
Presented to
The Academic Faculty

By

Bryan Alexander Baker

In Partial Fulfillment
Of the Requirements for the Degree
Doctor of Philosophy in Materials Science and Engineering

Georgia Institute of Technology

May 2010

Employing Double-Stranded DNA Probes on Colloidal Substrates for Competitive Hybridization Events

Approved by:

Dr. Valeria Milam, Advisor
School of Materials Science and Engineering
Georgia Institute of Technology

Dr. Andrés García
School of Mechanical Engineering
Georgia Institute of Technology

Dr. Barbara Boyan
Wallace H. Coulter Department of Biomedical Engineering
Georgia Institute of Technology

Dr. Seung Soon Jang
School of Materials Science and Engineering
Georgia Institute of Technology

Dr. Ken Gall
School of Materials Science and Engineering
Georgia Institute of Technology

Date Approved: March 23, 2010

ACKNOWLEDGEMENTS

I would like to thank all those who walked with me through this process. Dr. Milam, your patience and dedication to teaching enabled me to fail, learn, and grow. Chris Tison and James Hardin, you both made the joys and frustrations of research more bearable and provided suggestions, criticism, and friendship along the way. Didi Eze, Alex Weller, and Rick Sullivan who became colleagues and friends near the end of my work. Rebecca, Sonya, and Gita, thanks for being patient with my mentorship and working with professionalism beyond your years. I would also like to thank Professor Hong Liu and Professor Chenguo Hu for being two of the best friends I have had since coming to graduate school. I learned so much from you both. To Andrea, Christian and Johannes for sharing your stories with me. To Sara, who's friendship got me through the first year. To Anthony, Sherry, Gregory, Jeff and Ms. Yvonne for having a cheerful word. To Mechelle, who made the day a little brighter every time we spoke. I could not complete this without a debt of gratitude to my family who has always been there and never gave up on me. Finally and most importantly, I owe all that I am and have learned to Christ who has patiently taught me more during this time than any book could hold.

TABLE OF CONTENTS

LIST OF TABLES

LIST OF FIGURES

LIST OF ABBREVIATIONS

A	Adenine
BSA	Bovine Serum Albumin
C	Cytosine
CML	Carboxylate- Modified Latex
COOH	Carboxylic Acid
DLVO	Derjaguin-Landau-Verwey-Overbeek Theory
DNA	Deoxyribonucleic Acid
dsProbe	Double-Stranded DNA Probe
EDAC	*N*-Ethyl-*N'*-(3-dimethylaminopropyl) Carbodiimide Hydrochloride
Fluor	Fluorescein
FITC	Fluorescein Isothiocyanate
G	Guanine
HODM	High Oligonucleotide Density Microsphere
k_{obs}	Observed Displacement Rate
LODM	Low Oligonucleotide Density Microsphere
MES	2-(N-Morpholino) Ethane Sulfonic Acid
MESF	Mean Equivalent Soluble Fluorophore
NN	Nearest Neighbor
PBS	Phosphate Buffered Saline
RNA	Ribonucleic Acid
ssProbe	Single-Stranded DNA Probe
T	Thymine
T_m	Melting Temperature
Tris/EDTA	Tris-Ethylenediaminetetraacetic Acid Disodium Salt Dihydrate
Tween	Tween^{TM} 20 Detergent

SUMMARY

DNA has found application beyond its biological function in the cell in a variety of materials assembly systems as well as nucleic acid-based detection devices. In the current research, double-stranded DNA probes are applied in both a colloidal particle assembly and fluorescent assay approach utilizing competitive hybridization interactions. The responsiveness of the double-stranded probes (dsProbes) was tuned by sequence design and tested against a variety of nucleic acid targets. Chapter 1 provides a review of the particle substrate used in the current research, colloidal particles, as well as examines previous applications of DNA in assembly and nucleic acid detection formats. Chapter 2 discusses the formation of fluorescent satellites, or similarly termed fluorescent micelles, via DNA hybridization. The effects of DNA duplex sequence, temperature at which assembly occurs, and oligonucleotide density are variables considered with preferential assembly observed for low oligonucleotide density particles. Chapter 3 demonstrates the controlled disassembly of these satellite structures via competitive hybridization with a soluble target strand. Chapter 4 examines DNA duplexes as fluorescent dsProbes and characterizes the kinetics of competitive hybridization between immobilized dsProbes and solution targets of interest. The sequence-based affinities of dsProbes as well as location of an embedded target sequence are both variables explored in this study. Based on the sequence design of the dsProbes, a range of kinetics responses are observed. Chapter 5 also examines the kinetics of competitive hybridization with dsProbes but with a focus on the specificity of competitive target by including mismatches within a short 15 base competitive target. Chapter 6 examines the effects of dsProbe orientation relative to

the particle surface as well as substrate particle size. The kinetics of displacement of DNA targets with those of RNA targets of analogous sequence are also discussed. The results of this study indicate discrimination in competitive hybridization between perfectly matched and mismatched targets, targets of varied mismatch location, and DNA versus RNA competitive targets. In Chapter 7 key aspects of the nearest neighbor thermodynamic model are examined from the literature to analyze the dsProbes and secondary duplexes. Discrepancies are discovered between the predicted and experimentally observed competitive displacement of the dsProbes by various targets. Finally, Chapter 8 compares and contrasts the use of dsProbes with modern nucleic acid assay methodologies. General guidelines are suggested for future applications of dsProbes in nucleic acid detection formats.

Chapter 1

Introduction to DNA as a Materials Tool for Assembly and Detection

1.1 DNA as a Biological and Chemical Macromolecule

DNA has been a widely studied biological macromolecule in large part to its importance in living organisms as well as its complex yet clearly defined molecular structure. In the environment of the cell, the dominant structure of DNA is two strands of complementary base pairs running in an anti-parallel orientation with adenine bases pairing with thymine and cytosine bases pairing with guanine to form a double helix[1]. Watson and Crick's composite analysis of experimental results led to the first correct report of DNA structural characteristics in 1953. Their work combined 1) Erwin Chargoff's discovery that a given DNA sample has equivalent numbers of adenine and thymine as well as guanine and cytosine bases 2) Jerry Donahue's demonstration of the correct tautomeric forms of the bases, which directly affect the prediction of hydrogen bonding and 3) Rosalind Franklin's X-ray diffraction studies to arrive at the correct form of the double-stranded helix[2]. Watson and Crick's analysis also correctly predicted that both strands of DNA serve as template strands during the replication process of cellular division[3]. Since their work, more detailed structural information on DNA duplexes has been obtained. In its native form, DNA appears most commonly as a B form in which the double helical diameter is ~ 2 nm with one helical turn occurring every 10-11 bases at a vertical rise of 0.34 nm between each base pair. DNA can also exist in either an A or Z form. The A form DNA takes 11 bases to complete one helical turn and has a 20° tilt of

its base pairs. The A form is known as the dehydrated form of DNA and appears in high ionic strength solutions. Z form DNA has a left-handed chirality in contrast to the right handedness of both B and A form DNA[1, 2].

The bases of DNA are categorized as either purines (adenines and guanine) or pyrimidines (cytosine and thymine) depending on the aromatic ring structures within each molecule (Figure 1.1.1). Each base is bonded to the C1 position of a 2' deoxyribose sugar. The phosphate group attached to C5 position of the sugar imparts the negative charge groups characteristic of the DNA backbone. Hydrogen bonding in Watson-Crick base pairing occurs between the adenine and thymine bases via two hydrogen bonds while each cytosine pairs with guanine via three hydrogen bonds. Both hydrogen bonding between the base pairs and stacking of the aromatic bases in the interior of the helix influence the structure of duplex DNA. The hydrophobic nature of the bases results in a strong driving force for the helical conformation in order to minimize contact of the hydrophobic aromatic rings with a polar aqueous environment[1]. This propensity of complementary DNA strands to form duplexes in buffered aqueous solutions based on Watson-Crick pairings and hydrophobic base stacking is an essential component of the current research.

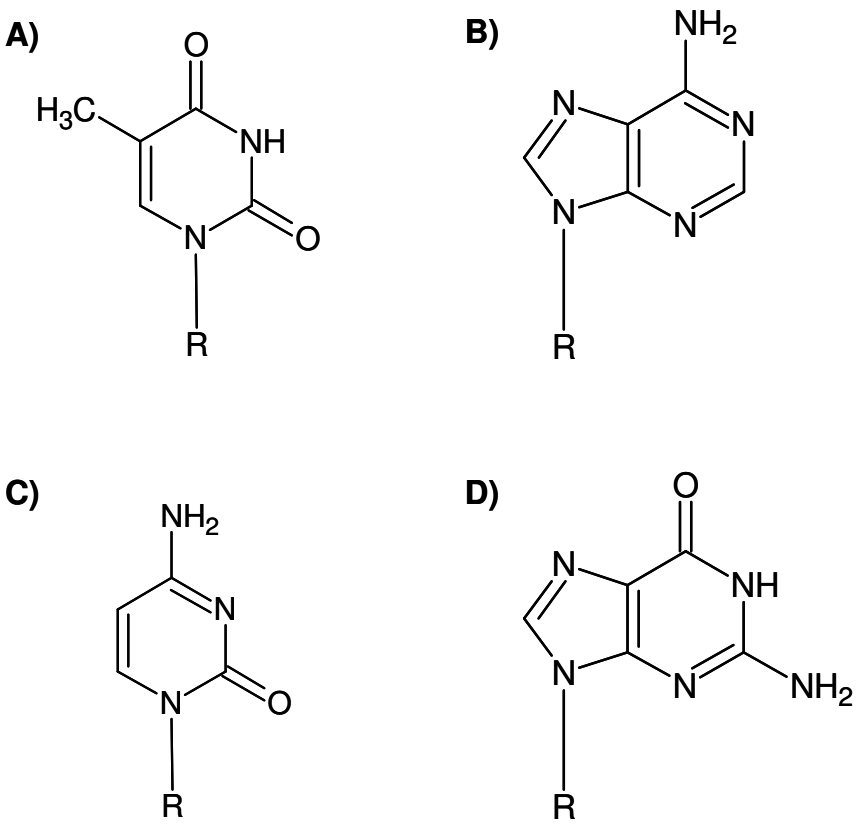

Figure 1.1.1. The chemical structure of the DNA bases A) Thymine B) Adenine C) Cytosine and D) Guanine. A) and C) are pyrimidines. B) and D) are purines. The formation of hydrogen bonds occurs between adenine and thymine and between guanine and cytosine in Watson-Crick base pairing. Image created in ChemSketch.

The ability to incorporate various chemical modifications and fluorescent tags has extended the applicability of DNA beyond its purely physiological context to a diverse array of bio-related applications. Acrydite [4, 5], fluorescent dye[6], and amine[5] modifications are only a few of the more common chemical modifications available for conjugating the end of single DNA strands to either a tag or to a material substrate. Often these modifications are synthesized through an altered base structure or phosphate group. Additionally, chemical modifications to the interior backbone of DNA have further expanded the capabilities DNA. Locked nucleic acids (LNA) are DNA analogs in which

a 2' hydroxyl is connected with the 4' carbon by a methylene bridge[7, 8], PNA or peptide nucleic acids eliminate the negative charge by using modified glycine residues to form the backbone[9], and 2´ methyl-oligonucleotides contain a 2' hydroxyl blocked by bond formation with a methyl group[8, 10]**.** Such backbone modifications decrease susceptibility of DNA to enzymatic cleavage. Other internal modifications include phosphorothioate moieties along the interior of the DNA backbone which facilitates binding to gold substrates[11] which have been used in a variety DNA-based platforms.

The study of DNA beyond its natural physiological context has also resulted in characterization of the mechanical[12], electrical[13, 14] and thermal melting properties of DNA. Particularly, the duplex melting temperature (T_m) is one of the most important properties related to DNA-based applications. This temperature corresponds to the temperature at which a solution of complementary DNA strands exists as 50% duplexes and 50% single strands and is dependent on base length, sequence, and percentage of G-C pairs[2]. The melting temperature of duplex DNA is commonly determined from UV absorbance spectra at 260 nm. The aromatic rings within the bases result in a hyperchromic effect observed when DNA transitions from a double-stranded to a single stranded form. Experimentally determining the duplex melting temperature, T_m, as a function of concentration provides the thermodynamic parameters describing the free energy of duplex formation from the relationship

$$\frac{1}{T_m} = \frac{R}{\Delta H^\circ} \ln C_T + \frac{\Delta S^\circ}{\Delta H^\circ} \qquad (1)$$

where R refers to the universal gas constant, ΔH° and ΔS° are the enthalpy and entropy of formation, respectively, and C_T is the total strand concentration[15-18]. The results of

such thermodynamic analysis have lead to predictive models of DNA stability, one of which is the nearest-neighbor (NN) model[19-21] in which the work of SantaLucia et al has been a prominent influence. In addition to developing the general NN parameters for DNA duplexes, SantaLucia and colleagues have also examined the effects of incorporating specific types of mismatches [15, 16] as well as dangling ends[17] on the melt temperature of duplexes in solution. Both of these sequence variables are considered in the current research for immobilized oligonucleotides. The work of SantaLucia and others has prompted development of web-based applications such as Zuker and Markham's DINA Fold server which allows users free access to software to calculate melting temperature of custom nucleic acid sequences[22-24]. Duplex melting temperatures for the sequences used in this work were determined with the aid of this open-access program.

1.2 DNA as a Materials Assembly Tool

The unique polymer properties, based on transitions form single to double-stranded forms, and the innate degree of control available from complementary base pairing have prompted many investigations into the potential applications of DNA as a material assemblies tool. For example, these properties have appeared in DNA nanofabrication techniques[25] by using carefully selected duplex sequences optimized for preferred hybridization and thermodynamic behavior. Investigators such as Nadrian Seeman have used these approaches to assemble DNA architectural subunits into intricate structures of interlocking chains forming 2D crystalline DNA arrays[26, 27]. Other applications incorporating the polymeric properties of oligonucleotides have included

DNA as crosslinking agents in acrylamide-based hydrogels[28], enzymatically crosslinked DNA hydrogels[29], and DNA block copolymers for capsule formation[30]. Beyond polymer applications, DNA has been used as a template in functional materials synthesis of array structures[31-35], circuit and nanoelectric components[36], and aided in programmable growth of CdTe luminescent crystals[11].

The materials application of DNA has also been instrumental in the development of particle suspensions with tunable and responsive properties. Pioneered in large part by the efforts of Chad Mirkin and colleagues, the first and most widely cited paper describing gold nanoparticle aggregation driven by DNA hybridization was published in 1996[37] along with concurrent contributions from Paul Alivisatos' group[38]. Since then, Mirkin's group has done prolific work in the area of nanoparticle structures mediated by DNA hybridization[39-45]. Analysis of sequence, DNA length, spacer length[46-48], salt concentration[43] and the effect of multivalent linkages [42] in three-dimensional nanoparticle aggregates have all been explored as variables of interest. More recent efforts have focused on the development of DNA mediated crystal structures with defined lattice parameters corresponding to FCC and BCC unit cells[49, 50]. More recently, DNA functionalized gold nanoparticles have been arranged in defined tetrahedral symmetries with controlled chirality[51].

Design and development of these nanoparticle-based systems has prompted investigation into the thermal stability of immobilized DNA. Results from analysis show that thermal transitions from a double-stranded to a single-stranded form of oligonucleotides immobilized between the surfaces of particles occur over a more narrow temperature range than soluble oligonucleotides. These sharper transitions also occur at

higher temperatures[37, 52] implying additional stabilization of the duplexes occurs within the aggregate network. These attenuated thermal transitions are believed to be a result of cooperative melting effects driven in large part by a reduction in local counterion concentration surrounding the neighboring DNA duplexes[43, 53]. As duplexes denature, the counterion concentration decreases locally which alters the screening of negative charges along the DNA backbone. This reduction in charge screening facilitates further DNA melting and ultimately particle redispersion. Charge screening has also been studied in hybrid duplexes such as PNA/DNA-linked particle aggregates[9] with similar cooperative melting transitions observed. DNA hybridization within an aggregate structure is not only influenced by ionic strength of the dispersive medium, but also by the three-dimensional proximity of the strands confined between adherent particle surfaces. The multivalent character of the DNA linkages mediating particle-particle interaction is thought to further stabilize the duplex structure[42]. Additionally, the curvature of the particle surfaces may facilitate some non-Watson-Crick base pairing which may contribute to stability of the nanoparticle aggregate[40].

Particle size also plays a role in maintaining aggregate structure. As particle size increases, T_m increases due to the increase in surface area meaning a larger absolute number of DNA strands to form bridges between particles[42, 54]. As the number of DNA strands, and therefore potential linkages on the particle surface increases, the enthalpy due to complementary base-pairing increases giving rise to higher melting temperatures[55] despite the loss of entropy that occurs by reducing the conformational freedom of the DNA strands[56]. These combined factors contribute to the reported increase in the effective melting temperatures of DNA duplexes bridging nanoparticle

aggregates in comparison to their soluble duplex counterparts[37, 42, 52]. For colloidal particles with length scales on the order of micrometers, similar studies examining DNA mediated aggregation have been completed, often using readily available polystyrene particles[57-62]. A more detailed discussion on colloid properties and colloid-colloid interactions is saved for the next section.

Finally, the potential of DNA as a materials assembly tool is further enabled by its response to other biological macromolecules such as enzymes. As a biological molecule *in vivo* DNA is subject to a number of enzymatic processes, a condition that persists in appropriately buffered *in situ* environments. Studies have demonstrated enzymatic control of immobilized DNA strands on particle surfaces via cleavage[63], extension[64], and ligation[65]. Also, the use of nucleases in conjunction with DNA-functionalized particles has demonstrated an added level of control in mediating particle aggregation[66]**.** While enzymatic manipulation of DNA is not presented in the current work, these research efforts outlined above reinforce the concept that innate sequence-based specificity makes DNA a versatile materials assembly tool.

1.3 Nonspecific and Specific Interactions in Colloidal Suspensions

As the majority of the work in this thesis is dependent on colloid particle platforms, a more detailed discussion of select colloid science fundamentals is warranted. Colloidal particles can range in size from 1 nm to 10 μm [67-69] though particles in the size range of 1 nm to 100 nm are commonly referred to as nanoparticles. Due to their high surface area to volume ratio and ubiquitous van der Waals attractive interactions, colloids dispersed in suspension tend to aggregate to reduce surface tension between the

interface of the colloid and dispersive media unless otherwise stabilized[70] through electrostatic, steric, or electrosteric repulsive interactions. Colloids in suspension undergo temperature dependent Brownian motion[71] which facilitates particle interaction via collisions. Colloidal particles are subject to a number of nonspecific interactions such as van der Waals; hydrophobic; steric (assuming an adsorbed or grafted polymer layer); hydration and solvation forces (depending on the liquid medium); and electrostatic (as mediated by the electric double layer)[72]. A variety of nonspecific interactions have been used to manipulate colloid dispersions. The assembly of colloids into packed monolayers has been demonstrated with controlled drying approaches[73, 74]. Heterocoagulation has generated defined 3D architectures largely driven by steric stabilization of two disparate sized particle populations influenced by solution conditions[75]. Excellent control of 3D architectures has been achieved using magnetostatic interactions to assemble paramagnetic and non-magnetic colloidal structures and to control the assemblies with varying ferrofluid concentrations[76]. Common to these techniques is the nonspecific nature of the interactions between particles based largely on long-range forces or environmental / solution conditions.

The contributions of two particular nonspecific interactions are evaluated for dilute suspensions of spherical particles in Derjaguin-Landau-Verwey-Overbeek theory, more commonly referred to as DLVO theory. DLVO describes the pairwise interaction of particles based on 1) attractive van der Waals forces arising from induced dipoles of both the solvent and particle and 2) repulsive electrostatic forces arising from the diffuse electrical double layer surrounding the charged particle surface in an aqueous medium[77, 78]. Assumptions that are critical to the DLVO theory are that the

interacting bodies can be treated as having flat solid surfaces, uniform surface charge on these surfaces with no charge redistribution, a fixed counterion and surface ion concentration profile, and a stable surface chemistry (i.e. no surface oxidation, etc.)[79]. The contributions of van der Waals attractions and electrostatic repulsion is additive and is expressed as the total, distant-dependent interaction energy $U_{tot}(x)$

$$U_{tot}(x) = U_{vdW}(x) + U_{el}(x) \tag{2}$$

where $U_{vdW}(x)$ is van der Waals interactions and $U_{el}(x)$ is the electrostatic interactions. A representative of this interaction potential is illustrated for comparison in Figure 1.3.1.

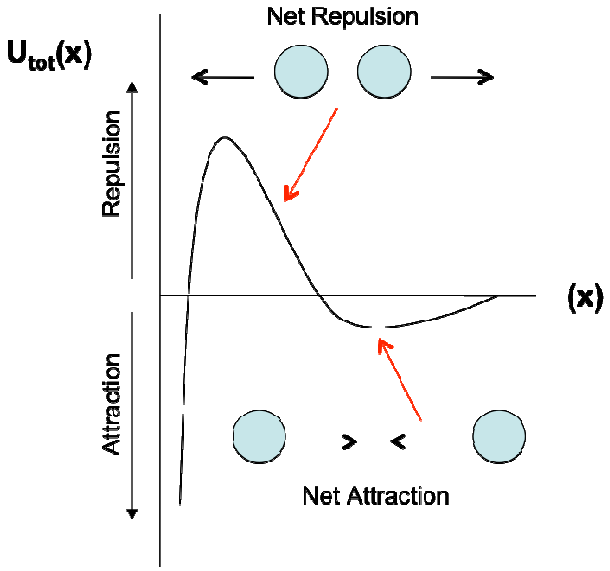

Figure 1.3.1. Representation of the interaction potential of two colloidal particles in solution based on van der Waals attractive and electrostatic repulsive interactions.

As two particles undergo Brownian motion and collide, the magnitude of this interaction energy changes with separation distance. For the interaction potential shown in Figure 1.3.1, at moderate separations a weak attractive interaction results in a meta-stable association. At shorter separation distances the repulsive barrier arises as a result of electrostatics. If the system has enough energy to overcome this barrier then a steep drop in the interaction energy corresponds to the dominance of van der Waals attractive forces at small separation distances. This short-range attraction is strong and non-reversible and the particles aggregate. The contribution from van der Waals interaction is simplified by the Derjaguin approximation that relates the interaction between two spheres as a case of interaction between two flat surfaces. The resulting attractive potential is described for colloids of the same size by

$$U_{vdW}(D) = -\frac{AR}{12D} \tag{3}$$

where A is the Hamaker constant, R is the particle radius, and D is the separation distance, and is a valid assumption when the radii of the particles is greater than the particle separation distance[78, 80].

Countering this attractive potential is electrostatic repulsion. The electrostatic interaction potential, after applying the Derjaguin approximation, for the simple case of two equally charged particles of the same radius is given by the expression

$$U_{el}(D) = \left(\frac{64\pi \cdot kTR\rho_{\infty} \cdot \gamma^2}{\kappa^2}\right)\exp[-\kappa D] \tag{4}$$

where k is the Boltzmann constant, T is temperature in Kelvin, ρ refers to the ion concentration, $\gamma = \tanh(e\psi_0 / 4kT)$ from the Guoy-Chapman theory describing charge potential variation from a surface of potential ψ_0 in ionic solutions, and κ is the inverse Debye length. The Debye length is an important parameter in aqueous media since it defines the thickness of the electric double layer surrounding the particle as

$$\kappa^{-1} = \left(e^2 \frac{\sum_i \rho_{\infty i} z_i^2}{\varepsilon \cdot \varepsilon_0 \cdot k \cdot T} \right)^{-\frac{1}{2}} \tag{5}$$

in which e is the electronic charge, z is the valency of the ions, ε is the permittivity of the media, ε_0 is the permittivity of free space[78]. The Debye length is also the characteristic decay length of the Debye-Huckel approximation of Guoy-Chapman theory, $\psi_x = \psi_0 \exp[-\kappa x]$, which states that the surface potential, ψ_x, changes as a function of distance, x, away from the particle surface[78]. The Debye length is heavily influenced by the ionic strength of the dispersive media, which poses a limitation to application of the DLVO theory. Specifically, it has been demonstrated that experimental deviations from DLVO predictions occur at high ionic concentrations [80, 81] making the theory less applicable for physiological conditions.

Further, the requirements for successful application of the DLVO theory are a dilute particle suspension, simple or spherical particle geometry, a diffusion-regulated double layer, and the absence of interactions other than van der Waals and electrostatic interactions[79]. As DNA-DNA interactions are based on sequence dependent hydrogen

bonding often in relatively high ionic strength solutions, colloids interacting via DNA linkages represent a departure from the central assumptions of DLVO theory. DNA-mediated interactions are more appropriately described as the interplay between 1) specific, short-range attraction based on complementary base sequence and 2) electrosteric repulsion from negatively charged DNA chains immobilized to the particle surface.

Specific, short-range attractive forces require close proximity and favorable orientation between the adhesive moieties similar to receptor-ligand interactions in biological systems. Binary particle suspensions have been specifically assembled by receptor-ligand interactions such as streptavidin and biotin[82], carbohydrate-selectin linkages[83] and DNA-DNA interactions for both nano-[84] and micron-sized particles[61]. Assembly of defined 3D particle structures, termed colloidal satellites or colloidal micelles, using DNA mediated adhesion has been demonstrated by ensuring the number ratio in a bidisperse particle population results in an excess of smaller particles relative to the larger core particles. This type of satellite or micelle structure based on specific attractive interactions has been demonstrated both for the nanometer scale[84, 85] and the micron scale[83].

A myriad of platforms utilizing the short-range, attractive interactions of complementary DNA sequences include Janus particles[86, 87], quantum dots[88], diatoms[89], and liposomes[90, 91]. Though these possibilities speak to the versatility of DNA-mediated particle interactions, the current research limits the discussion of DNA-mediated assembly to defined colloidal structures called colloidal satellites, each

comprised of a template microsphere surrounded by a layer of smaller, fluorescent particles.

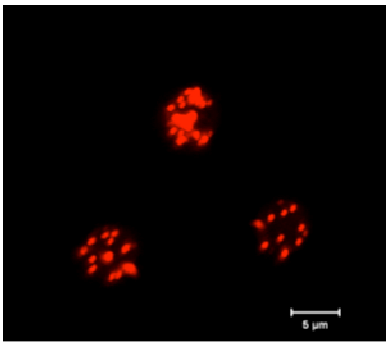

Figure 1.3.2. Representative confocal micrograph of fluorescent satellite assembly mediated by DNA linkages.

1.4. DNA-Based Detection Platforms and Factors Affecting Hybridization

In addition to serving as a materials assembly tool, DNA has been developed as a probe for capture and detection of physiological nucleic acid targets [92-94], small ion species[95-97] which is an issue of particular importance in water quality and purification[98, 99], and even chemical molecules of interest[100, 101]. The potential impact of nucleic acid-based detection strategies is readily apparent for clinical screenings and has received attention in the literature for use in genotyping[1, 102], screening for pathogens[92, 103-105], detecting environmental and food contaminants[106] and narcotics detection[107]. The following discussion of DNA-based detection platforms will be classified into three broad categories: solution, planar arrays, and particle substrates.

Solution probe systems are either single-stranded or double-stranded and include the popular molecular beacon design[108, 109] as well as labeled double-stranded DNA duplexes[110]. The advantage of this approach is the simplicity of the probe itself. The translational freedom of a soluble probe in solution allows the probe to freely diffuse to the target of interest and vice versa. The disadvantages of such an approach are that once released, the probes cannot be specifically tracked unless separately labeled by some characteristic dye that corresponds to a particular sequence. As a result, the number of discrete probes that can be screened simultaneously is limited to the number of dyes that can be individually identified. For targeting of cellular components, infiltration and stability of nucleic acid probes are considerable challenges. Subsequently, techniques such as the Southern blotting methods, use hybridization to detect targets separately via electrophoresis[111] after the cell has been lysed and the contents purified.

2D arrays or microarrays are a powerful alternative detection platform in nucleic acid analysis. They are often fabricated using lithographic techniques on substrates of glass or silicon[112]. Deposition of polymer-bound oligonucleotide probes[113] and hydrogel spotting with DNA probes have been also used to pattern array formats[5, 114]. The advantage of a microarray approach is the ability to control the spatial location of distinct probe sequences and thus obtain a library of information on a large population of target species that by the spatial mapping of the probes. Electrochemical probes of DNA aptamers deposited on 2D gold substrates[107, 115, 116] are an adaptation of the 2D format similar to microarrays.

Hybridization on 2D substrates is influenced primarily by the ability of targets to interact with the probe strands immobilized to the substrate. The surface density of DNA

probe strands directly affects the ability of targets to interact and orient themselves with the probe sequences. Thus, the concept of optimal density of DNA probes has been suggested for maximizing detectable hybridization events. At this probe density hybridization would occur efficiently and result in a discernable signal[117, 118]. Generally, both the hybridization rate and efficiency, or percentage of total probes that have hybridized to a target of interest, are increased at lower DNA surface density[119]. On 2D surfaces possible DNA target diffusion pathways include target diffusing directly to a probe, target diffusing first on the surface then across the surface to the probe, and lastly, target dissociation from a neighboring probe to a second or more complementary probe[117]. Collectively, these pathways make hybridization a diffusion limited process on 2D systems.

The last category of nucleic acid detection platforms described is particle substrate systems in which DNA strands are chemically linked to or adsorbed on particle surfaces. This category includes particles at both the nanometer and micrometer length scales such as aggregates[46], core-satellite structures[85] and single particles with covalently bound DNA probes[92, 93, 120]. A particle-based analog to the DNA microarray has developed with the advent of spectrally distinct polystyrene colloids which can achieve, by various dye combinations, several hundred discrete particles for a given assay[102]. The probe strands corresponding to each particle are encoded by a unique spectral wavelength. Targets that hybridize to these probes are labeled in a secondary labeling step separate from the capture or hybridization step. The cumulative fluorescence intensity of the dye label is quantified to determine the concentration of hybridized targets. This method has been successfully applied in the clinically relevant

demonstrated in the characterization of transcriptional expression of miRNA's in cancer tissues[93] by utilizing flow cytometry, one of the techniques applied in the current research.

Compared to a stationary planar array, DNA hybridization on the surface of microparticles more closely approximates the interaction of DNA strands freely diffusing throughout solution as the particles themselves undergo Brownian motion. Thus, where a diffusion-limited reaction may occur in a 2D array format, evidence suggests that a microparticle detection platform results in reaction limited hybridization kinetics[121]. In steady state conditions the diffusive boundary layer of a particle system is proportional to the radius of the particle[122], giving an advantage to small particles in minimizing the limitation of diffusion. Reaction limited hybridization has been approximated as a two-state all or nothing event[123]. Surface density of DNA is also a factor affecting hybridization rate on microparticle systems with low-density probe coverage resulting in higher association rates between targets and probes[121]. A five-fold slower rate of hybridization has been observed on the surface of microparticles compared to hybridization occurring in oligonucleotide solutions[124]. However, the ability to easily manipulate particle-bound DNA probes and readily exchange buffer solutions outweigh the disadvantage of slower hybridization rates in the application of this project.

1.5. Kinetics of Primary Hybridization and Competitive Hybridization

The mechanism underlying DNA-based detection of nucleic acid targets can be categorized as either a direct or primary hybridization event of the target to the DNA probe or a competitive hybridization event in which the original hybridization partner a double-stranded probe is displaced by the target. Competitive hybridization is driven by an affinity difference between the initial duplex and the secondary duplex or by fluctuations in the dynamic equilibrium of the duplex. Previous research has focused on understanding the kinetics of these events with particular emphasis on primary hybridization kinetics[119, 121, 125-128] and to a lesser degree competitive hybridization kinetics[110, 129, 130]. Often, these kinetic studies characterize DNA hybridization as a gain in signal event. This signal is commonly measured as an increase in fluorescence intensity as reported in molecular beacon [94], planar substrates[126] and particle-based[92] hybridization studies. Measuring mass increase due to hybridization on a quartz crystal microbalance is yet another characterization approach[128].

The general form of the reaction describing primary hybridization is as follows

$$P + T \underset{k_2}{\overset{k_1}{\rightleftharpoons}} PT$$

in which the forward reaction rate is given by k_1, the reverse reaction rate is give by k_2 and **P**, **T** and **PT** correspond to the probe, target and resulting duplex after hybridization, respectively. This process is schematically illustrated in Figure 1.5.1 using the example of a molecular beacon as the signal-on strategy.

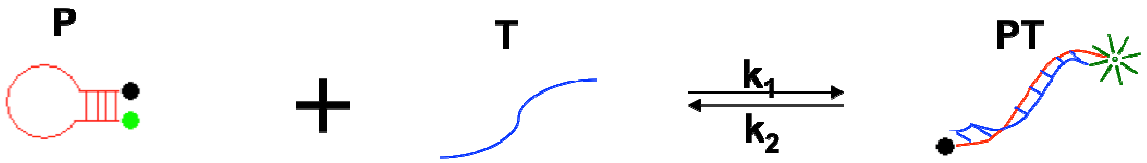

Figure 1.5.1. An example of a "signal on" reaction in which the interaction of probe **P** and target **T** result in the increase of a fluorescence signal with product **PT** as the quencher an dye on the probe are physically separated during hybridization.

Since the parameter being evaluated is an increase in concentration of **PT** over time the reaction rate is described by

$$\frac{d[PT]}{dt} = k_1[P][T] \qquad (6)$$

in which the forward reaction is highly favored over the reverse due to excess concentration of the target **T**. The presence of excess **T** is critical to the assumption of the forward progression of the reaction. The reaction for a signal *loss* event, such as occurs in competitive hybridization, which involves labeled primary duplexes becoming unlabeled secondary duplexes, is given in the same general manner but with a slight variation. Assuming that the same general reaction statement holds true

$$PT_1 + T_2 \underset{k_2}{\overset{k_1}{\rightleftharpoons}} PT_2 + T_1$$

where the forward reaction rate is given by k_1 and the reverse reaction rate is give by k_2, but now the components $\mathbf{PT_1}$, $\mathbf{T_2}$ and $\mathbf{PT_2}$ correspond to the initial duplex, target and

resulting secondary duplex, respectively, the rate equation can be expressed by following the loss of a signal from the initial labeled duplex, $\mathbf{PT_1}$, over the course of time.

$$\frac{d[PT_1]}{dt} = -k_1[PT_1][T_2] \qquad (7)$$

where again the forward reaction is highly favored due to the excess concentration of unlabeled target, $\mathbf{T_2}$. In the context of competitive hybridization the physical meaning of this equation is illustrated schematically in Figure 1.5.2 where $\mathbf{PT_1}$ describes the concentration of the labeled dsProbe species and $\mathbf{T_2}$ describes the concentration of the unlabeled target species. The resulting product $\mathbf{PT_2}$ is the new duplex resulting from competitive hybridization events between the target and the original hybridization partner in the initial dsProbe duplex.

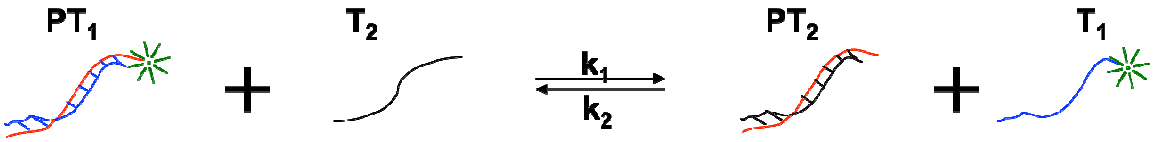

Figure 1.5.2. An example of a "signal off" reaction in which the competitive displacement of $\mathbf{T_1}$ in $\mathbf{PT_1}$ by the target $\mathbf{T_2}$ results in a fluorescence decrease with the formation of the secondary duplex $\mathbf{PT_2}$. If the probes are conjugated to particle substrates, then the fluorescently labeled initial hybridization partner can be removed from the suspension via washing.

In this analysis, the result of competitive hybridization can be presented either as the fraction of single-stranded probe DNA or the fraction of the initial probe displaced[130]. The reaction kinetics are second order if the concentration of

complementary strands is equal and pseudo-first order if the concentration of one of the strands is considered to be in excess[131]. Reynaldo et al also use a pseudo first order approximation in which the target is in excess and report the fraction of probe displaced instead of fraction of single-stranded DNA. Beginning by considering probe loss due to thermal dissociation and competitive hybridization, Reynaldo et al. develop the following reaction rate

$$\frac{d[PT_1]}{dt} = -k_1[PT_1] - k_2[PT_1][T_2] \tag{8}$$

in which k_1 corresponds to the dissociation rate due to thermal dissociation of the initial duplex $\mathbf{PT_1}$ and k_2 corresponds to the dissociation rate due to competitive hybridization with $\mathbf{T_2}$. By making the substitution

$$k_{obs} = k_1 + k_2[T_2] \tag{9}$$

they define the term k_{obs} to describe the dissociation rate of the initial duplex $\mathbf{PT_1}$ from both thermal dissociation and competitive hybridization. Solving for this new expression results in a description of the fraction of the initial duplex remaining as a function of time, t, given by

$$\frac{[PT_1]}{[PT_1]_0} = \exp[-k_{obs}t] \tag{10}$$

An observed displacement rate was obtained by fitting experimental data to the expression

$$f = f_0 + (f_\infty - f_0)(1 - \exp(-k_{obs}t)) \quad (11)$$

where f, f_0, and f_∞ correspond to fraction of single-stranded labeled oligonucleotides, and the fractions of single stranded oligonucleotides at $t = 0$ and the reaction equilibrium, respectively. This expression has taken the fraction of the initial duplex, **PT$_1$**, remaining and converted to fraction of the labeled target, **T$_1$**, displaced. The fitted parameter is the observed dissociation rate k_{obs} in s^{-1}. This approach is adopted for this project in order to facilitate characterization of competitive hybridization reactions. In order to minimize the contribution of the thermal dissociation pathway represented by k_1, the current research uses both an excess of the target, **T$_2$**, and an affinity difference between the initial duplex, **PT$_1$**, and the secondary duplex, **PT$_2$**, based on the high affinity of the target **T$_2$**.

1.6. Overview of Current Research

In the current research, described in subsequent chapters, is a continuation of these efforts to understand and characterize DNA as a materials tool with a specific emphasis on double-stranded DNA probes (dsProbes) immobilized on colloidal particle substrates for detection. Specifically, tuning the affinity of dsProbes has been examined in both the context of colloidal particle assembly and in fluorescence-based kinetics studies involving soluble hybridization partners. The particle assembly approach utilizes

DNA duplexes of varying affinity due to the incorporation of center mismatches or different base lengths in the initial hybridization partners. The dsProbes ultimately serves as bridges between a template microsphere and a surrounding layer of smaller fluorescent particles. The assembly of these satellite structures is assessed as a function of duplex sequence design, temperature of assembly, and DNA density of the template microsphere. The resulting satellites are then examined as optical detection platforms for (competitive) nucleic acid targets in solution. Following assembly, the colloidal satellites (or colloidal micelles) were then incubated with a competitive target sequence possessing a high affinity for the immobilized probe strand. Successful competitive hybridization results in the release of the smaller fluorescent particles from the colloidal satellite leaving a bare template microsphere. Changes in the extent of assembly formation and disassembly were assessed with confocal fluorescence microscopy techniques.

Fluorescently labeled double-stranded DNA probes (dsProbes) were also immobilized on microspheres and then suspended in solution with several competitive target sequences. The kinetics of displacement of the fluorescently labeled initial hybridization partner by the competitive targets was quantitatively analyzed using flow cytometry. DNA strands of varying base lengths and "complementarity" were used to vary both the affinity of the dsProbe and the competitive targets. Additionally, the effects of sequence context were also assessed by embedding a complementary recognition sequence at different locations within a longer competitive target strand. Changes in fluorescence intensity as a function of incubation time with competitive targets were monitored using flow cytometry and presented as kinetic analysis with experimentally determined displacement rates.

This work is motivated by the need for both specificity and robustness in nucleic acid based detection devices. Double-stranded DNA probes may provide an alternate approach to ensuring specificity that is not dependent on environmental or solution factors. In the popular microarray approach, specificity and fidelity of Watson-Crick base pairing is maintained by imposing stringency with elevated temperatures of hybridization. Promoting target specificity by increasing temperature requires a high degree of environmental control, conditions that are not always favorable for field use. Designing stringency into the DNA probes themselves represents an intrinsic approach and first steps towards methodology that may find employment beyond the controlled environment of the lab bench. Additionally, many nucleic acid based assays in which the target of interest is hybridized directly to a single-stranded probe require some form of chemical modification to the target of interest in order to report the hybridization event. In the proposed dsProbe approach, only the initial hybridization partner is required to be fluorescently labeled, thus reducing the need for modification of the target of interest. Discussions of the kinetics of competitive hybridization as well as comparison with current thermodynamic models of DNA duplexes are offered to compare and contrast the competitive hybridization approach with current understanding of DNA hybridization behavior. Suggestions for further direction and study are provided within the context of these comparisons.

1.7 References

1. Calladine, C.R., et al., *Understanding DNA*. 2004, Elsevier Academic Press: Amsterdam. p. 18-38.

2. Voet, D., J. Voet, and C.W. Pratt, *Fundamentals of Biochemistry*. 2002, New York: John Wiley & Sons, Inc.

3. Watson, J.D. and F.H.C. Crick, *Genetic Implications of the Structure of Deoxyribonucleic Acid.* Nature, 1953. 171: p. 964 - 967.

4. Rehman, F.N., et al., *Immobilization of acrylamide-modified oligonucleotides by co-polymerization.* Nucleic Acids Research, 1999. 27(2): p. 649 - 655.

5. Rubina, A.Y., et al., *Hydrogel drop microchips with immobilized DNA: properties and methods for large-scale production.* Analytical Biochemistry, 2004. 325: p. 92 - 106.

6. Smith, L.M., et al., *The synthesis of oligonucleotides containing an aliphatic amino group at the 5' terminus: synthesis of fluorescent DNA primers for use in DNA sequence analysis.* Nucleic Acids Research, 1985. 13(7): p. 2399 - 2412.

7. Yang, C.J., et al., *Synthesis and investigation of deoxyribonucleic acid/locked nucleic acid chimeric molecular beacons.* Nucleic Acids Research, 2007. 35(12): p. 4030 - 4041.

8. Ng, P.-S. and D.E. Bergstrom, *Alternative Nucleic Acid Analogues for Programmable Assembly: Hybridization of LNA to PNA.* Nano Letters, 2005. 5(1): p. 107 - 111.

9. Lytton-Jean, A.K.R., et al., *Highly Cooperative Behavior of Peptide Nucleic Acid-Linked DNA-Modified Gold-Nanoparticle and Comb-Polymer Aggregates.* Advanced Materials, 2009. 21: p. 706 - 709.

10. Xu, F., A.M. Pellino, and W. Knoll, *Electrostatic repulsion and steric hindrance effects of surface probe density on deoxyribonucleic acid (DNA)/peptide nucleic acid (PNA) hybridization.* Thin Solid Films, 2008. 516: p. 8634 - 8639.

11. Ma, N., E.H. Sargent, and S.O. Kelley, *One-step DNA-programmed growth of luminescent and biofunctionalized nanocrystals.* Nature Nanotechnology, 2009. 4: p. 121 - 125.

12. Smith, S.B., Y. Cui, and C. Bustamante, *Overstretching B-DNA: The Elastic Response of Individual Double-Stranded and Single-Stranded DNA Molecules.* Science, 1996. 271: p. 795-799.

13. Wagenknecht, H.-A., *Principles and Mechanisms of Photoinduced Charge Injection, Transport, and Trapping in DNA*, in *Charge Transfer in DNA: From Mechanism to Application*, H.-A. Wagenknecht, Editor. 2005, Wiley-VCH. p. 1 - 26.

14. Zwolak, M. and M.D. Ventra, *Physical approaches to DNA sequencing and detection.* Reviews of Modern Physics, 2008. 80: p. 141-165.

15. Allawi, H.T. and J. John SantaLucia, *Thermodynamics and NMR of Internal G-T Mismatches in DNA.* Biochemistry, 1997. 36: p. 10581 - 10594.

16. Allawi, H.T. and J. John SantaLucia, *Thermodynamics of internal C-T mismatches in DNA.* Nucleic Acids Research, 1998. 26(11): p. 2694 - 2701.

17. Bommarito, S., N. Peyret, and J.S. Jr., *Thermodynamic parameters for DNA sequences with dangling ends.* Nucleic Acids Research, 2000. 28(9): p. 1929 - 1934.

18. Sugimoto, N., et al., *Improved thermodynamic parameters and helix initiation factor to predict stability of DNA duplexes.* Nucleic Acids Research, 1996. 24(22): p. 4501 - 4505.

19. SantaLucia, J., *A unified view of polymer, dumbbell, and oligonucleotide DNA nearest-neighbor thermodynamics.* Proceedings of the National Academy of Sciences of the United States of America 1998. 95: p. 1460 - 1465.

20. Peyret, N., et al., *Nearest-Neighbor Thermodynamics and NMR of DNA Sequences with Internal A-A, C-C, G-G and T-T Mismatches.* Biochemistry, 1999. 38: p. 3468 - 3477.

21. Breslauer, K.J., et al., *Predicting DNA duplex stability from the base sequence.* Proceedings of the National Academy of Sciences of the United States of America 1986. 83: p. 3746 - 3750.

22. Markham, N.R. and M. Zuker, *MFold*. http://dinamelt.bioinfo.rpi.edu/. Accessed 9/16/08.

23. Markham, N.R. and M. Zuker, *DINAMelt web server for nucleic acid melting prediction.* Nucleic Acids Research, 2005. 33: p. W577 - W581

24. Markham, N.R. and M. Zuker, *UNAFold: software for nucleic acid folding and hybriziation*, in *Bioinformatics, Volume II. Structure, Functions and Applications*, J.M. Keith, Editor. 2008, Humana Press: Totowa, NJ. p. 3 - 31.
25. Li, H., J.D. Carter, and T.H. LaBean, *Nanofabrication by DNA self-assembly.* Materials Today, 2009. 12(5): p. 24 - 32.

26. LaBean, T.H., et al., *Construction, Analysis, Ligation, and Self-Assembly of DNA Triple Crossover Complexes.* Journal of the American Chemical Society, 2000. 122: p. 1848-1860.

27. Winfree, E., et al., *Design and self-assembly of two-dimensional DNA crystals.* Nature, 1998. 394: p. 539 - 544.

28. Lin, D.C., B. Yurke, and N.A. Langrana, *Mechanical Properties of a Reversible, DNA-Crosslinked Polyacrylamide Hydrogel.* Journal of Biomechanical Engineering, 2004. 126: p. 104 - 110.

29. Um, S.H., et al., *Enzyme-catalysed assembly of DNA hydrogel.* Nature Materials, 2006. 5: p. 797 - 801.

30. Johnston, A.P.R. and F. Caruso, *Stabilization of DNA Multilayer Films Through Oligonucleotide Crosslinkg.* Small 2008. 4(5): p. 612-618.

31. Yan, H., et al., *DNA-Templated Self-Assembly of Protein Arrays and Highly Conductive Nanowires.* Science, 2003. 301: p. 1882 - 1884.

32. Ongaro, A., et al., *DNA-Templated Assembly of a Protein-Functionalized Nanogap Electrode.* Advanced Materials, 2004. 16(20): p. 1799 - 1803.

33. Kim, S., et al., *DNA-Assisted Monolayer Immobilization of 2D Opaline Arrays.* Advanced Functional Materials, 2006. 16: p. 1590 - 1598.

34. Deng, Z., et al., *DNA-Encoded Self-Assembly of Gold Nanoparticles into One-Dimensional Arrays.* Angewandte Chemie International Edition, 2005. 44: p. 3582 - 3585.

35. Niemeyer, C.M., et al., *Bifunctional DNA-gold nanoparticle conjugates as building blocks for the self-assembly of cross-linked particle layers.* Biochemical and Biophysical Research Communications, 2003. 311: p. 995 - 999.

36. Eichen, Y., et al., *Self-assembly of nanoelectrical components and circuits using biological templates.* Acta Polymer, 1998. 49: p. 663 - 670.

37. Mirkin, C.A., et al., *A DNA-based method for rationally assembling nanoparticles into macroscopic materials.* Nature, 1996. 382: p. 607-609.

38. Alivisatos, A.P., et al., *Organization of 'nanocrystal molecules' using DNA.* Nature, 1996. 382: p. 609 - 611.

39. Cao, Y.C., et al., *A two-color change, nanoparticle-based method for DNA detection.* Talanta, 2005. 67: p. 449-455.

40. Hill, H.D., S.J. Hurst, and C.A. Mirkin, *Curvature-Induced Base Pair "Slipping" Effects in DNA-Nanoparticle Hybridization.* Nano Letters, 2009. 9(1): p. 317 - 321.

41. Huo, F., A.K.R. Lytton-Jean, and C.A. Mirkin, *Asymmetric Functionalization of Nanoparticles Based on Thermally Addressable DNA Interconnects.* Advanced Materials, 2006. 18: p. 2304-2306.

42. Hurst, S.J., H.D. Hill, and C.A. Mirkin, *"Three-Dimensional Hybridization" with Polyvalent DNA-Gold Nanoparticle Conjugates.* Journal of the American Chemical Society, 2008. 130: p. 12192 - 12200.

43. Jin, R., et al., *What Controls the Melting Properties of DNA-Linked Gold Nanoparticle Assemblies?* Journal of the American Chemical Society, 2003. 125: p. 1643-1654.

44. Storhoff, J.J. and C.A. Mirkin, *Programmed Materials Synthesis with DNA.* Chemical Reviews, 1999. 99: p. 1849-1862.

45. Loweth, C.J., et al., *DNA-Based Assembly of Gold Nanocrystals.* Angewandte Chemie International Edition, 1999. 38(12): p. 1808 - 1812.

46. Storhoff, J.J., et al., *One-Pot Colorimetric Differentiation of Polynucleotides with Single Base Imperfections Using Gold Nanoparticle Probes.* Journal of the American Chemical Society, 1998. 120: p. 1959 - 1964.

47. Storhoff, J.J., et al., *What Controls the Optical Properties of DNA-Linked Gold Nanoparticle Assemblies?* Journal of the American Chemical Society, 2000. 122: p. 4640 - 4650.

48. Lytton-Jean, A.K. and C.A. Mirkin, *A Thermodynamic Investigation into the Binding Properties of DNA Functionalized Gold Nanoparticle Probes and Molecular Fluorophore Probes.* Journal of the American Chemical Society, 2005. 127: p. 12754 - 12755.

49. Park, c.Y., et al., *DNA-programmable nanoparticle crystallization.* Nature, 2008. 451: p. 553-556.

50. Nykypanchuk, D., et al., *DNA-guided crystallization of colloidal nanoparticles.* Nature, 2008. 451: p. 549-552.

51. Mastroianni, A.J., S.A. Claridge, and A.P. Alivisatos, *Pyramidal and Chiral Groupings of Gold Nanocrystals Assembled Using DNA Scaffolds.* Journal of the American Chemical Society, 2009. 131: p. 8455 - 8459.

52. Elghanian, R., et al., *Selective Colorimetric Detection of Polynucleotides Based on the Distance-Dependent Optical Properties of Gold Nanoparticles.* Science, 1997. 277: p. 1078 - 1081.

53. Gibbs-Davis, J.M., G.C. Schatz, and S.T. Nguyen, *Sharp Melting Transitions in DNA Hybrids without Aggregate Dissolution: Proof of Neighboring-Duplex Cooperativity.* Journal of the American Chemical Society, 2007. 129: p. 15535 - 15540.

54. Park, S.Y. and D. Stroud, *Theory of melting and the optical properties of gold/DNA nanocomposites.* Physical Review E, 2003. 67: p. 212202.

55. Sun, Y., N.C. Harris, and C.-H. Kiang, *The reversible phase transition of DNA-linked colloidal gold assemblies.* Physica A, 2005. 354: p. 1 - 9.

56. Dreyfus, R., et al., *Simple Quantitative Model for the Reversible Association of DNA Coated Colloids.* Physical Review Letters, 2009. 102: p. 048301.

57. Kim, A.J., P.L. Biancaniello, and J.C. Crocker, *Engineering DNA-Mediated Colloidal Crystallization.* Langmuir, 2006. 22: p. 1991-2001.

58. Kim, A.J., et al., *Probing interfacial equilibration in microspheres crystals formed by DNA-directed assembly.* Nature Materials, 2009. 8: p. 52 - 55.

59. Biancaniello, P.L., et al., *DNA-Mediated Phase Behavior of Microsphere Suspensions.* Langmuir, 2007. 23: p. 2688-2693.

60. Biancaniello, P.L., A. Kim, and J.C. Crocker, *Colloidal Interactions and Self-Assembly Using DNA Hybridization.* Physical Review Letters, 2005. 94: p. 058302.

61. Milam, V.T., et al., *DNA-Driven Assembly of Bidisperse, Micron-Sized Colloids.* Langmuir, 2003. 19: p. 10317-10323.

62. Tison, C.K. and V.T. Milam, *Reversing DNA-mediated Adhesion at a Fixed Temperature.* Langmuir, 2007. 23: p. 9728-9736.

63. Wang, Z., et al., *Enzymatic DNA processing in gold nanoparticles.* Journal of Materials Chemistry, 2004. 14: p. 578-580.

64. Pena, S.R.N., et al., *Hybridization and Enzymatic Extension of Au Nanoparticle-Bound Oligonucleotides.* Journal of the American Chemical Society, 2002. 124: p. 7314 - 7323.

65. Kanaras, A.G., et al., *Site-Specific Ligation of DNA-Modified Gold Nanoparticles Activated by the Restriction Enzyme StyI.* Small, 2007. 3(1): p. 67-70.

66. Tison, C.K. and V.T. Milam, *Manipulating DNA Probe Presentation via Enzymatic Cleavage of Diluent Strands.* Biomacromolecules, 2008. 9: p. 2468 - 2476.

67. Xia, Y., et al., *Colloidal Crystals: Recent Developments and Niche Applications*, in *Colloids and Colloid Assemblies*, F. Caruso, Editor. 2004, Wiley-VCH Verlag GmbH & Co. KGaA, Weinheim: Weinheim. p. 603.

68. Russel, W.B., D.A. Saville, and W.R. Schowalter, *Colloidal Dispersions*. 1989: Cambridge University Press. 525.

69. Birdi, K.S., *Surface and Colloid Chemistry*, in *Handbook of Surface and Colloid Chemistry*, K.S. Birdi, Editor. 1997, CRC Press: Boca Raton. p. 1-4.

70. Zhong, Z., et al., *From Discrete Particles to Spherical Aggregates: A Simple Approach to the Self-Assembly of Au Colloids.* Chemistry: A European Journal, 2005. 11: p. 1473-1478.

71. Weitz, D.A. and W.B. Russel, *New Developments in Colloid Science.* MRS Bulletin, 2004. 29(2): p. 82-84.

72. Somasundaran, P., et al., *Colloid Systems and Interfaces-Stability of Dispersions through Polymer and Surfactant Adsorption*, in *Handbook of Surface and Colloid Chemistry*, K.S. Birdi, Editor. 2003, CRC Press: Boca Raton. p. 387-435.

73. Prevo, B.G. and O.D. Velev, *Controlled, Rapid Deposition of Structured Coatings from Micro- and Nanoparticle Suspensions.* Langmuir, 2004. 20: p. 2099-2107.

74. Gangwal, S., et al., *Induced-Charge Electrophoresis of Metallodielectric Particles.* Physical Review Letters, 2008. 100: p. 058302.

75. Wu, Q., et al., *A Facile Strategy for Controlling the Self-Assembly of Nanocomposite Particles Based on Colloidal Steric Stabilization Theory.* Langmuir, 2008. 24: p. 7778 - 7784.

76. Erb, R.M., et al., *Magnetic assembly of colloidal superstructures with multipole symmetry.* Nature, 2009. 457: p. 999 - 1002.

77. Kralchevsky, P.A., K.D. Danov, and N.D. Denkov, *Chemical Physics of Colloid Systems and Interfaces*, in *Handbook of Surface and Colloids Chemistry*, K.S. Birdi, Editor. 1997, CRC Press: Boca Raton. p. 333 - 494.

78. Israelachvili, J.N., *Intermolecular and Surface Forces*. 1985, Academic Press: London. p. 161-193.

79. Cao, G., *Nanostructures & Nanomaterials: Synthesis, Properties & Applications*. 2004: Imperial College Press.

80. Behrens, S.H., et al., *Charging and Aggregation Properties of Carboxyl Latex Particles: Experiments versus DLVO Theory.* Langmuir, 2000. 16: p. 2566 - 2575.

81. Bostrom, M., D.R.M. Williams, and B.W. Ninham, *Specific Ion Effects: Why DLVO Theory Fails for Biology and Colloids Systems.* Physical Review Letters, 2001. 87(16): p. 168103.

82. Hiddessen, A.L., D.A. Weitz, and D.A. Hammer, *Rheology of Binary Colloidal Structures Assembled via Specific Biological Cross-Linking.* Langmuir, 2004. 20: p. 6788-6795.

83. Hiddessen, A.L., et al., *Assembly of Binary Colloidal Structures via Specific Biological Adhesion.* Langmuir, 2000. 16: p. 9744-9753.

84. Yao, H., et al., *DNA-directed self-assembly of gold nanoparticles into binary and ternary nanostructures.* Nanotechnology, 2007. 18: p. 015102.

85. Sebba, D.S., et al., *Reconfigurable Core--Satellite Nanoassemblies as Molecularly-Driven Plasmonic Switches.* Nano Letters, 2008. 8(7): p. 1803-1808.

86. Bajaj, M.G. and P.E. Laibinis, *Selective DNA-Directed Assembly on Dual-Functionalized Microparticles.* Materials Research Society Proceedings, 2004.

87. Perro, A., et al., *Design and synthesis of Janus micro- and nanoparticles.* Journal of Materials Chemistry, 2005. 15: p. 3745-3760.

88. Mitchell, G.P., C.A. Mirkin, and R.L. Letsinger, *Programmed Assembly of DNA Functionalized Quantum Dots.* Journal of the American Chemical Society, 1999. 121: p. 8122-8123.

89. Rosi, N.L., C.S. Thaxton, and C.A. Mirkin, *Control of Nanoparticle Assembly by Using DNA-Modified Diatom Templates.* Angewandte Chemie International Edition, 2004. 43: p. 5500-5503.

90. Jakobsen, U., A.C. Simonsen, and S. Vogel, *DNA-Controlled Assembly of Soft Nanoparticles.* Journal of the American Chemical Society, 2008. 130: p. 10462-10463.

91. Beales, P.A. and T.K. Vanderlick, *Specific Binding of Different Vesicle Populations by the Hybridization of Membrane-Anchored DNA.* Journal of Physical Chemistry A, 2007. 111: p. 12372 - 12380.

92. Dunbar, S.A., et al., *Quantitative, multiplexed detection of bacterial pathogens: DNA and protein applications of the Luminex LabMAP™ system.* Journal of Microbiological Methods, 2003. 53: p. 245-252.

93. Lu, J., et al., *MicroRNA expression profiles classify human cancers.* Nature, 2005. 435(9): p. 834-838.

94. Bao, G., A. Tsourkas, and P.J. Santangelo, *Engineering Nanostructured Probes for Sensitive Intracellular Gene Detection.* Mech Chem Biosyst, 2004. 1(1): p. 23 - 36.

95. Li, J. and Y. Lu, *A Highly Sensitive and Selective Catalytic DNA Biosensor for Lead Ions.* Journal of the American Chemical Society, 2000. 122: p. 10466 - 10467.

96. Yim, T.-J., et al., *Highly Active and Stable DNAzyme - Carbon Nanotube Hybrids.* Journal of the American Chemical Society, 2005. 127: p. 12200 - 12201.

97. Chang, I.-H., et al., *Miniaturized Lead Sensor Based on Lead-Specific DNAzyme in a Nanocapillary Interconnected Microfluidic Device.* Environmental Science and Technology, 2005. 39(10): p. 3756 - 3761.

98. Shannon, M.A., et al., *Science and technology for water purification in the coming decades.* Nature, 2008. 452: p. 301 - 310.

99. Wernette, D.P., et al., *Functional-DNA-Based Nanoscale Materials and Devices for Sensing Trace Contaminants in Water.* MRS Bulletin, 2008. 33: p. 34-41.

100. Liu, J., D. Mazumdar, and Y. Lu, *A Simple and Sensitive "Dipstick" Test in Serum Based on Lateral Flow Separation of Aptamer-Linked Nanostructures.* Angewandte Chemie International Edition, 2006. 45: p. 7955 - 7959.

101. Lu, Y. and J. Liu, *Functional DNA nanotechnology: emerging applications of DNAzymes and aptamers.* Current Opinion in Biotechnology, 2006. 17: p. 580 - 588.

102. Battersby, B.J., et al., *Colloids for Encoding Chemical Libraries: Applications in Biological Screening*, in *Colloids and Colloid Assemblies: Synthesis.*

Modification, Organization and Utilization of Colloid Particles, F. Caruso, Editor. 2004, Wiley-VCH. p. 507 - 560.

103. Call, D.R., M.K. Borucki, and F.J. Loge, *Detection of bacterial pathogens in environmental samples using DNA microarrays.* Journal of Microbiological Methods, 2003. 53: p. 235 - 243.

104. Dunbar, S.A., *Applications of Luminex^{R} xMAP^{TM} technology for rapid, high-throughput multiplexed nucleic acid detection.* Clinica Chimica Acta, 2006. 363: p. 71-82.

105. Guschin, D.Y., et al., *Oligonucleotide Microchips as Genosensors for Determinative and Environmental Studies in Microbiology.* Applied and Environmental Microbiology, 1997. 63(6): p. 2397 - 2402.

106. Baeumner, A.J., *Biosensors for environmental pollutants and food contaminants.* Analytical and Bioanalytical Chemistry 2003. 377: p. 434 - 445.

107. White, R.J., et al., *Optimization of Electrochemical Aptamer-Based Sensors via Optimization of Probe Packing Density and Surface Chemistry.* Langmuir, 2008. 24: p. 10513 - 10518.

108. Tsourkas, A., et al., *Hybridization kinetics and thermodynamics of molecular beacons.* Nucleic Acids Research, 2003. 31(4): p. 1319 - 1330.

109. Santangelo, P.J., et al., *Dual FRET molecular beacons for mRNA detection in living cells.* Nucleic Acids Research, 2004. 32(6): p. e57.

110. Li, Q., et al., *A new class of homogeneous nucleic acid probes based on specific displacement hybridization.* Nucleic Acids Research, 2002. 30: p. 2e5.

111. Southern, E.M., *Detection of Specific Sequences Among DNA Fragments Separated by Gel Electrophoresis.* Journal of Molecular Biology, 1975. 98: p. 503 - 517.

112. Ramsay, G., *DNA chips: State-of-the art.* Nature Biotechnology, 1998. 16: p. 40 - 44.

113. Livache, T., et al., *Polypyrrole DNA Chip on a Silicon Device: Example of Hepatitis C Virus Genotyping.* Analytical Biochemistry, 1998. 255: p. 188 - 194.

114. Soto, C.M., et al., *Immobilization and Hybridization of DNA in a Sugar Polyacryalte Hydrogel.* Biotechnology and Bioengineering, 2005. 92(7): p. 934 - 942.

115. Fan, C., K.W. Plaxco, and A.J. Heeger, *Electrochemical interrogation of conformational changes as a reagentless method for the sequence-specific detection of DNA.* Proceedings of the National Academy of Sciences of the United States of America 2003. 100(16): p. 9134 - 9137.

116. Xiao, Y., et al., *Single-step electronic detection of femtomolar DNA by target-induced strand displacement in an electrode-bound duplex.* Proceedings of the National Academy of Sciences of the United States of America 2006. 103(45): p. 16677 - 16680.

117. Chan, V., D.J. Graves, and S.E. McKenzie, *The Biophysics of DNA Hybridization with Immobilized Oligonucleotide Probes.* Biophysical Journal, 1995. 69: p. 2243 - 2255.

118. Hagan, M.F. and A.K. Chakraborty, *Hybridization dynamics of surface immobilized DNA.* The Journal of Chemical Physics, 2004. 120(10): p. 4958 - 4968.

119. Peterson, A.W., R.J. Heaton, and R.M. Georgiadis, *The effect of surface probe density on DNA hybridization.* Nucleic Acids Research, 2001. 29(24): p. 5163 - 5168.

120. Cram, L.S., *Flow cytometry, an overview.* Methods in Cell Science, 2002. 24: p. 1-9.

121. Henry, M.R., et al., *Real-Time Measurements of DNA Hybridization on Microparticles with Fluorescence Resonance Energy Transfer.* Analytical Biochemistry, 1999. 276: p. 204 - 214.

122. Stenberg, M. and H. Nygren, *Kinetics of antigen-antibody reactions at solid-liquid interfaces.* Journal of Immunological Methods, 1988. 113: p. 3 - 15.

123. Stevens, P.W., M.R. Henry, and D.M. Kelso, *DNA hybridization on microparticles: determining capture-probe density and equilibrium dissociation constants.* Nucleic Acids Research, 1999. 27(7): p. 1719 - 1727.

124. Wolf, S.F., et al., *Rapid hybridization kinetics of DNA attached to submicron latex particles.* Nucleic acids Research, 1987. 15(7): p. 2911 - 2926.

125. Tawa, K., D. Yao, and W. Knoll, *Matching base-pair number dependence of the kinetics of DNA-DNA hybridization studied by surface plasmon fluorescence spectroscopy.* Biosensors and Bioelectronics, 2005. 21: p. 322 - 329.

126. Glazer, M., et al., *Kinetics of oligonucleotide hybridization to photolithographically patterned DNA arrays.* Analytical Biochemistry, 2006. 358: p. 225 - 238.

127. Vainrub, A. and B.M. Pettit, *Coulomb blockage of hybridization in two-dimensional DNA arrays.* Physical Review E, 2002. 66: p. 041905.

128. Okahata, Y., et al., *Kinetic Measurements of DNA Hybridization on an Oligonucleotide-Immobilized 27-MHz Quartz Crystal Microbalance.* Analytical Chemistry, 1998. 70: p. 1288 - 1296.

129. Homann, M., W. Nedbal, and G. Sczakiel, *Dissociation of long-chain duplex RNA can occur via strand displacement in vitro: biological implications.* Nucleic Acids Research, 1996. 24(22): p. 4395-4400.

130. Reynaldo, L.P., et al., *The Kinetics of Oligonucleotide Replacements.* Journal of Molecular Biology, 2000. 297: p. 511-520.

131. Wetmur, J.G., *DNA Probes: Applications of the Principles of Nucleic Acid Hybridization.* Critical Reviews in Biochemistry and Molecular Biology, 1991. **26**: p. 227 - 259.

CHAPTER 2

Quantification of Double-Stranded Probes and Formation of Satellite Assemblies[1]

2.1 Introduction

This chapter discusses the process of covalently attaching DNA to colloidal particles, quantification of double-stranded DNA probes using fluorescently tagged hybridization partners, and the DNA-mediated assembly of fluorescent satellites. The first part of the chapter will discuss the hybridization of soluble dye-labeled targets to immobilized single-stranded DNA probe strands on the microsphere surface to form labeled dsProbes quantified via flow cytometry. By covalently coupling DNA to the surface of polystyrene microspheres, we can easily handle the DNA-functionalized particles via centrifugation and washing steps to allow for facile buffer exchange as well as the addition and removal of target species and smaller fluorescent particles. The second part of the chapter will discuss the process of colloidal satellite formation mediated by DNA duplex bridges between particle surfaces of varying base length and with or without mismatches. Differences in fluorescent particle coverage in populations of colloidal satellites is assessed as a function of the oligonucleotide density on the surface of the microsphere templates as well as the temperature conditions used for satellite assembly.

---

[1] Results of this chapter are also discussed in
Baker, B. A. and V. T. Milam, "*DNA Density-Dependent Assembly Behavior of Colloidal Micelles*," Langmuir, in press.

2.2 Experimental Methods.

Materials. DNA was purchased from Integrated DNA Technologies with either an amine or fluorescein modification to the 5' end (IDT, Coralville, IA). HPLC purification was performed by the manufacturer. 5.1 μm or 0.2 μm carboxylate modified polystyrene particles were purchased from Invitrogen (Molecular Probes, Eugene, OR). 5.0 μm COOH modified polystyrene particles were purchased from Bangs Laboratories (Fishers, Indiana). *N*-Ethyl-*N'*-(3-dimethylaminopropyl) carbodiimide hydrochloride (EDAC) and 10x phosphate buffered saline (PBS) were purchased from Sigma (St. Louis, MO). Tris-ethylenediaminetetraacetic acid disodium salt dihydrate (Tris/EDTA) buffers of pH 7.4 and pH 8.0 were purchased from Fisher Scientific (Pittsburgh, PA). The 2-(N-morpholino) ethane sulfonic acid (MES) was purchased from Acros Organics (New Jersey, USA). Proclin 300 was purchased from Supelco (Bellefonte, PA). Tween 20 was purchased from Calbiochem (EMD Biosciences, La Jolla, CA).

Buffer Preparation. Diamond Nanopure water was used in all buffer formulations (Barnstead International, Dubuque, IA). PBS/Tween buffer was made with 5 mL of 10x PBS, 45 mL of nanopure water, and 100 μL of Tween 20 mixed end-over-end for ~ 1 h. Coupling Buffer (CB) followed a formulation by Bangs Laboratories (Fishers, IN) used in their PolyLink Coupling Kit but was prepared in our lab. 50 mM MES and 0.05% Proclin 300 were diluted in nanopure water at a pH of 5.2 and mixed by end-over-end mixing. All buffers were filtered through a 0.2 μm syringe cap filter before use.

Conjugation of Single-Stranded Probe to Template Microspheres. Template microspheres with COOH functionalities were coupled via a standard EDAC conjugation protocol as described previously[1]. In order to arrive at a final particle concentration of

1% w/v solids, 25 µL of 4% w/v Invitrogen particles and 10 µL of 10% w/v Bangs Laboratories particles were centrifuged at 9.1 x 1000 g for 2 minutes (same for all centrifugation steps) and resuspended in 100 µL of the Coupling Buffer (CB). A second centrifugation step followed with resuspension into 150 µL of CB. 55 µL of CB was then added to 10 mg of pre-weighed and N_2 backfilled EDAC. Immediately after vortexing, 25 µL of the EDAC/CB solution was added to the particle suspension along with 200 µL of 10 µM probe DNA. The suspension was vortexed and incubated with end-over-end mixing for two hours. Following mixing the single-stranded, probe-coupled particles were centrifuged and washed two times in PBS/Tween buffer and resuspended in 100 µL PBS/Tween at a final concentration of 1% w/v solids.

A schematic of this process is presented in Figure 2.3.1. EDAC coupling is a common technique for the formation of an amide bond between a COOH group and primary amine group. The single-stranded DNA probe strand is coupled to the template microsphere (both Molecular Probes and Bangs Laboratories microspheres) via a primary amine group on the 5' end separated from the DNA bases by a 12 carbon spacer. During the coupling reaction, an O-acylisourea intermediate is formed between the EDAC molecule and a COOH group on the particle surface. This intermediate is displaced by the amide bond formation between the COOH residue on the particle surface and the amine group on the DNA probe strand resulting in an isourea leaving group[2]. The EDAC-coupling buffer solution must be made immediately prior to addition as the EDAC molecule is susceptible to hydrolysis. After coupling, the final product is stored at 4-6 °C until use.

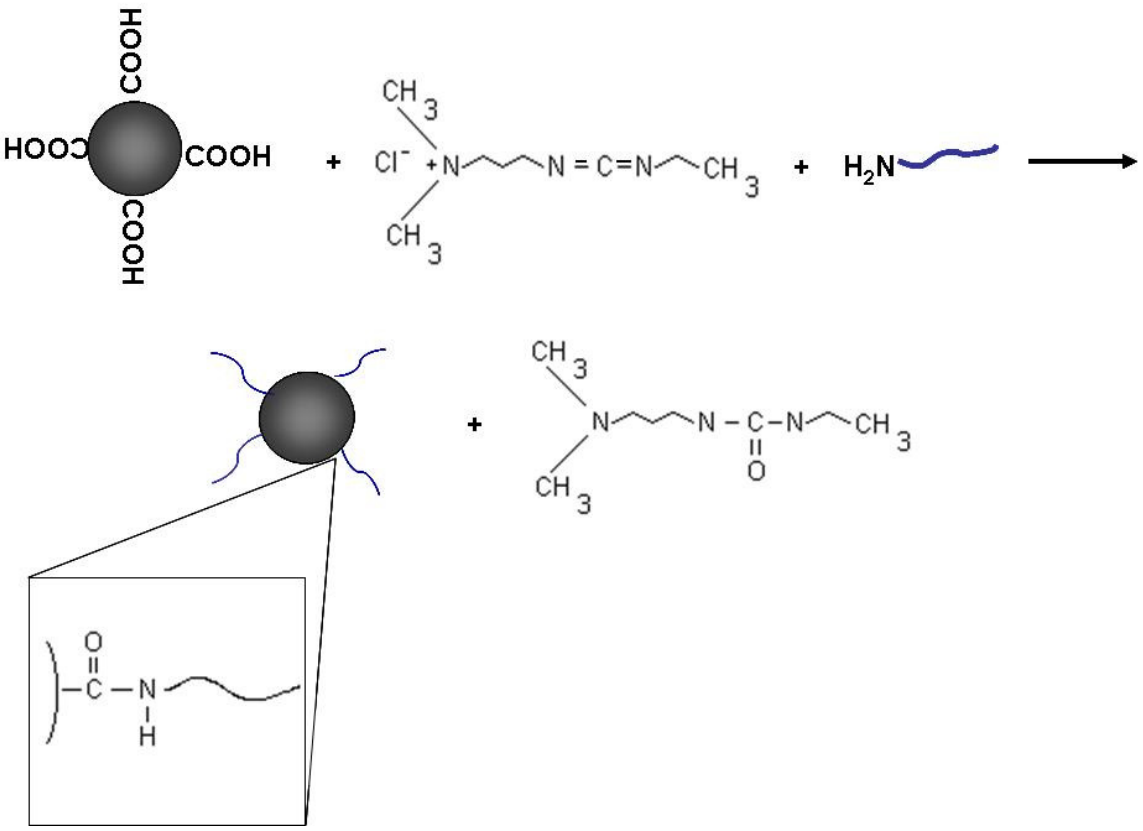

Figure 2.2.1. Schematic of reactants and products involved in conjugating aminated DNA to COOH-modified polystyrene particles. Inset: Schematic of the amide bond formed between the amine end group on DNA and the carboxylic acid group on the surface of the particle.

Conjugation of Target Strand to Template Microspheres. The 0.2 µm fluorescent particles were prepared similarly. 50 µL of 2% w/v fluorescent particles were centrifuged at 14 x 1000 g for 5 minutes then resuspended in 100 µL of CB. After a second centrifugation step followed by resuspension into 150 µL of CB, 50 µL of EDAC/CB solution was added to the particle suspension followed by 200 µL of 10 µM primary target DNA. The particles were incubated with end-over-end mixing for two hours and then washed two times. The final resuspension was a 1% w/v solids concentration in 100 µL PBS/Tween.

Primary Hybridization of Soluble Targets to Form dsProbes. For both Invitrogen and Bangs Laboratories template microspheres, a suspension of the probe-functionalized microspheres was incubated in a 5 µM concentration of fluorescently labeled primary targets. The following is adapted from the protocol developed by Chris Tison[1]. The Invitrogen particles were prepared by taking 12 µL of probe functionalized particles and diluting in 188 µL of PBS/Tween. After a washing step followed by resuspension in 200 µL of PBS/Tween, 200 µL of 10 µM fluorescently-labeled target DNA were added resulting in a concentration of 5 µM. After 6 h incubation the samples were given two complete washing steps. 20 µL of the hybridized suspension was removed and diluted to a final volume of 100 µL with PBS/Tween. The Bangs Laboratories microspheres were prepared similarly though begin with 2 µL of probe functionalized particles diluted to 100 µL and centrifuged. After resuspension in 100 µL PBS/Tween, 100 µL of 10 µM fluorescently labeled DNA was added resulting in a concentration of 5 µM DNA. After 6 h incubation the sample was washed a total of two times and resuspended in 100 µL of PBS/Tween. This process is schematically illustrated in Figure 2.2.2.

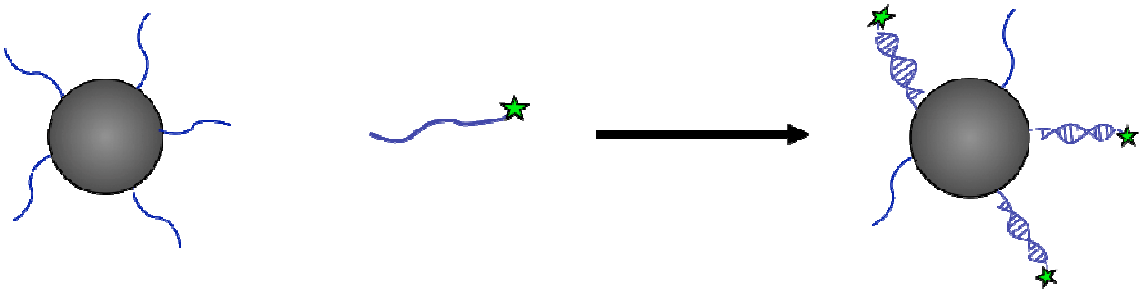

Figure 2.2.2. Schematic of primary hybridization between the DNA single-stranded probe coupled to the particle surface and the fluorescently-labeled hybridization partner to form dsProbes on the particle surface.

The primary hybridization partner (primary target) is fluorescein-labeled on the 5' end so that once hybridized, the fluorophore will extend away from the particle surface. This fluorescent labeling allows the use of flow cytometry to quantify the number of duplexes on the particle surface. Preparation for flow cytometry is completed by diluting the 100 μL particle suspension with 900 μL of PBS/Tween. The final 1 mL sample is analyzed with a Becton Dickinson FACS II flow cytometer (Becton Dickinson, San Jose, CA). Generally, hybridized samples are stored at 4 – 6 °C conditions prior to analysis with flow cytometry occurring the next day. For each series of measurements, a negative control of probe functionalized template microspheres was analyzed. FITC calibration standards from Bangs Laboratories were used to calibrate the measured fluorescence intensity and convert to duplex density.

2.3 Quantifying Duplex Density on Template Microspheres

2.3.1 Hybridization Events with Soluble, Fluorescently-Labeled Targets

In order to ensure that there was no significant signal difference due to storage and handling, a series of controls was performed to quantify the duplex density of the dsProbes on the particle surfaces using flow cytometry. Hybridization partners of 11, 13, or 15 bases in length that are perfectly complementary to the immobilized probe strands were incubated with the probe-functionalized 5.1 μm microspheres in order to allow primary hybridization to occur. Four handling and storage conditions were examined: 6 h of incubation followed by flow cytometry, 6 h of incubation followed by storage at

room temperature for 24 h before flow cytometry, 6 h of incubation followed by storage at 4 – 6 °C for 24 h before flow cytometry, and 24 h of incubation directly followed by flow cytometry. The primary target duplex density values were compared across all four of these categories. In order to determine the duplex density, observed fluorescence intensity was compared to calibration standards of mean equivalent soluble fluorophore (MESF) purchased from Bangs Laboratories (Fisher, IN). Once an MESF number is determined for a given sample, dividing by the surface area of the particle (for 5.1 μm particles the surface area is 81.72 μm^2) results in the average duplex density of the fluorescently-labeled primary targets hybridized to probes immobilized on the particle surface.

Figure 2.3.1 shows the results of these studies. The 15 base primary hybridization partner (**T15**) has the highest observed duplex density followed by **T13** then **T11** for all conditions studied. The observed duplex density values are consistent and demonstrate only moderate variation across the four conditions studied. This results indicates that the common storage and handling conditions for subsequent experiments have significantly less influence on duplex density than base length of the hybridization partner. From these results a six-hour hybridization time was deemed sufficient to result in consistent duplex density values for a given particle population. Following hybridization, samples may be stored at 4 – 6 °C conditions prior to flow cytometry without significantly affecting the observed duplex density values.

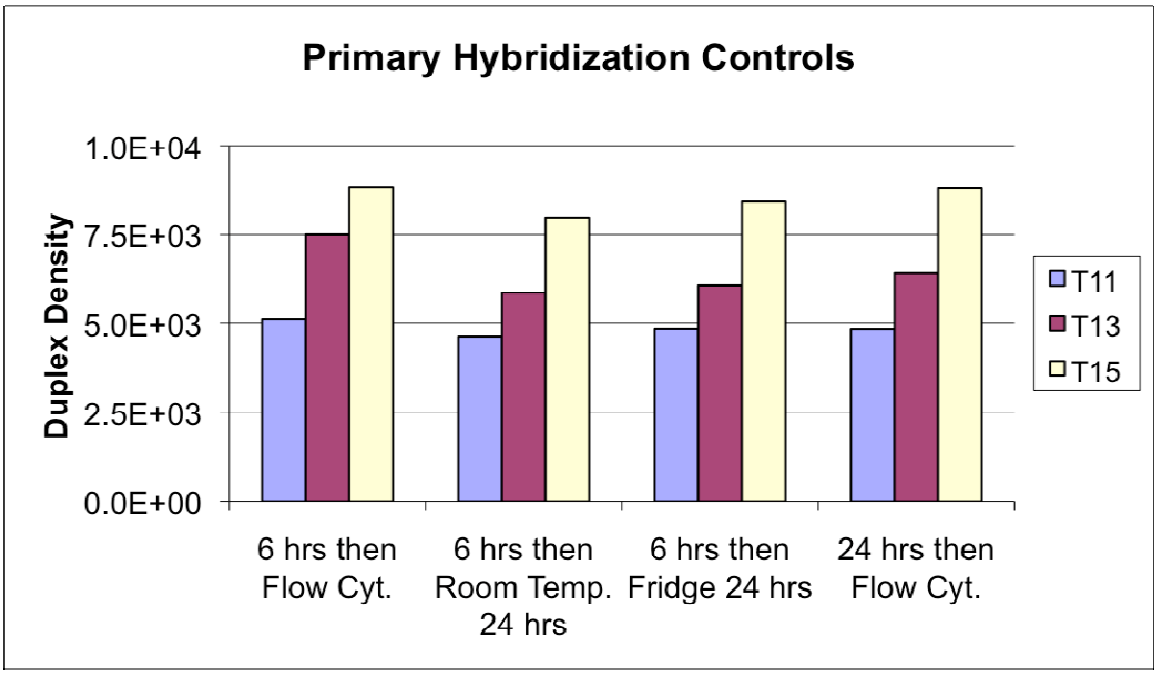

Figure 2.3.1. Density of labeled duplexes under various handling and storage conditions after target incubation and prior to flow cytometry for perfectly complementary targets of 11 bases (**T11**), 13 bases (**T13**), and 15 bases (**T15**).

After coupling and initial studies of storage and handling conditions, a more extensive list of candidate dsProbe sequences was studies using flow cytometry. While flow cytometry has been historically used as a quantification tool in cell studies[3, 4] its application to nucleic acid capture and detection has been successfully demonstrated[5, 6]. The probe and its fluorescently-labeled hybridization partners used for the study are listed in Table 2.3.1.

Table 2.3.1. List of oligonucleotide sequences and their function (probe vs. target). The probe strand, highlighted in blue, is the strand immobilized on the particle surface. The center mismatches are highlighted in red. The fluorescent label on the target is highlighted in green and listed as "T-Fluor" as the fluorophore is incorporated on a modified thymine base that does not participate in hybridization.

Name	Sequence
Probe	5' – Amine-(carbon12) CTC GTC ACA CTA TCA – 3'
T11	3' –AG TGT GAT AGT (T-fluor) – 5'
T11m	3' –AG TGT CAT AGT (T-fluor) – 5'
T13	3' – G CAG TGT GAT AGT (T-fluor) – 5'
T13m	3' – G CAG TGA GAT AGT (T-fluor) – 5'
T15	3' – GAG CAG TGT GAT AGT (T-fluor) – 5'
T15m	3' – GAG CAG TCT GAT AGT (T-fluor) – 5'
TH18	3' – TTT TTT TTT TTT TTT TTT (T-fluor) – 5'

As a negative control, coupled microspheres that were not incubated with the original, dye-labeled targets were prepared for flow cytometry and included in every measurement. This negative control was used to establish the autofluorescence of the polystyrene lattices as these samples were not exposed to fluorescent targets. Representative fluorescence histograms taken from flow cytometry data are shown in Figures 2.3.2 and 2.3.3. The histograms show peaks for the fluorescence intensity associated with a population of single-stranded probe functionalized particles incubated with a series of either perfectly-matched sequences and mismatched sequences for Invitrogen and Bangs Laboratories template microspheres, respectively. For all samples the blank particles showed almost no fluorescence. Both Invitrogen (Figure 2.3.2) and Bangs Laboratories (Figure 2.3.3) microspheres demonstrated increasing fluorescence, as

indicated by higher peak location on the FITC scale, for longer target strands. Comparing the perfectly complementary targets to the mismatched targets in both cases indicates a shift to lower fluorescence values for the set of mismatched targets. Comparisons between the two types of microspheres show consistently lower fluorescence values for target hybridization to the Bangs Laboratories microspheres for a given target.

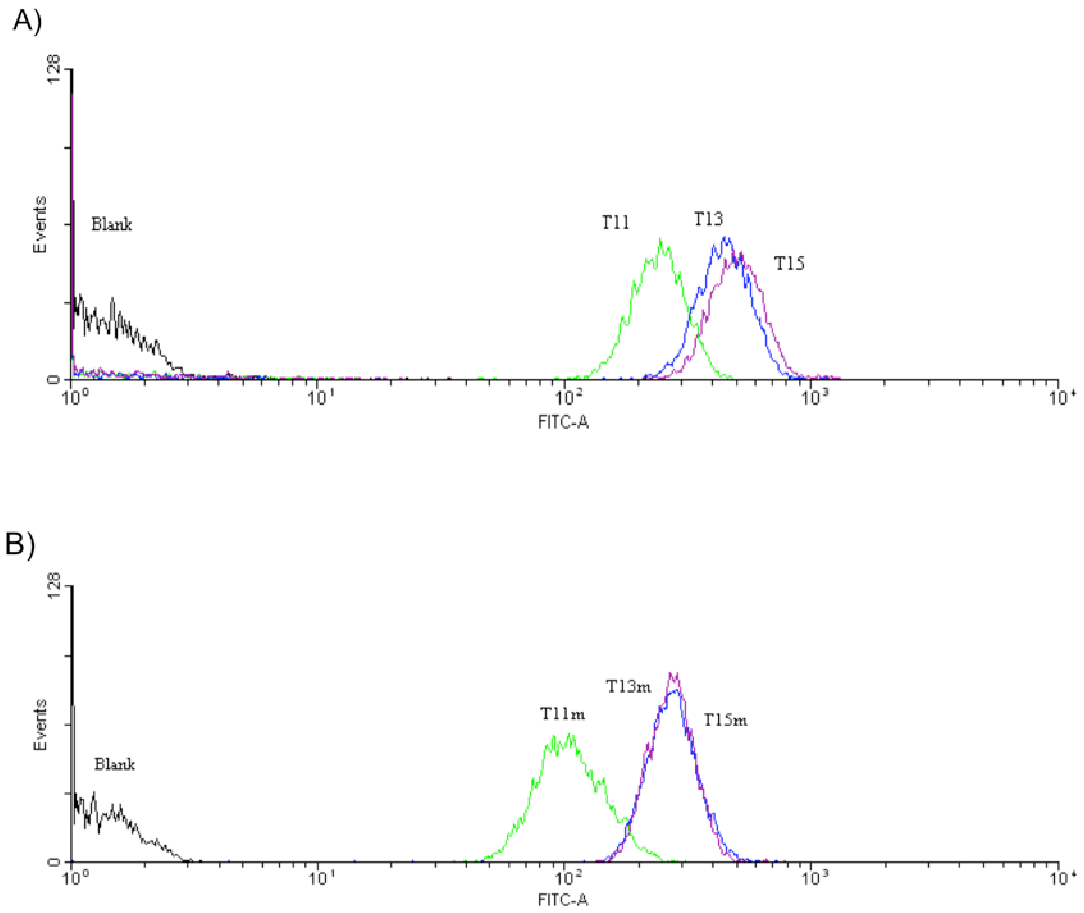

Figure 2.3.2. Representative flow cytometry histogram showing the relative fluorescence intensity associated with single-stranded probe functionalized particles incubated with A) **T11**, **T13** or **T15** targets or B) **T11m**, **T13m**, or **T15m** targets. The Blank peak is a negative reference corresponding to probe functionalized particles alone (no fluorescent targets). Invitrogen particles were used for these studies.

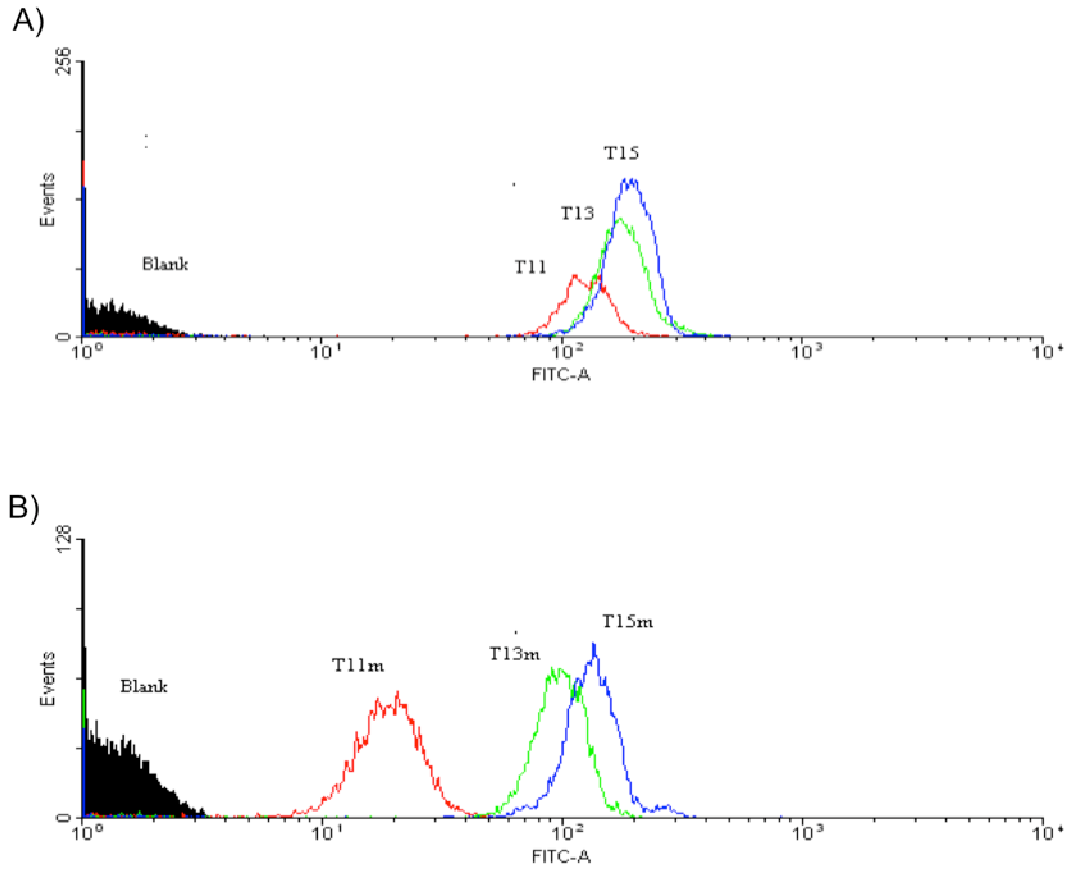

Figure 2.3.3. Representative flow cytometry histogram showing the relative fluorescence intensity associated with single-stranded probe functionalized particles incubated with A) **T11**, **T13** or **T15** targets or B) **T11m**, **T13m**, or **T15m** targets. The Blank peak is a negative reference corresponding to probe functionalized particles alone (no fluorescent targets). Bangs Laboratories particles were used for these studies.

Table 2.3.2 shows the measured duplex densities for both Invitrogen and Bangs Laboratories particles determined from the flow cytometry studies. Each duplex density value corresponds to the average of three separate measurements. Included in this series is a second negative control in which single-stranded probe functionalized particles were incubated with **TH18**, a fluorescently-labeled 18 base thymine sequence that has no specific affinity for the probe strand. The low duplex density values reported (8.58 duplexes per μm^2 for the Molecular Probes microspheres and 13.78 duplexes per μm^2 for the Bangs Laboratories microspheres) indicate minimal nonspecific interaction between the fluorescently labeled targets and the probe-conjugated microspheres. Subsequently, we conclude that reported duplex density values correspond to specific hybridization events. Longer base lengths result in higher duplex densities for both Invitrogen and Bangs Laboratories particles. Duplexes that incorporate a center mismatch result in a lower duplex density than their perfectly matched counterparts. The Invitrogen particles, however, consistently resulted in higher duplex density values than the Bangs Laboratories microspheres for all analogous sequences tested. As indicated by the variations in duplex density value, the differences in duplex length and the inclusion of a center mismatch provide a mechanism to incorporate affinity differences within the dsProbe. These affinity differences will next be assessed in the context forming particle assemblies using dsProbes.

Table 2.3.2. Measured densities of DNA duplexes on various microspheres based on flow cytometry and the calculated number of duplex linkages between a template microsphere and a fluorescent particle based on measured duplex density on microspheres and the projected contact area.

1° Target	Duplex Density (duplex /μm²)		Calculated Duplex Number Between Particles	
	Invitrogen	Bangs Labs.	Invitrogen	Bangs Labs.
TH18	9	14	NA	NA
T11	6,303	2,719	5	2
T11m	309	365	< 1	< 1
T13	11,816	4,112	11	4
T13m	5,654	2,103	5	2
T15	12,923	4,321	13	4
T15m	6,392	2,879	7	3

2.3.2 Calculating Contact Area and Number of Duplex Linkages

In order to better understand how the characteristic of duplex length and fidelity in base pair matching might affect DNA-mediated colloidal particle assembly, the number of duplexes that were expected to form between a template microsphere and each fluorescent particle surfaces were calculated using flow cytometry data and geometric considerations of the projected contact area between colloidal particles. The following calculations to determine the contact area between the template particle and fluorescent particles are based largely on the approach of Biancaniello and colleagues[7]. One necessary adaptation of our system is to account for the difference in particle sizes. The particle radius of the smaller particle is used in calculation, as it is the size-limiting component of our bi-disperse particle system. Figure 2.3.6 shows a schematic of the contact area between the two particle surfaces and the relevant geometric parameters.

The contact area is defined not only by the radius of the smaller particle but also the stretch length of the hybridized duplex that still allows complete hybridization of all bases within the duplex. As duplexes are formed from the center of the contact region outward to the edges, they undergo more stretching in order to form perfectly complementary duplexes. This stretching is a result of the radius of curvature of the particle surface, here limited by the smaller particle. Work by Smith et al. has demonstrated that duplex DNA has a stretch length of approximately 1.7 times its un-stretched contour length[8]. If we assume that the length of a DNA duplex is 0.34 nm between each base pair, which is the rise between each base pair of the helix, then the number of rises between base pairs participating in the hybridization duplex (or one less than the number of bases in the duplex) multiplied by this number gives the unstretched contour length of the duplex. For the cases of mismatched duplexes containing one center mismatch, the length is approximated to be the same as its perfectly matched equivalent. The difference between the stretched length and unstretched contour length is the quantity s which will be used to calculate the radius of the projections, r.

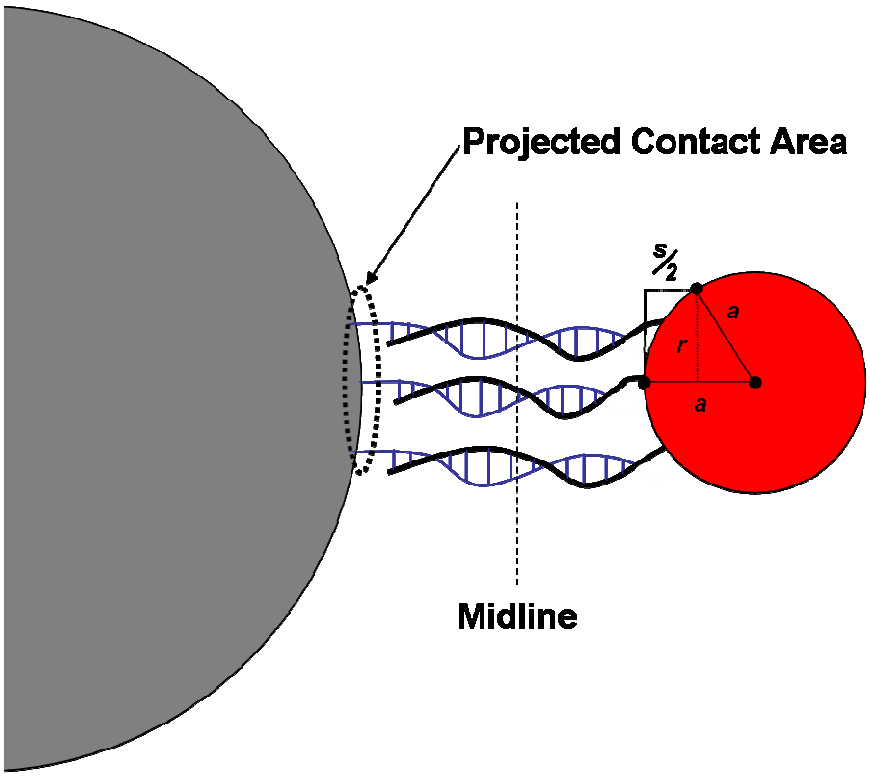

Figure 2.3.4. The projected contact area between the template microsphere and smaller fluorescent particle is defined by the geometry of the smaller radius of the fluorescent particle and the stretch length of the DNA duplex. Here, *a* corresponds to the radius of the smaller fluorescent particle, *r* corresponds to the radius of the contact area, and *s* is the difference in length of an unstretched DNA duplex in the center of the contact zone and a stretched DNA duplex near the periphery of the contact zone.

From the geometry in Figure 2.3.6, *r* is equal to $\sqrt{a^2-(a-s/2)^2}$. The term $s/2$ corresponds to the difference in length of un-stretched DNA and stretched DNA that falls on either side of the midline indicated. Since each DNA duplex is serving as a linkage or bridge between two differently sized particles the radius of curvature of both particles affects the total number of duplexes that do not exceed the maximum stretch length of a duplex. Thus, the difference in length *s* is distributed equally across both sides of the midline. This assumption is true for Biancaniello's system in which both particles are the

same size. In our system where the template particle is significantly larger than the 200 nm fluorescent particle, stretching of the duplex may not occur as equitably but the same assumption is applied in order to simplify the calculation.

Using the above methods, the calculated contact area values are as follows: 11 base duplex corresponds to a contact area of 743.13 nm^2, 13 base duplex corresponds to a contact area of 890.83 nm^2, and 15 base duplex corresponds to an area of 1,038.1 nm^2. This contact area multiplied by the duplex density on the surface of the template microsphere obtained from flow cytometry is used to approximate the number of DNA duplexes in the contact area between each particle listed in Table 2.3.2. Further details on these calculations are shown in Appendix A.

Comparison of all targets tested indicates that longer more perfectly complementary strands have higher duplex densities and result in higher values of predicted duplex linkages within the contact region. This trend is true for both the Invitrogen and Bangs Laboratories template microspheres. Comparisons across template microspheres indicate that for a given target the number of predicted duplexes is higher for the Invitrogen template microspheres due to their higher duplex density values. For example, the **T15** target is predicted to form approximately 13 duplex linkages within the contact area for a Invitrogen template microsphere compared to only 4 duplexes for the Bangs Laboratories template microspheres. Additional UV-vis studies to determine the ssDNA probe density on the particle surface after coupling indicated a modestly higher probe density occurs on the Invitrogen microspheres. Full details are given in Appendix B. (It should be noted that there was a time delay between the completion of the assembly studies and UV-vis measurements of the ssDNA probe density. After the

ssDNA probe density was determined, unexpected primary hybridization activity was observed for the same lot of Invitrogen particles used in the ssDNA density study. The reason for this behavior is not certain nor is its effect clear, but aging of the microspheres may have occurred. While the author believes the ssDNA density study does reflect density differences between the Invitrogen and Bangs Laboratories microspheres, only general trends are assessed from the data in light of the unexplained hybridization activity later observed.)

As a matter of convenience and in light of consistently higher duplex densities for all targets examined, the Molecular Probes template microspheres will be referred to as High Oligonucleotide Density Microspheres (HODM) and the Bangs Laboratories template microspheres will be referred to as Low Oligonucleotide Density Microspheres (LODM). For both template microspheres the **T11m** target is predicted to form less than one duplex within the contact region. Based on these calculations alone, one would expect limited if any assembly formation for the **T11m** case. On the other hand, one would expect that longer targets and perfectly matched targets will more likely form DNA-linked colloidal satellite structures for both template microspheres though perhaps Invitrogen microspheres may show more extensive fluorescent particle coverage on each template microsphere due to its higher duplex densities.

2.4 Satellite Assembly

2.4.1 Initial Studies

In order to generate particle assemblies mediated by DNA hybridization, primary targets functionalized with amine groups and a 12 carbon spacer instead of fluorescein at the 5' end were used. Through the amine group located on the 5' end of the DNA backbone, EDAC coupling was used to functionalize the surface of the 200 nm fluorescent particles with the target DNA strands. Flow cytometry was not used to quantify the number of DNA duplexes on these particles as their diameter was below the optimal size resolution capability of the instrument. The duplex melting temperatures as well as hairpin melting temperatures for the target sequence were calculated from Michael Zuker's DNAFold server[9-11]. The melting temperatures obtained allowed for selection of incubation conditions that were well below the melting point for most DNA duplexes studied. Table 2.4.1 is a summary of the modified primary target sequences and melting temperature analysis.

Table 2.4.1. Calculated duplex and hairpin melting temperatures using 3.51 mM target concentration and 154 mM Na+ concentration conditions for duplexes. For hairpin melting temperatures, 25 °C conditions 154 mM Na+ concentration were used. The underlined base indicates a mismatch between the probe and target.

* Duplex melting temperature calculated from M. Zuker MFold (accessed 9/16/08): http://dinamelt.bioinfo.rpi.edu/hybrid2.php

** Hair pin melting temperature calculated from Zuker Quickfold (accessed 9/16/08): http://dinamelt.bioinfo.rpi.edu/quikfold.php

Nomenclature	Sequence	Melt Temp.*	HP**
P21	5' – Amine-(carbon12) CTC GTC ACA CTA TCA – 3'	NA	6.6°C
NC	3' – ACT ATC ACA CTG CTC (carbon12)- Amine – 5'	22.2°C	6.6°C
T11	3' –AG TGT GAT AGT (carbon12)- Amine – 5'	62.4 °C	-64°C
T11m	3' –AG TGT CAT AGT (carbon12)- Amine – 5'	43.0 °C	-64°C
T13	3' – G CAG TGT GAT AGT (carbon12)- Amine – 5'	67.8 °C	-3.2°C
T13m	3' – G CAG TGA GAT AGT (carbon12)- Amine – 5'	58.4 °C	-64°C
T15	3' – GAG CAG TGT GAT AGT (carbon12)- Amine – 5'	71.8 °C	-3.2°C
T15m	3' – GAG CAG TCT GAT AGT (carbon12)- Amine – 5'	59.5 °C	12.4°C

Initial studies examined different buffer and particle size conditions before a general protocol was established. To form colloidal satellite (or colloidal micelle) assemblies, the template microspheres were incubated with an excess of fluorescent particles at room temperature with end-over-end mixing. PBS/BSA buffer prepared with heat denatured BSA (56 ºC for 30 minutes) was selected as an initial assembly buffer with the expectation that the BSA would block any nonspecific agglomeration of the particles. A negative control of HODM and fluorescent particles was prepared in which both types of particles were coupled with the probe strand. This condition should limit the ability of these particles to assemble via DNA duplexes since the sequences were not

complementary. Additionally, fluorescent particles functionalized with the perfectly complementary targets were also evaluated for assembly formation with probe-functionalized template microspheres. The results are shown in Figure 2.4.1. While assemblies involving perfectly complementary targets **T11**, **T13** and **T15** did form in PBS/BSA buffer, the negative control sample (Figure 2.4.1 (a)) also showed unexpected assembly between noncomplementary particles. In light of this, PBS/Tween was tested as an alternative buffer. The results shown in subsequent figures indicated minimal nonspecific adhesion between particles. All subsequent assembly studies, therefore, were prepared using PBS/Tween buffer.

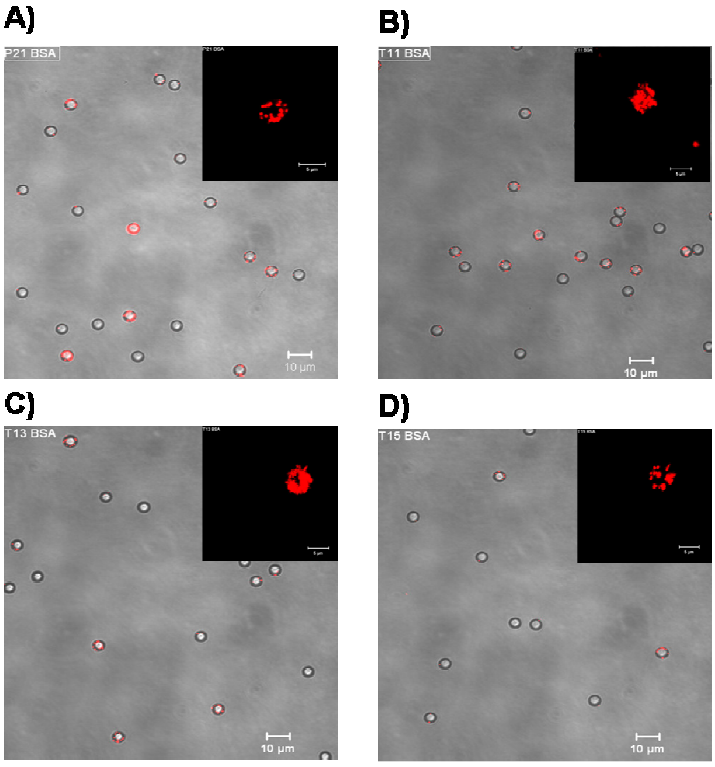

Figure 2.4.1. Assemblies prepared in PBS/BSA buffer with HODM as the template microsphere. The fluorescent particles were functionalized with a) **P21,** the same sequence as the probe strand on HODM, b) **T11,** c) **T13** and d) **T15**. The large field of view scale bar is 10 µm. The inset shows a 3D projection of a representative colloidal satellite with a scale bar of 5 µm.

We next incubated the HODM and complementary 1µm fluorescent particles together in order to form satellite assemblies. Figure 2.4.2 shows the results of assembly attempts at room temperature and 30 °C conditions with 1 µm fluorescent particles functionalized with perfectly matched target strands. In all cases there was negligible assembly formation. As shown in subsequent figures, repeating these assembly attempts with 200 nm fluorescent particles was more successful. As a result of these initial studies, the 200 nm fluorescent particles were selected for all other assembly studies.

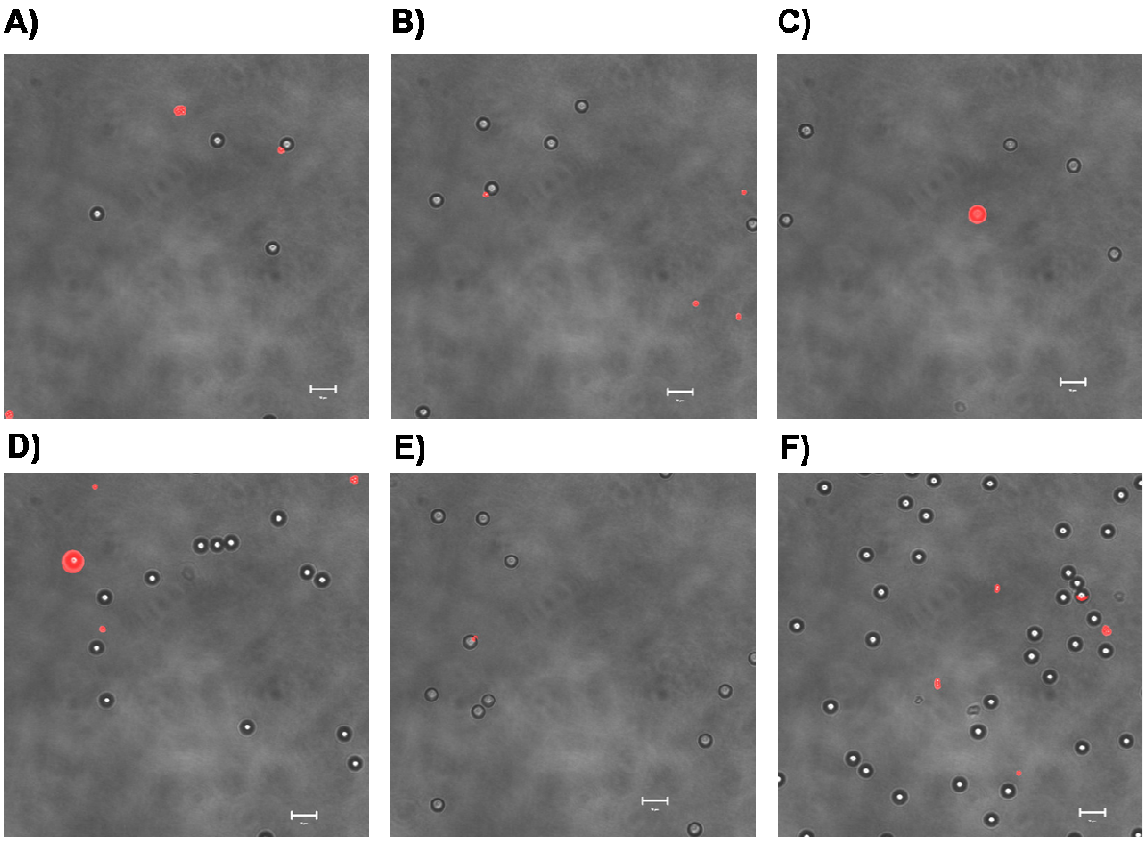

Figure 2.4.2. Assemblies made with HODM and 1 µm fluorescent particles in PBS/Tween buffer. Figures a – c were incubated at room temperature conditions while figures d – f were incubated at 30 °C. Fluorescent particles were functionalized with a) **T11**, b) **T13**, c) **T15**, d) **T11**, e) **T13**, or f) **T15** target strands.

2.4.2 Experimental Approach to Form and Image DNA-Linked Colloidal Satellites

Following initial assembly studies, a general protocol for assembly formation and imaging was established for all future assemblies. Following coupling the template microspheres and 200 nm fluorescent particles were diluted from a 1% w/v solids concentration to a 0.5% w/v solids concentration in PBS/Tween. Immediately prior to assembly, each separate particle population was sonicated for 20 – 30 seconds to break apart any agglomerates. 5 μL of template microspheres, 25 μL of fluorescent particles and 20 μL of PBS/Tween were mixed by brief vortexing. The suspension was incubated at room temperature for 48 h with end-over-end mixing unless otherwise noted. At the conclusion of the 48 h, a series of washing steps were performed to remove any excess, non-adherent fluorescent particles. These washing steps consisted of 10 gentle centrifugation steps at 3.0 x 1000 g for 1 minute. After each centrifugation step the assemblies were resuspended in 50 μL of PBS/Tween and gently vortexed at medium speeds. After the final wash, the remaining particles were resuspended in 100 μL of PBS/Tween.

Confocal microscopy was used to image the assemblies. A Zeiss 510 LSM (Germany) confocal microscope was used with a 63x oil objective. For each assembly sample, 20 μL of PBS/Tween was added to a 25 μL well formed by an adhesive spacer on the surface of a glass slide. To this well, an additional 5 μL of assembly suspension was added then covered flush by a square cover slip. One limitation of confocal microscopy is the narrow depth of field in the resulting image, which means that information may be lost above and below the focal plane. In an effort to compensate for this insets are included in which three-dimensional projections are made through one axis

of one or more representative colloidal satellites to include projected fluorescence from the entire assembly structure.

In order to ensure that the assemblies were being formed as a result of DNA hybridization events, a non-complementary control (**NC**) was included for both the HODM and the LODM systems. The fluorescent particles for this study were functionalized with the same sequence immobilized on the template microspheres, which should not result in complementary base pairing. The results of this assembly experiment are shown in Figure 2.4.3. For both template microspheres, only limited coverage of fluorescent particles is observed. The inset images for this control case included template microspheres with the maximum coverage observed. These results indicate that any nonspecific attractive interactions or imperfect base hybridizations of DNA strands are not appreciable. This result for the negative control is particularly clear if compared to Figures 2.4.4 and 2.4.5 in which complementary DNA sequences are immobilized to the template microsphere and fluorescent particles resulting in significant assembly formation.

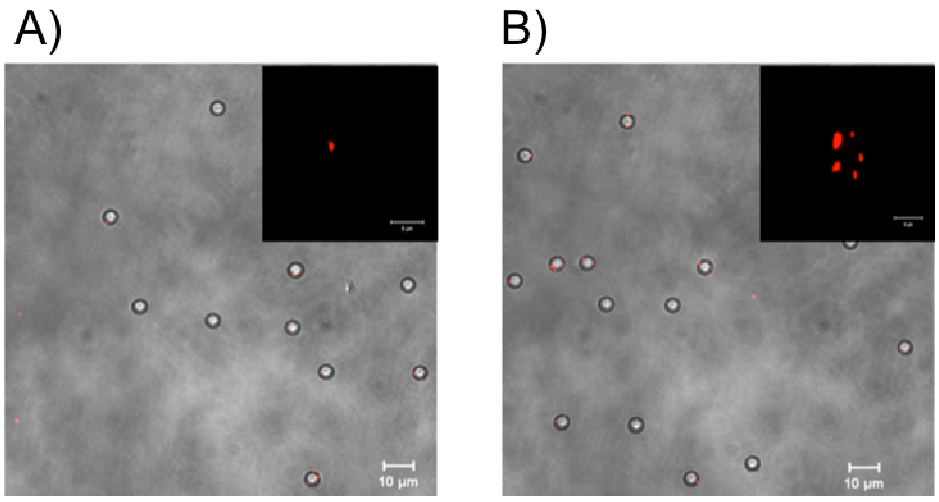

Figure 2.4.3. Assemblies with **NC** 200 nm red fluorescent particles incubated at room temperature using both a) HODM and b) LODM. Scale bar is 10 µm. Inset scale bar is 5 µm.

Figure 2.4.4 shows assemblies made with the HODM at room temperature. The **T11** and **T13** assemblies show the greatest extent of coverage by red fluorescent particles indicating the adhesion of the fluorescent particles is favorable. Unexpectedly, the **T15** assemblies resulted in relatively sparse fluorescent particle coverage compared to **T11** and **T13**. The **T11m** and **T13m** mismatched assemblies show generally less fluorescence coverage than their perfectly matched counterparts. For the **T15m** assemblies there again is noticeably poor fluorescence coverage. At first, these results appear inconsistent with the flow cytometry measurements in which the longer **T15** and **T15m** fluorescence targets resulted in the highest duplex densities (12, 923 and 6,392 duplexes per μm^2) for the perfectly matched and mismatched targets, respectively. If we assume that duplex densities taken from flow cytometry correlate to affinity of the probe-target duplex, then the lowest affinity duplexes correspond with **T11m** and **T13m** duplexes with respective duplex densities of 309 and 5.654 duplexes per μm^2. Yet, both of these targets

successfully formed assemblies with the HODM. Comparing **T11** and **T15m** duplexes which have similar duplex density values (6,303 duplexes per μm^2 for **T11** and 6,392 duplexes per μm^2 for **T15m**) and also similar number of predicted duplex linkages (5 and 7, respectively) shows that similar affinity in hybridization activity of soluble fluorescent targets does not necessarily translate to similar assembly behavior once targets are immobilized to particle surfaces. Looking at the sequences themselves, there are two noticeable differences: the presence of a mismatch in **T15m** and the fact that **T11** is four bases shorter than **T15m**. Neither of these factors appears to have an appreciable effect on the affinity of these targets as their duplex densities are very close in value for the soluble studies. However, the variation in length may contribute to the differences observed in assembly as the longer target would have to penetrate closer to the surface of the particle in order to completely hybridize. Comparing **T13** and **T15** targets shows the result in which hybridization of soluble targets resulted in similar duplex densities (11,816 versus 12, 923 duplexes per μm^2 respectively) and predicted duplex linkages in the contact area (11 versus 13 respectively). Figure 2.4.4 demonstrates the distinction between the two targets in terms of assembly formation with **T13** assemblies showing more fluorescent coverage on the HODM. For these two targets the only difference in sequence is the additional two bases in **T15**.

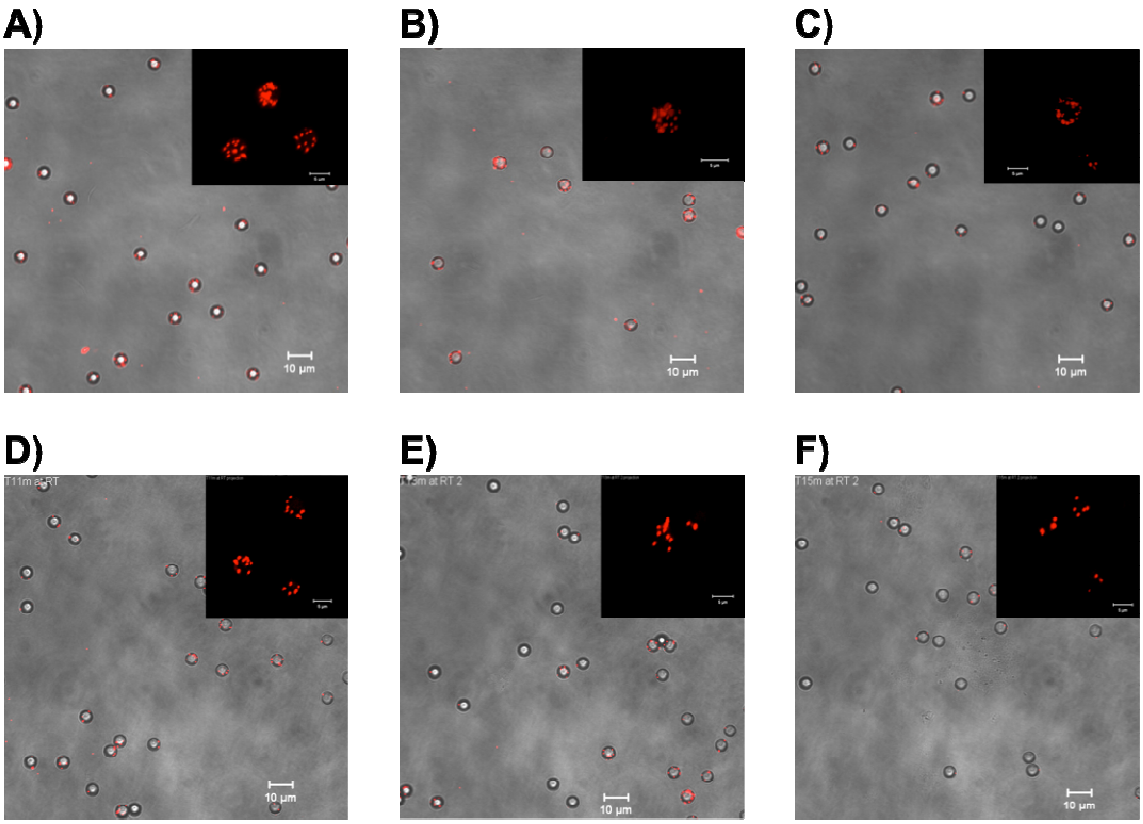

Figure 2.4.4. Assemblies of probe-functionalized HODM and 200 nm red fluorescent particles at room temperature with fluorescent particles functionalized with the targets a) **T11**, b) **T13**, c) **T15**, d) **T11m**, e) **T13m**, or f) **T15m**. Scale bar is 10 µm. Inset scale bar is 5 µm.

Previous studies have shown that hybridization of DNA strands on both planar[12] and particle[13] substrates with high densities of DNA probes have reduced hybridization efficiency between the immobilized probes and soluble targets. Since the length differences are a consistent explanation for the differences of assembly behavior observed in the current work, reducing the density of the DNA probes on the particle surface may facilitate hybridization with **T15** and **T15m** targets resulting in more extensive satellite formation. As shown in Table 2.3.2, the LODM have consistently lower duplex density values for all targets tested and have lower ssDNA probe coupling

density (see Appendix B) and thus serve to test the effects of oligonucleotide density on assembly formation.

Figure 2.4.5 shows the results of incubating the LODM with complementary fluorescent particles. All target cases resulted in an observable amount of fluorescence, including for the **T15** and **T15m** targets that were previously unsuccessful with the HODM. While duplex density values for **T15** and **T15m** targets are approximately one third of the values seen on the HODM (4,321 and 2,879 duplexes per μm^2 versus 12,923 and 6,392 duplexes per μm^2, respectively) the LODM showed significant coverage by fluorescent particles compared to their HODM counterparts. These results, in conjunction with the measured probe densities and duplex densities for LODM and HODM, support the conclusion that the higher probe density of the HODM is hindering assembly formation for the longest targets (**T15** and **T15m**) since these two targets must penetrate closer to the particle surface in order to form completely hybridized duplex bridges between particle surfaces.

Another contributing factor may also be the synthesis methods used by the suppliers of the template microspheres. The HODM, corresponding to the Invitrogen 5.1 μm CML particles, are characterized by the suppliers as having a "fluffy" surface due to the side chains used to generate COOH groups on the surface of the microsphere. The supplier does not describe the LODM, corresponding to the Bangs Laboratories 5.0 μm carboxylated particles, as having a similar topography. This difference between the LODM and HODM may result in a different steric or electrostatic impediment to assembly. However, differences in these nonspecific interactions would be expected to affect all the targets equally for a given template microsphere. The **T11**, **T11m**, **T13** and

T13m target cases allow DNA-mediated assemblies to form with both template microspheres. Subsequently, the surface density and length of the **T15** and **T15m** appear to be the determining factors in fluorescent particle coverage on the template microsphere. For DNA-linked colloidal satellites to form for these longest targets, the oligonucleotide density needed to be lower.

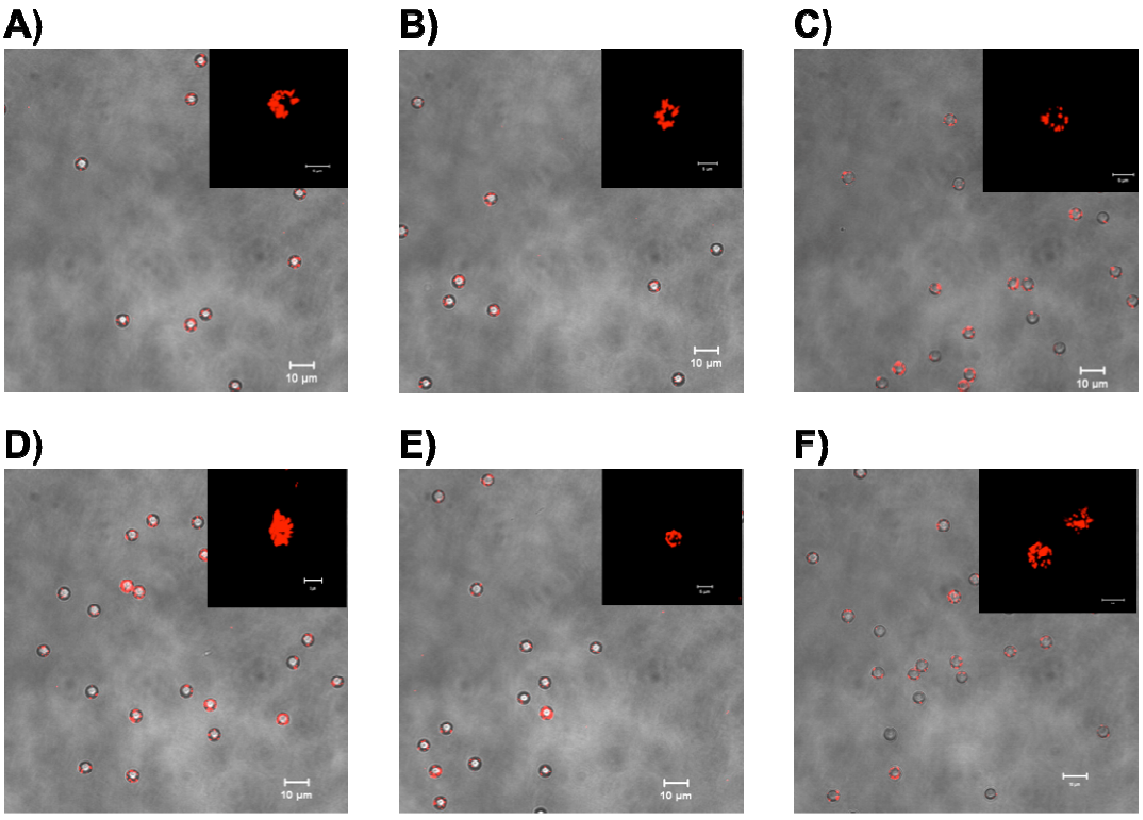

Figure 2.4.5. Assemblies of probe-functionalized LODM and 200 nm red fluorescent particles at room temperature with fluorescent particles functionalized with the targets a) **T11**, b) **T13**, c) **T15**, d) **T11m**, e) **T13m**, or f) **T15m**. Scale bar is 10 µm. Inset scale bar is 5 µm.

Given the success of the LODM in forming particle assemblies for all probe-target duplexes studied, another approach was attempted to generate low probe density template microspheres using the HODM. HODM were prepared with an altered coupling protocol in order to reduce the number of probe strands on the particle surface. Instead of coupling with a probe DNA concentration of 5 μM in the reaction solution, the DNA concentration was reduced to 0.5 μM while keeping the final volume the same. Quantitative hybridization studies of soluble, fluorescein-labeled **T15** with these modified-HODM were also performed using flow cytometry as described before. Duplex density values of soluble **T15** hybridization for modified-HODM was 3,940 duplexes per μm^2 compared to 12, 923 duplexes per μm^2 for standard HODM and 4,321 duplexes per μm^2 for LODM. The duplex density value reported for the hybridization with modified-HODM represents only one measurement, as this study was intended as a test case. Figure 2.4.6 shows a comparison of assemblies made with standard HODM, modified HODM (incubated with 0.5 μM probe DNA), and standard LODM. The results are not conclusive on the effect of reducing the conjugated probe density on the Invitrogen template particles, though the large field of view image for the LODM qualitatively appears to have a larger number of fluorescent satellites.

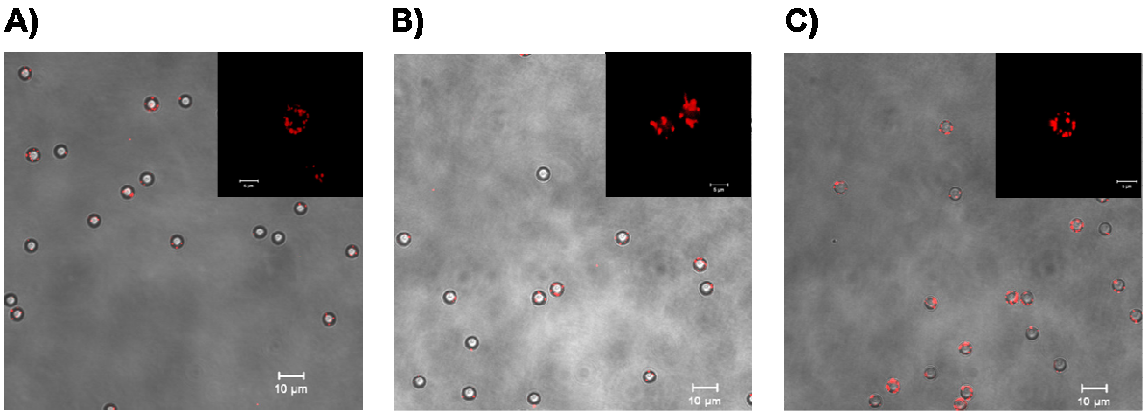

Figure 2.4.6. Assemblies with **T15** dsProbe duplexes and assembled at room temperature with a) HODM prepared with standard coupling protocol of 5 µM probe DNA, b) HODM prepared with only 0.5 µM probe DNA and c) LODM prepared with standard coupling protocol of 10 µM probe DNA.

2.4.3 Effect of Assembly Temperature on Satellite Formation.

In an effort to further investigate the causes of low fluorescent particle coverage by **T15** and **T15m** targets on HODM, a series of temperature studies were devised using 30 °C and 40 °C incubation conditions for both the perfectly matched and mismatched targets using both template microspheres. These studies were designed to investigate the possibility that **T15** and **T15m** targets could more readily form assemblies at elevated temperatures by minimizing any latent secondary structure in the probe strand or imperfect base pairing interactions at these elevated temperatures. The only change to the assembly protocol is that the 48 h incubation occurs in a hybridizing oven set to the indicated temperature with end-over-end mixing. Once this incubation time has concluded the suspensions are immediately washed as previously described. Figures 2.4.7 and 2.4.8 show the results of assembly formation at the given incubation temperatures for assemblies with HODM. Assemblies made with the perfectly matched

duplexes are shown in Figure 2.4.7 and with mismatched duplexes in Figure 2.4.8. Looking specifically at the **T15** assemblies, there is limited fluorescent particle coverage observed even when incubated at 30 °C and 40 °C. In contrast the **T11** and **T13** assemblies show good satellite formation at both these temperatures. For all perfectly matched targets, the predicted duplex melting temperatures are well above these incubation temperatures (Table 2.4.1). For the mismatches DNA targets, the effects of elevated incubation temperature conditions are more noticeable. Generally, the larger field of view images show fewer fluorescent satellites compared to the perfectly matched assemblies. Assemblies with the **T11m** target in particular result in fewer fluorescent assemblies within the larger field of view. While the inset image does show fluorescence coverage, it represents the highest fluorescence coverage observed from this sample and thus is not a truly representative colloidal satellite. The 40 °C assembly temperature also approaches the 43 °C predicted melting temperature for **T11m** duplexes and thus it is reasonable to expect **T11m** duplexes may be too weak to allow significant DNA-linked colloidal satellite formation. From these studies, it also does not appear that increased incubation temperature provides any noticeable advantage favoring assembly formation with the **T15** and **T15m** targets for either template microsphere system.

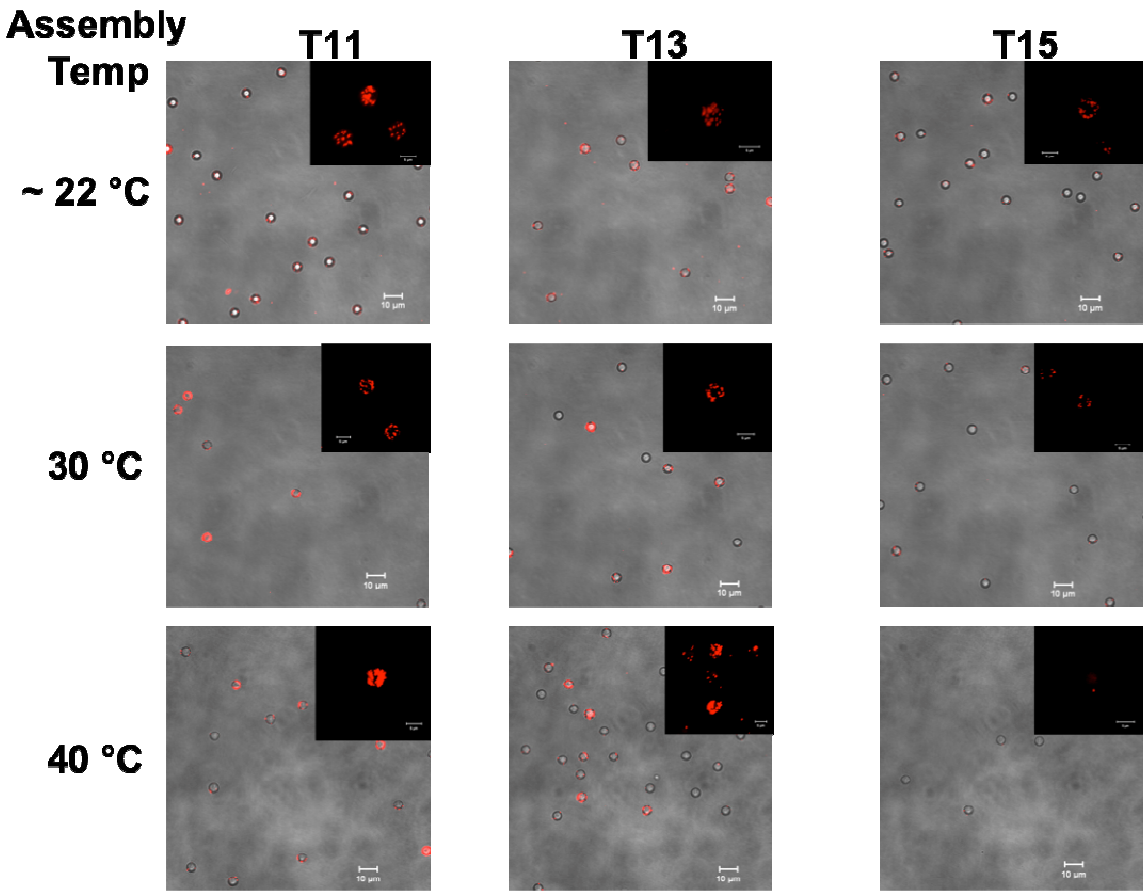

Figure 2.4.7. Assemblies of HODM and fluorescent particles for perfectly matched probe-target duplexes incubated at room temperature, 30 °C, or 40 °C conditions. Scale bar is 10 µm. Inset scale bar is 5 µm.

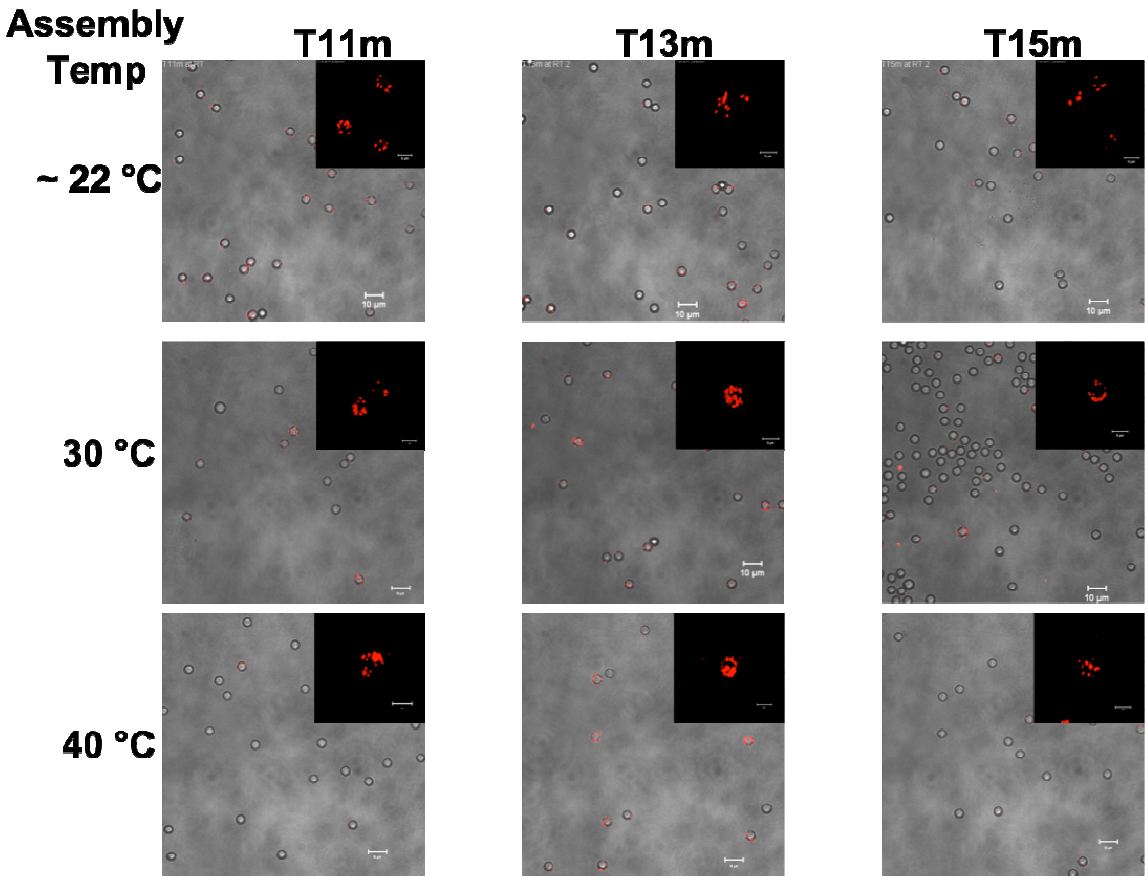

Figure 2.4.8. Assemblies of HODM and fluorescent particles for mismatched probe-target duplexes incubated at room temperature, 30 °C, or 40 °C conditions. Scale bar is 10 µm. Inset scale bar is 5 µm.

Assembly formation at elevated temperatures was also evaluated for the LODM system. Figures 2.4.9 and 2.4.10 summarize these results of perfectly matched and mismatched targets, respectively. All perfectly matched targets, including **T15**, were again able to form satellites at all temperatures in contrast to results for the HODM. The mismatched assemblies in Figure 2.4.10 also show generally good assembly formation for **T13m** and **T15m** at all temperatures examined. The one exception, however, is the **T11m** case which demonstrates decreasing assembly formation as the assembly temperature approached the 43 °C melting temperature of the **T11m** duplex. Since this temperature effect is observed in both template microsphere systems, the **T11m** duplex simply appears to be too unstable at 40 °C to allow satellite formation.

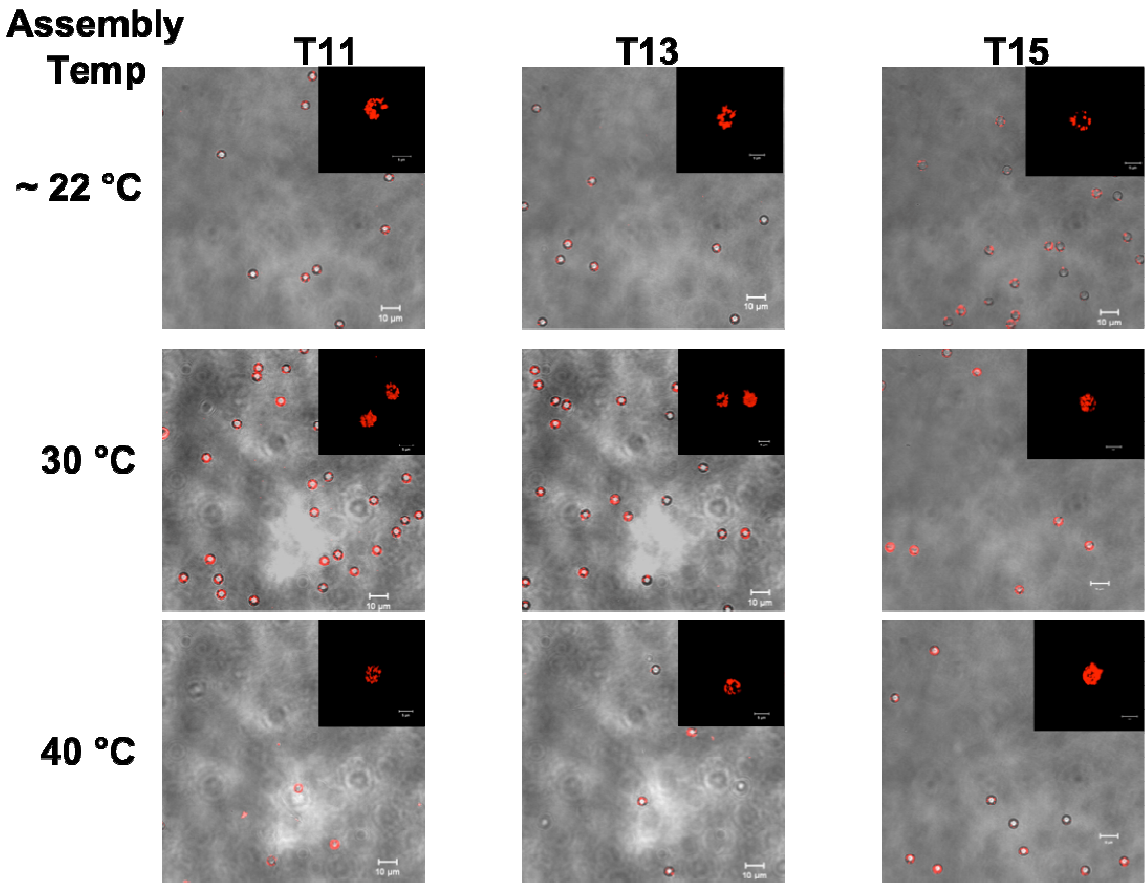

Figure 2.4.9. Assemblies of LODM and fluorescent particles for perfectly matched probe-target duplexes incubated at room temperature, 30 °C, or 40 °C conditions. Scale bar is 10 µm. Inset scale bar is 5 µm.

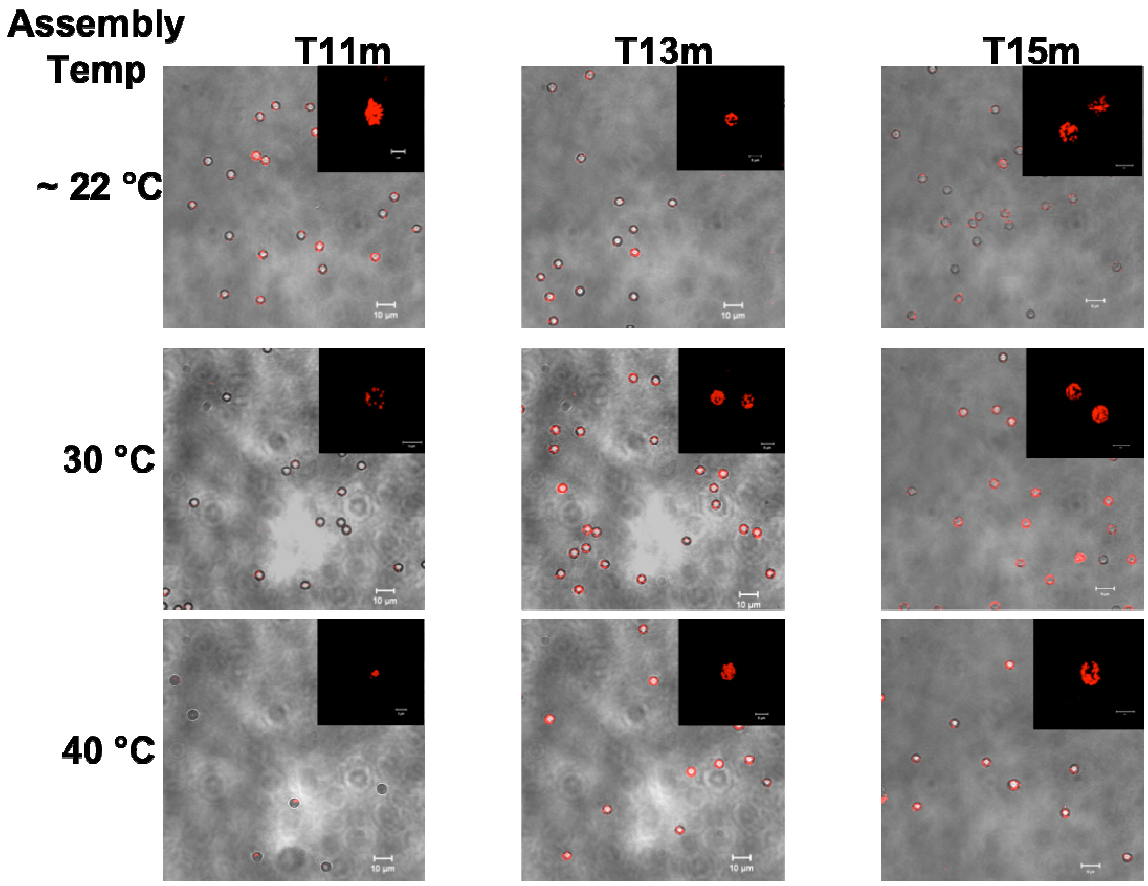

Figure 2.4.10. Assemblies of LODM and fluorescent particles for mismatched probe-target duplexes incubated at room temperature, 30 °C, or 40 °C conditions. Scale bar is 10 µm. Inset scale bar is 5 µm.

2.5 Conclusions

In summary, a 15 base DNA probe sequence patterned after the work of Dunbar et al.[14] and complementary to a genomic recognition sequence for *Salmonella* served as our design basis for DNA linkages within a fluorescent particle assembly. Incubation of soluble targets with varying degrees of affinity (based on length and presence of mismatches) for the immobilized probe strand was carried out with two different template microspheres. The Invitrogen 5.1 μm particles resulted in consistently higher duplex density values over the Bangs Laboratories 5 μm particles. Subsequently these template microspheres were renamed for convenient reference as HODM (for high oligonucleotide density microspheres) and LODM (for low oligonucleotide density microspheres). Assemblies of fluorescent satellite structures comprised of 200 nm fluorescent particles with either HODM or LODM were attempted for all targets studied at varying temperature conditions. Generally, satellite structures were observed for both the HODM and LODM though assembly with the HODM resulted in limited assembly for the longest targets, **T15** and **T15m**. Poor satellite formation on the HODM with the 15 base long targets is attributed to the added electrostatic repulsion due to higher oligonucleotide density on the surface of the HODM.

Finally, assemblies with the **T11m** target highlight an interesting comparison between the soluble target hybridization activity quantified by flow cytometry and the assembly studies in which the target is immobilized on the surface of fluorescent particles. While the calculated number of duplex linkages formed by **T11m** targets with probes in the contact area for both the HODM and LODM is less than one, Figures 2.4.4 and 2.4.5 show significant satellite formation for this weak affinity target, most

noticeably with the LODM. It is not the opinion of the author that one duplex is sufficient to result in stable assembly formation in the current experimental protocol. This discrepancy in hybridization activity points to differences in hybridization behavior for targets that are soluble in solution and for targets immobilized to fluorescent particles. In the soluble case, each dye-labeled target is allowed to interact relatively independently (if we ignore concentration gradient effects) of the other targets with the surface of the template microsphere. Thus, hybridization resulting in duplex formation with soluble targets is largely a function of affinity of the target for the probe. For those targets immobilized to the fluorescent particle surface, their interactions are not independent as multiple targets are proximal to the probe strands within the contact area. As the two particle surfaces approach one another during assembly, multiple hybridization events can occur between multiple probe-target pairs. The cooperative nature of this interaction may help to stabilize the formation of otherwise low affinity duplexes such as **T11m**. A similar effect has been reported in 3D aggregates of DNA-functionalized gold nanoparticles in which duplexes with a few as one Watson-Crick base pair were credited with aggregate formation due to the multivalent interaction within the aggregate[15]. Thus, low affinity duplexes can still result in DNA-linked colloidal satellites in part due to the multivalent nature of the hybridization events between immobilized target strands.

2.6 References

1. Tison, C.K. and V.T. Milam, *Reversing DNA-mediated Adhesion at a Fixed Temperature.* Langmuir, 2007. 23: p. 9728-9736.

2. Hermanson, G.T., *Bioconjugate Techniques*. 1996, San Diego: Academic Press, INC. 785.

3. Horan, P.K. and Leon L. Wheeless, Jr., *Quantitative Single Cell Analysis and Sorting.* Science, 1977. 198: p. 149 - 157.

4. Cram, L.S., *Flow cytometry, an overview.* Methods in Cell Science, 2002. 24: p. 1-9.

5. Fulton, R.J., et al., *Advanced multiplexed analysis with the FlowMetrix^{TM} system.* Clinical Chemistry, 1997. 43(9): p. 1749 - 1756.

6. Lu, J., et al., *MicroRNA expression profiles classify human cancers.* Nature, 2005. 435(9): p. 834-838.

7. Biancaniello, P.L., et al., *DNA-Mediated Phase Behavior of Microsphere Suspensions.* Langmuir, 2007. 23: p. 2688-2693.

8. Smith, S.B., Y. Cui, and C. Bustamante, *Overstretching B-DNA: The Elastic Response of Individual Double-Stranded and Single-Stranded DNA Molecules.* Science, 1996. 271: p. 795-799.

9. Markham, N.R. and M. Zuker, *MFold*. http://dinamelt.bioinfo.rpi.edu/. Accessed 9/16/2008.

10. Markham, N.R. and M. Zuker, *DINAMelt web server for nucleic acid melting prediction.* Nucleic Acids Research, 2005. 33: p. W577 - W581

11. Markham, N.R. and M. Zuker, *UNAFold: software for nucleic acid folding and hybriziation*, in *Bioinformatics, Volume II. Structure, Functions and Applications*, J.M. Keith, Editor. 2008, Humana Press: Totowa, NJ, p. 3 - 31.

12. Peterson, A.W., R.J. Heaton, and R.M. Georgiadis, *The effect of surface probe density on DNA hybridization.* Nucleic Acids Research, 2001. 29(24): p. 5163 - 5168.

13. Henry, M.R., et al., *Real-Time Measurements of DNA Hybridization on Microparticles with Fluorescence Resonance Energy Transfer.* Analytical Biochemistry, 1999. 276: p. 204 - 214.

14. Dunbar, S.A., et al., *Quantitative, multiplexed detection of bacterial pathogens: DNA and protein applications of the Luminex LabMAP^{TM} system.* Journal of Microbiological Methods, 2003. 53: p. 245-252.

15. Hurst, S.J., H.D. Hill, and C.A. Mirkin, *"Three-Dimensional Hybridization" with Polyvalent DNA-Gold Nanoparticle Conjugates.* Journal of the American Chemical Society, 2008. 130: p. 12192 - 12200.

CHAPTER 3

Disassembly of Satellites Using Competitive Hybridization Events[2]

3.1 Introduction

While the assembly and aggregation of particles based on specific binding or recognition events has been extensively considered, the redispersion of aggregates or disassembly of DNA-linked particles based on specific recognition events, such as DNA hybridization itself, has not received much attention. Lu's group has demonstrated DNAzyme-linked gold nanoparticle aggregates that redispersed due to cleavage of the DNA if Pb^{2+} associated with the "binding pocket" of the DNAzyme[1]. In this study, the rate of redispersion was enhanced with invasive DNA strands that function in a similar manner to competitive targets. In a separate example, Lim et al. used DNA strands not to aid redispersion or disassembly directly, but to impede gold nanoparticle aggregate formation after melting[2]. Here the competitive strands serve not to destabilize the DNA linkages but rather prevent their re-association after melting. Considering work with colloidal assemblies, our group has demonstrated DNA directed redispersion under room temperature conditions of DNA-linked aggregates[3]. The current work discusses disassembly of DNA-linked colloidal satellites under isothermal conditions using competitive DNA hybridization events. Having demonstrated the ability to assemble morphologically distinct satellite structures using DNA linkages, we next sought to selectively disassemble those satellites by promoting competitive displacement of the

[2] Results of this chapter are also discussed in
Baker, B. A. and V. T. Milam, "*DNA Density-Dependent Assembly Behavior of Colloidal Micelles*," Langmuir, in press.

original hybridization partner. The driving force for competitive displacement stems from affinity differences between the DNA linkages forming the assemblies and the competitive target. This affinity difference can be due to differences in sequence length and incorporation of center mismatches as previously discussed. In the following chapter, we describe the process of competitive hybridization with soluble DNA targets as well as the negative controls used to ensure disassembly was a product of competitive events. Examples of successful disassembly experiments are presented.

3.2 Experimental Methods

Satellite assemblies were prepared as described in Chapter 2. Following satellite formation, 10 μL of the assembly suspension was added to 10 μL of PBS/Tween for a final suspension volume of 20 μL. For the reference sample no further additions were made. For the negative and positive samples either 20 μL of Tris/EDTA buffer (pH 7.4) only or 20 μL of 10 μM DNA was added bringing the final volume to 40 μL and the final concentration of competitive DNA to 5 μM, which is consistent with prior concentrations used in flow cytometry studies. This concentration of competitive target is well in excess of the predicted concentration of duplexes forming DNA linkages of the satellite assemblies (see Appendix C). Suspensions were incubated at 37 °C with aliquots removed for imaging at 48 and 72 h. The progress of disassembly was imaged directly after samples were removed from the disassembly suspension using a Zeiss 510 LSM confocal microscope (Germany). For disassembly studies, 10 μL of disassembly suspension is loaded into the 25 μL adhesive wells followed by 15 μL of PBS/Tween. A cover slip is used to cap the well and pressed flush for good adhesion.

3.3 Results and Discussion

A schematic of the process of disassembly by competitive hybridization with a target DNA strands in solution is demonstrated in Figure 3.3.1. The driving force for competitive hybridization and subsequent disassembly is the affinity difference between the competitive target and the initial duplex partner generated by selecting sequences of varying lengths and incorporating center mismatches in the target strand immobilized on the fluorescent particle. The competitive strand selected for these studies was **T15**, a 15 base strand that is perfectly complementary to the probe strand immobilized on the template microsphere surface.

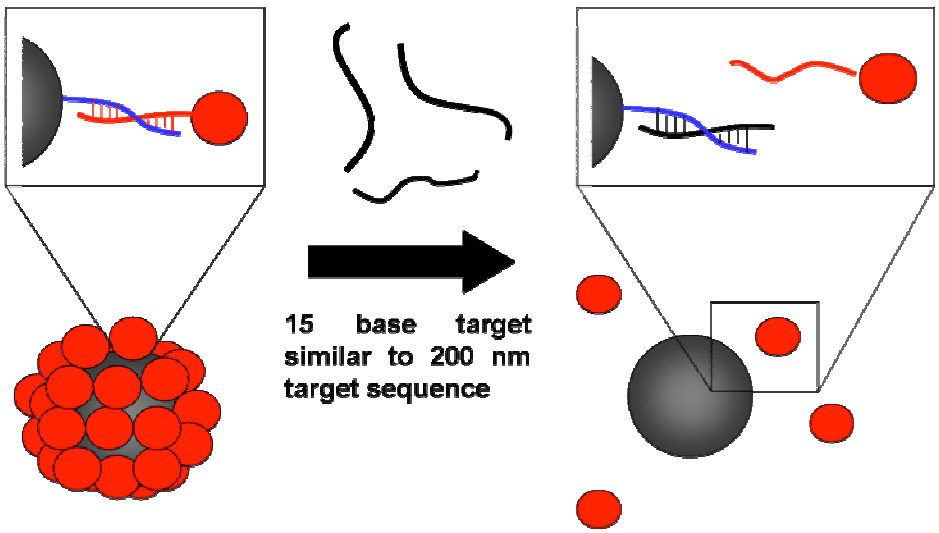

Figure 3.3.1. Schematic illustrating the process of disassembly via competitive hybridization. As the competitive target strand hybridizes to double-stranded probe, it displaces the primary target strand. This displacement event in turn releases the fluorescent particles and results in a visible change from fluorescent satellites to nonfluorescent template microspheres. For simplicity only one DNA linkage is shown.

Due to the consistent coverage of fluorescent particles observed in satellite assemblies (Chapter 2), low oligonucleotide density microspheres (LODM) were selected as the template microspheres for all disassembly studies. As part of these studies, a series of negative controls was devised to ensure that disassembly does not result from nonspecific interactions or instability of the colloidal satellites. The first control was a reference sample of the assemblies incubated in PBS/Tween at 37 °C with no other additions. The second control was the assemblies incubated in PBS/Tween plus Tris/EDTA (pH 7.4) in the same volume used with the competitive target sample. This control was selected to ensure that the addition of this buffer, used to handle and store the DNA, did not itself destabilize the satellite structures. The final control was the assemblies incubated in the presence of amine functionalized, 20-thymine DNA sequence referred to as **TH20**. This non-complementary control was selected to ensure that short strands of non-complementary DNA do not destabilize the assembly structure. Finally, the positive sample consisted of the assemblies incubated in the presence of soluble **T15** as these target strands are perfectly complementary to the probe strand on the template microsphere. In many of these attempts there was little disassembly observed. Figure 3.3.2 is an example, which illustrates no significant difference between the negative controls of the reference sample, the Tris/EDTA sample, the **TH20** sample and the positive **T15** sample. This result is included as an illustration of what is considered to be an unsuccessful disassembly attempt, meaning the presence of **T15** did not result in loss of fluorescent particle coverage on the template microsphere. Both the room temperature conditions as well as the shorter incubation time of 48 h may contribute to the lack of observable loss in fluorescent particle coverage in this case.

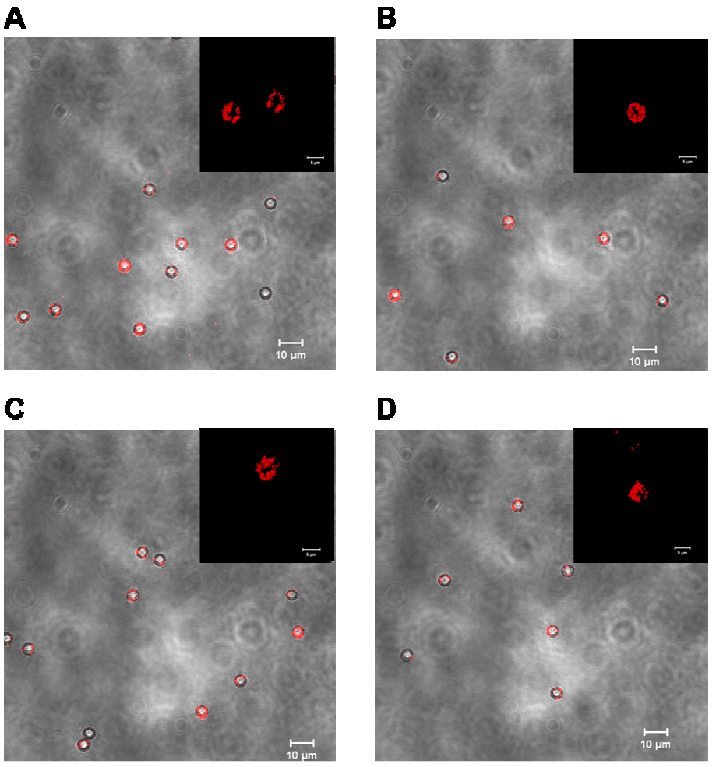

Figure 3.3.2. Disassembly attempt with **T11** assemblies formed at room temperature and incubated at room temperature for 48 h with a) PBS/Tween buffer, b) Tris/EDTA buffer, c) **TH20**, or d) **T15**. The scale bars in the large field of view image correspond to 10 µm. The inset scale bar corresponds to 5 µm.

From these initial disassembly attempts, several satellite assemblies were selected as good candidates to demonstrate the process of disassembly based on their stability with negative controls and responsiveness to the **T15** target strand. The satellites selected were all assembled at 30 °C incubation conditions and comprised duplex linkages of **T11**, **T13m** and **T15m**. With these satellites disassembly was performed at 37 °C and incubated up to 72 h in order to allow enough time for competitive hybridization to result in observable disassembly. While all disassembly attempts were imaged at both 48 h and 72 h using confocal microscopy, significant disassembly of samples incubated with **T15**

while maintaining stability of the negative controls was most consistently observed after 72 h.

Figure 3.3.3, the first of the successful disassembly results, shows the confocal images of observed disassembly of the **T11** satellites after 72 h of incubation. Good fluorescent particle coverage occurs for the reference sample, Tris/EDTA, and **TH20** samples as indicated by the larger images containing several fluorescent satellites within a given field of view in Figure 3.3.3 (a)-(c), respectively, indicating little if any disassembly occurs in these negative controls. In comparison, incubation with the **T15** target (Figure 3.3.3 (d)) results in nearly bare template microspheres with few if any red fluorescent particles remaining adherent. A more direct comparison can be made by comparing the inset image of Figure 3.3.3(a) with the inset image of Figure 3.3.3(d). In the former, a bright layer of fluorescence is evident on the surface of the template microsphere indicating that the satellites maintained stability throughout the incubation timeframe. Figure 3.3.3(d), on the other hand, shows only a few particles adhering to the surface of the template microsphere after incubation with **T15**. The contrast between the fluorescent coverage of the negative controls with the minimal fluorescence observed on microspheres for the sample incubated with **T15** indicates specific displacement must occur due to competitive hybridization events. In the soluble hybridization studies discussed in Chapter 2, **T11** targets resulted in a duplex density of approximately half that of **T15** (2,719 duplexes per μm^2 versus 4,321 duplexes per μm^2 for the LODM). Both the discrepancy in duplex density from the soluble studies and the observed stability of the **T11** negative control point to the higher affinity of **T15** as the driving force for disassembly events in this study.

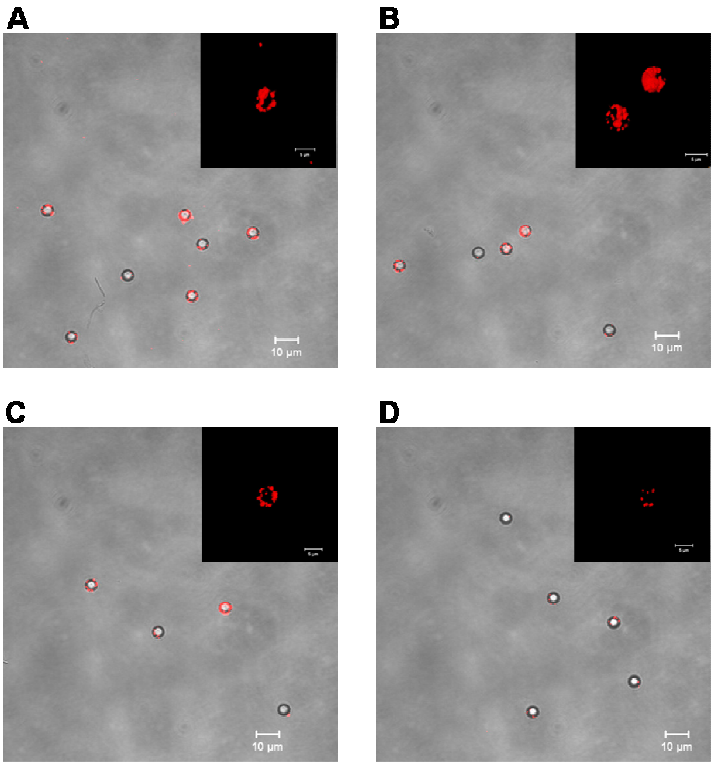

Figure 3.3.3. T11-linked assemblies formed at 30 °C and incubated at 37 °C for 72 h with a) PBS/Tween buffer, b) Tris/EDTA buffer, c) **TH20**, or d) **T15**. The scale bars in the large field of view image correspond to 10 µm. The inset scale bar corresponds to 5 µm.

Figure 3.3.4 show disassembly results for **T13m** satellites prepared at 30 °C and imaged after 72 h incubation. The negative control samples (Figure 3.3.4(a)-(c)) show fluorescent particle coverage after 72 h incubation while the satellites incubated in the presence of **T15** strands (Figure 3.3.4(d)) show almost complete disassembly. Again comparison between the reference inset image in Figure 3.3.4(a) with the inset of the positive **T15** sample in Figure 3.3.4(d) reveal a stark contrast in the level of fluorescence coverage between satellites incubated in the two conditions. The duplex density values obtained in the soluble hybridization studies suggest that **T13m** has an even lower affinity than **T11** (2,103 duplexes per μm^2 and 2,719 duplexes per μm^2, respectively). However, these assemblies maintain good stability when incubated with negative controls. Only the presence of **T15** results in an observable loss in fluorescent particle coverage. This optimization of a weakly stable, but responsive DNA duplex linkage is desirable for stimuli-responsive particle systems.

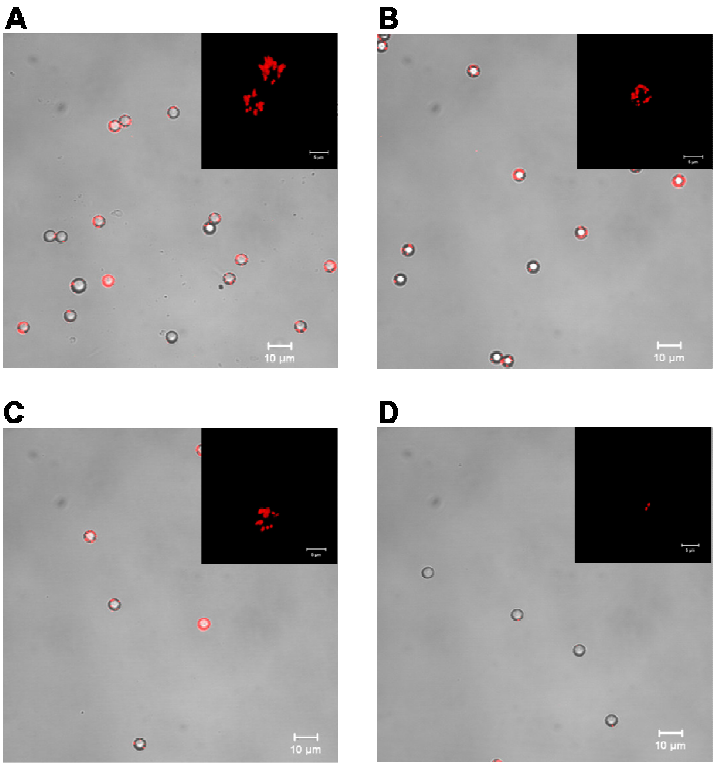

Figure 3.3.4. T13m-linked assemblies formed at 30 °C and incubated at 37 °C for 72 h with a) PBS/Tween buffer, b) Tris/EDTA buffer, c) **TH20**, or d) **T15**. The scale bars in the large field of view image correspond to 10 µm. The inset scale bar corresponds to 5 µm.

Finally, disassembly with the **T15m** satellites is shown in Figure 3.3.5. As in the other systems, the negative controls all show good fluorescence coverage at the conclusion of the 72 h study (Figure 3.4(a)-(c)). However, the satellites incubated with **T15** again show an observable loss in fluorescence over the time course of the study (Figure 3.4(d)). Recalling the duplex density values determined from the soluble hybridization studies (2,879 duplexes per μm^2), **T15m** is another moderate affinity probe-target pair. In this case, the presence of a center mismatch alone is enough to provide a sufficient affinity difference between the probe-target duplex and the competitive target, **T15**, resulting in the disassembly of the colloidal structures.

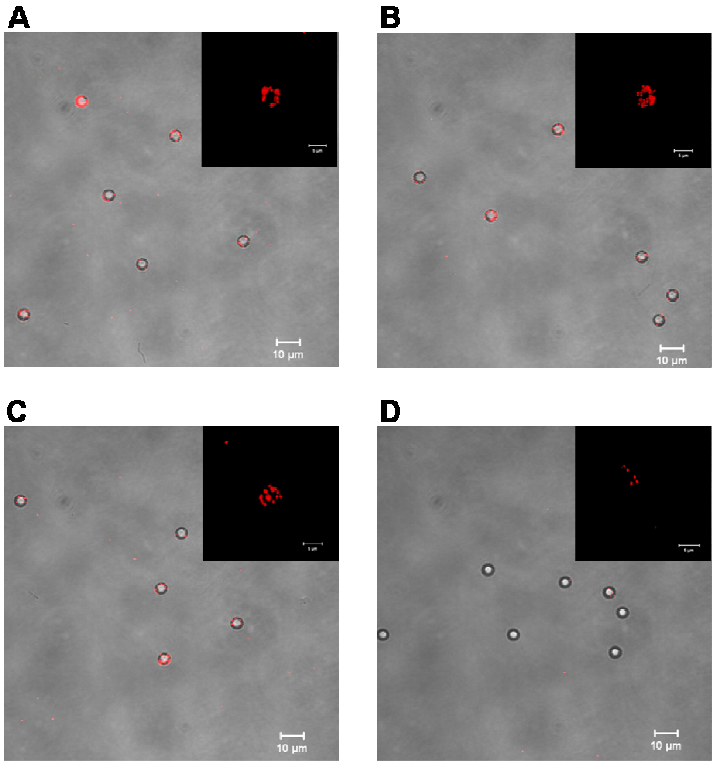

Figure 3.3.5. T15m-linked assemblies formed at 30 °C and incubated at 37 °C for 72 h with a) PBS/Tween buffer, b) Tris/EDTA buffer, c) **TH20**, or d) **T15**. The scale bars in the large field of view image correspond to 10 µm. The inset scale bar corresponds to 5 µm.

3.4 Conclusions

This chapter demonstrates the feasibility of competitive hybridization-based approaches to disassemble stimuli-responsive colloidal structures. As the DNA sequences used to design the duplex linkages were taken from a recognition sequence within the *Salmonella* genome, the application of competitive-based disassembly as a detection mechanism of nucleic acid targets is demonstrated as a proof of concept. However, the colloidal systems investigated here have key limitations that may affect their usefulness as detection platforms. One issue that has been present in both the assembly (Chapter 2) and disassembly studies (Chapter 3) has been the heterogeneous coverage of fluorescent particles. Within a given field of view, there are some template microspheres that are more completely covered with fluorescent particles than others. This observation is true for HODM and LODM in the assembly studies as well as the LODM in the disassembly studies. Due to the inconsistency in satellite formation, the current approach to disassembly is not considered a quantitative method. While the state of disassembly is a qualitative indicator of the presence of a competitive target, more sensitive methods are necessary to provide information on the concentration of a target or a quantitative characterization of specificity for a target of interest. Additionally, the above disassembly approach is based on *a priori* knowledge of the sequence of interest. Discrimination, however, between multiple targets has not been assessed in the current methodology.

Other stimuli-responsive particle platforms exist with the capacity to provide a discernable response to the presence of an analyte of interest in the visible light spectrum. Specifically, the plasmon resonance effect intrinsic to gold nanoparticles, which

facilitates a red to blue shift in suspensions transitioning from a disassembled to assembled state, is such an example. It is the opinion of the author that a colloidal particle assembly-disassembly approach to nucleic acid detection is not yet competitive with other techniques in terms of sensitivity and facile observation. However, colloidal particles allow much simpler handling and buffer exchange processes due to their larger size. As these disassembly studies focused on investigating the competitive interactions of the DNA strands as opposed to optimizing the particle characteristics (i.e. size, fluorescence, etc.), it was decided to focus the remainder of this project on examining the kinetics of these competitive hybridization events using single particles functionalized with double-stranded probes. The facile handling afforded by the colloidal particles previously used in this project is advantageous to this end. In the subsequent chapters, the kinetics of competitive hybridization is examined as a function of duplex sequence design as well as target specificity and context.

3.5 References

1. Liu, J. and Y. Lu, *Stimuli-Responsive Disassembly of Nanoparticle Aggregates for Light-Up Colorimetric Sensing.* Journal of the American Chemical Society, 2005. **127**: p. 12677 - 12683.

2. Lim, I.-I.S., et al., *Assembly--Disassembly of DNAs and Gold Nanoparticles: A Strategy of Intervention Based on Oligonucleotides and Restriction Enzymes.* Analytical Chemistry, 2008. **80**(15): p. 6038-6044.

3. Tison, C.K. and V.T. Milam, *Reversing DNA-mediated Adhesion at a Fixed Temperature.* Langmuir, 2007. **23**: p. 9728-9736.

CHAPTER 4

Competitive Hybridization of Double-Stranded DNA Probes with Varying Affinity

4.1 Introduction

In the following chapter, double-stranded DNA probes (dsProbes), having been fluorescently labeled and functionalized to a particle substrate, are studied in the context of competitive hybridization with a 15 base target sequence. This competitive target is presented as either a short 15 base single-stranded DNA molecule or an embedded 15 base sequence within a longer 100 base-long DNA strand. The dsProbes are designed with varying affinity based on duplex length and presence of mismatches within the original duplex. Successful competitive hybridization events involve displacing the original dye-labeled partner strand with the secondary, unlabeled target. Competitive hybridization is quantified by monitoring the time-dependent decrease in measured fluorescence intensity for a population of colloidal particles functionalized with the dsProbes and incubated with competitive targets. From this observed fluorescence change, the fraction of labeled initial hybridization partners displaced is measured and the kinetics are analyzed.

4.2 Experimental Methods

Materials. All DNA strand were purchased from Integrated DNA Technologies (IDT, Coralville, IA) and HPLC purified by the manufacturer. The immobilized probe strand was functionalized with an amine group at the 5´ end and a 12 carbon spacer to

separate the hybridizing segment from the particle surface. Primary targets were purchased functionalized with fluorescein via a modified, non-hybridizing thymine residue on the 5´ end. The non-complementary strand **NC-18** was purchased with a fluorescein modification attached at the 3´ end. The DNA was aliquoted in either 7.4 or 8.0 pH Tris/EDTA buffer (Fishers Scientific) at a concentration of 100 μM and stored at -20 °C. 5.1 μm carboxylate modified latexes were purchased from Invitrogen (Eugene, OR). *N*-Ethyl-*N'*-(3-dimethylaminopropyl) carbodiimide hydrochloride (EDAC) was purchased from Sigma-Aldrich (St. Louis, MO).

Primary and Secondary/Competitive Hybridization. The protocol for primary and secondary/competitive hybridization is schematically illustrated in Figure 4.2.1. To begin, 12 μL of coupled Invitrogen particles at 1% solids concentration were mixed with 188 μL of PBS/Tween. After centrifugation at 9.1 x 1000g for 2 minutes, the supernatant was removed and the particle pellet resuspended in 200 μL of PBS/Tween. 200 μL of fluorescently labeled primary target DNA at a concentration of 10 μM was added and the suspension briefly vortexed. The suspension, now at a total volume of 400 μL with a primary target concentration of 5 μM, was mixed via end-over-end mixing for 6 h at room temperature. Following incubation, the suspensions were centrifuged and resuspended to 400 μL three times. After the final centrifugation and resuspension, 20 μL of the suspension was removed as a reference sample to determine the initial duplex density of the labeled dsProbes. This 20 μL reference was diluted to a final volume of 100 μL and stored at 4-8 °C until sample preparation for flow cytometry. To begin secondary/competitive hybridization, 20 μL of unlabeled competitive target DNA at 100 μM was added and the suspension was briefly vortexed and mixed end-over-end. This

results in a total volume of the competitive hybridization suspension of 400 μL with a competitive target DNA concentration of 5 μM, as in prior studies. At specified time intervals of 0.25, 0.5, 0.75, 1, 6, 24, 48, and 72 h, 40 μL of the suspension was removed and diluted to a final volume of 100 μL in PBS/Tween. This time point sample was then centrifuged and resuspended three times in 100 μL of PBS/Tween. The samples were stored at 4-8 °C until prepared for flow cytometry.

Flow Cytometry. Primary hybridization reference samples and each competitive hybridization time point sample were prepared for analysis with flow cytometry by dilution with 900 μL of PBS/Tween, bringing the final volume of the sample to 1 mL. A FACS II flow cytometer from Becton Dickinson (Becton Dickinson, San Jose, CA) was used for all flow cytometry measurements. A sample of coupled particles never incubated with fluorescent targets was used as a negative control to account for autofluorescence of the microspheres. In order to obtain quantitative data, Quantum™ FITC MESF reference standards from Bangs Laboratories (Fishers, IN) were analyzed with each flow cytometry session and used to determine the average number of fluorescent DNA duplexes on the microsphere surface. Dividing this value by the known surface area of the microspheres yielded the average duplex density on the particle surface.

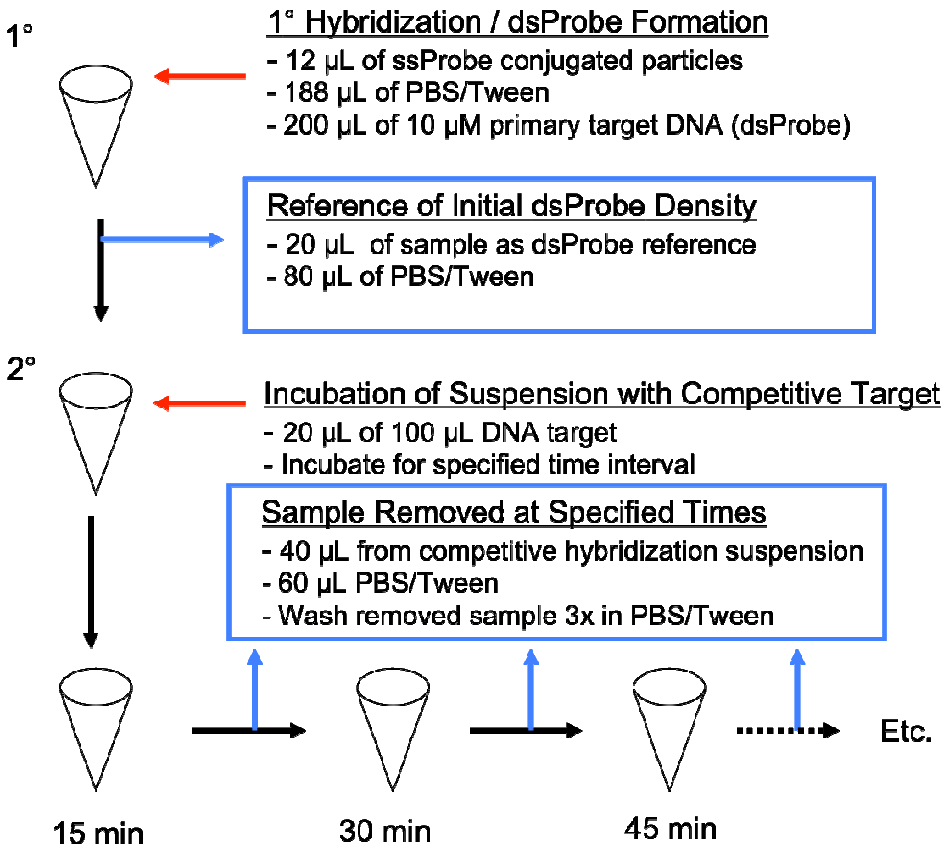

Figure 4.2.1. Schematic illustrating the batch protocol for preparing suspensions for time-dependent competitive hybridization studies. Addition of competitive targets and removal of aliquots or samples at specified time points is illustrated by arrows.

4.3 Background

Tuning the affinity of DNA duplexes by varying sequence length and incorporating mismatches has previously been discussed in the context of DNA mediated particle assembly (Chapter 2) and disassembly (Chapter 3). In this chapter we apply the same parameters of sequence design in a fluorescent assay approach. Using soluble, fluorescently labeled hybridization partners complementary to the immobilized probe strands, we have prepared double-stranded DNA probes (dsProbes) for studying the kinetics of competitive hybridization of targets patterned after a recognition sequence within the *Salmonella* genome. Dunbar et al. have previously incorporated this recognition motif in their experimental system by utilizing single-stranded DNA probes (ssProbes) immobilized to a particle surface[1]**.** A limitation of using single-stranded probes is that a separate labeling step of all candidate targets must occur for the detection event to be reported. This labeling step often involves some form of chemical modification of the target itself. In some assays, a second step following target capture is necessary in order to label the hybridized target via chemical modification. An example of this methodology involves labeling the target sequence with biotin during PCR then incubating with streptavidin-Phycoerythrin in order to report detection[93, 104, 132]. In a fluorescently labeled dsProbe approach, however, a detection event corresponds directly with capture as loss of fluorescence, which can be quantified for our colloidal substrates using such techniques as flow cytometry. Figure 4.3.1 illustrates the differences between the ssProbe and dsProbe assay approach.

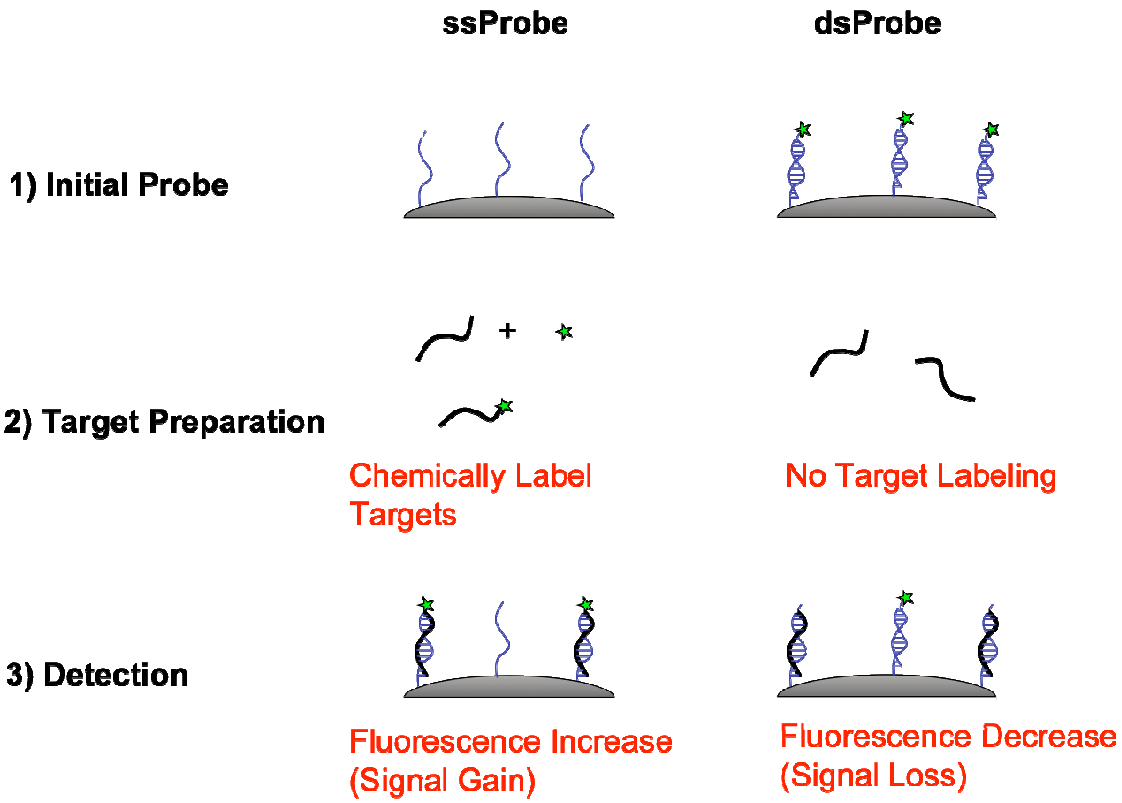

Figure 4.3.1. Schematic illustrating key differences between ssProbe and dsProbe assays for detecting the presence of targets of interest.

Additionally for single-stranded probe systems, in order to promote hybridization between the probe and perfectly-matched, soluble targets of interest, it is common for elevated temperatures to be used to select the matched target sequences and exclude or at least limit hybridization of mismatched targets[2]. As an alternative to elevated hybridization temperatures, longer incubation times at lower temperatures have also been used[5,6]. This approach requires environmental control of the assay conditions, which is not always available in point of use applications. The dsProbe approach offers an alternative to promoting specific hybridization that does not necessitate temperature control. In order for the original partner strand in the dsProbe to be displaced by the

target of interest, there must be a sufficient or higher affinity of the target for the probe to drive competition forward at room temperature. Thus, target sequences that are fully complementary to the immobilized probe strand are more likely to be successful at displacing the labeled strand than their mismatched counterparts. By tuning the affinity of the dsProbe this reaction can be made more or less responsive to the presence of target strands and thus more or less stringent in sensitivity based on the intrinsic probe design. The following chapter is a study of the kinetics of competitive hybridization in which the timing and extent of responsiveness varies based on sequence design of both the dsProbe and the competitive targets.

4.4 Results and Discussion

4.4.1 Incubation of dsProbes with Short Target

In order to assess the kinetics of competitive hybridization, several possible dsProbes were tested of varying sequence length with or without a center mismatch. For the first series of competitive hybridization studies, the competitive target was a 15 base strand perfectly complementary to the chemically immobilized probe strand on the microsphere surface. Table 4.4.1 shows the dsProbe sequences and the labeling scheme used throughout the dsProbe studies. Also in Table 4.4.1 are the measured initial duplex densities of each dsProbe on the microsphere surface prior to addition of the competitive target.

Table 4.4.1. List of dsProbe sequences and labeling scheme. The duplex density values represent the average of three separate flow cytometry measurements and correspond to the initial duplex density prior to incubation with competitive targets. The red bases correspond to a mismatch in the original hybridization partner of the probe strand. The green thymine base corresponds to the modification used by the supplier to incorporate the fluorescein into the DNA strand and is not intended to participate in hybridization.

dsProbe	Sequence	Average Duplex Density (oligos / μm^2)
P21:T11	5'– Amine (12 carbon) CTC GTC ACA CTA TCA – 3' 3'–AG TGT GAT AGT (T Fluor) – 5'	6,558
P21:T13	5' – Amine (12 carbon) CTC GTC ACA CTA TCA – 3' 3'– G CAG TGT GAT AGT (T Fluor) – 5'	12,294
P21:T15	5' – Amine (12 carbon) CTC GTC ACA CTA TCA – 3' 3'– GAG CAG TGT GAT AGT (T Fluor) – 5'	13,446
P21:T11m	5'– Amine (12 carbon) CTC GTC ACA CTA TCA – 3' 3'--AG TGT CAT AGT (T Fluor) – 5'	321
P21:T13m	5' – Amine (12 carbon) CTC GTC ACA CTA TCA – 3' 3'– G CAG TGA GAT AGT (T Fluor) – 5'	5,883
P21:T15m	5' – Amine (12 carbon) CTC GTC ACA CTA TCA – 3' 3'– GAG CAG TCT GAT AGT (T Fluor) – 5'	6,651

The variation in duplex density values for the different sequences provides an indication of the affinity difference of the dsProbes. Generally, longer dsProbes have higher duplex densities than their shorter counterparts. Also, compared to the perfectly-matched analogs, the presence of a center mismatch significantly decreases the measured duplex density. For example, the **P21:T13** dsProbe duplex density went from 12,294 to 5,883 duplexes per μm^2 with the addition of the center mismatch (**P21:T13m**). Based on these initial duplex density values, we hypothesized that competitive displacement would be faster for mismatched duplexes compared to their perfectly matched counterparts.

Similarly, we also expected the shorter duplexes to undergo competitive hybridization events more readily than their longer counterparts.

The short **T15** strand was chosen as a model competitive target for the first competition study. The results of this study are shown in Figure 4.4.1 as duplex density versus incubation time with **T15** competitive targets for all the dsProbes tested. Each data point represents the average of three separate sample runs with the error bars corresponding to the standard deviation. The non-complementary hybridization partner **NC-18** (18 consecutive thymine bases) was used as a negative control in this study to examine whether or not nonspecific adherence of the fluorescent primary targets occurred on the microsphere surface or to the probes themselves. The values for the **NC-18** duplex density were less than 10 duplexes per particle, a value significantly less than all other dsProbes with intended complementary base pairing. This result indicates negligible nonspecific association of the fluorescently labeled strands occurs with the microsphere surface or with the immobilized probes and thus the remaining dsProbes are formed as a result of complementary base pairing between the immobilized strands and the dye-labeled hybridization partner.

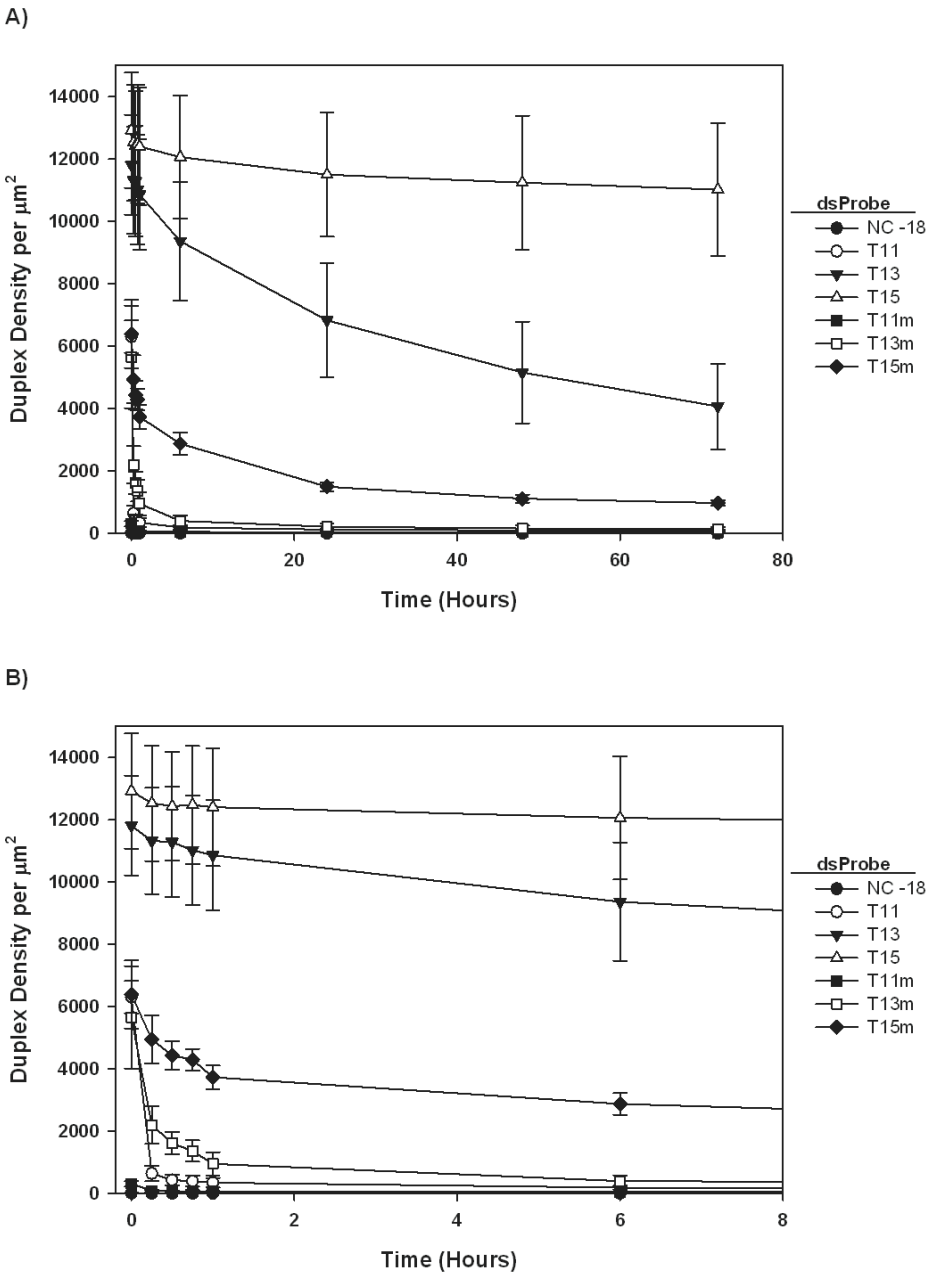

Figure 4.4.1. Duplex density of dsProbes (original hybridization partner listed) as a function of incubation time with the short competitive target **T15** following A) 72 h of incubation with an expanded view of B) the first 6 h of incubation.

In general, there was a decrease in duplex density as a function of incubation time with the **T15** competitive target for all dsProbe systems listed in Table 4.4.1. A significant amount of release occurs for all dsProbes within the first 6 h as shown in Figure 4.4.1 (b). Based on the initial duplex density values, it seems reasonable to conclude that **P21:T11**, **P21:T11m**, and **P21:T13m** are the weakest dsProbes. The initial duplex densities for these probes are 6,303; 309; and 5654 duplexes per μm^2, respectively. After the first hour of incubation with **T15** the duplex densities drop to 347, 71, and 948 duplexes per μm^2. This decrease in duplex density may be indicative of both competitive hybridization as well as dissociation due to the low stability of the dsProbes themselves. Release as a function of competitive hybridization versus dissociation is considered in more detail in subsequent sections. The longer dsProbes, **P21:T13**, **P21:T15** and **P21:T15m**, had initial duplex densities of 11,816; 12,923; and 6,392 duplexes per μm^2, respectively. After one hour these duplex density values had decreased modestly to 10,861; 12,405, and 3,729 demonstrating the greater stability of these dsProbes. Even after 72 h of incubation with **T15** targets, the **P21:T13** and **P21:T15** do not approach a plateau in duplex density values and thus do not reach equilibrium. In order to facilitate comparisons between the release kinetics of various dsProbes, the duplex densities of selected dsProbes were converted to fraction of initial dsProbe density released at a given time point. The zero point, which corresponds to the duplex density after primary hybridization, was used as the reference sample by which all subsequent time points were normalized. The results of this conversion from duplex density to fraction released are seen in Figure 4.4.2 (a) and (b) for the selected dsProbes. In this context, “release” refers to loss of the initial hybridization partner of the dsProbe

due to both thermal dissociation and competitive hybridization whereas "displacement" refers to loss of the initial hybridization partner due to competitive hybridization alone, after being normalized to exclude the contributions of thermal dissociation. The methods for determining displacement are detailed in Section 4.4.2.

Figure 4.4.2 shows the fraction of dsProbe released as a function of incubation time for **P21:T11**, **P21:T13**, **P21:T15**, and **P21:T15m** dsProbes. The selected dsProbes shown represent a range of kinetic responses including fast (**P21:T11**), moderate (**P21:T15m**), slow (**P21:T13**) and limited (**P21:T15**) release kinetics determined by their sequence design. The **P21:T15** dsProbe shows only minimal release over the time course of the experiment with a maximum of 15% released at 72 h. As the labeled strand in the **P21:T15** dsProbe is the same sequence as the competitive target, there is no driving force based on sequence affinity differences to induce displacement resulting in the minimal activity observed. This example illustrates the importance of designing a stable dsProbe that is still responsive to a target of interest. Due to its limited release, the **P21:T15** dsProbe is not studied in subsequent experiments. As a result of their range in kinetics responses, three dsProbes were selected for more detailed study, **P21:T11**, **P21:T13** and **P21:T15m**. The question next posed is how the release kinetics are altered if the competitive target is no longer presented as a short sequence, but rather as an embedded target or recognition sequence within the context of a longer DNA strand.

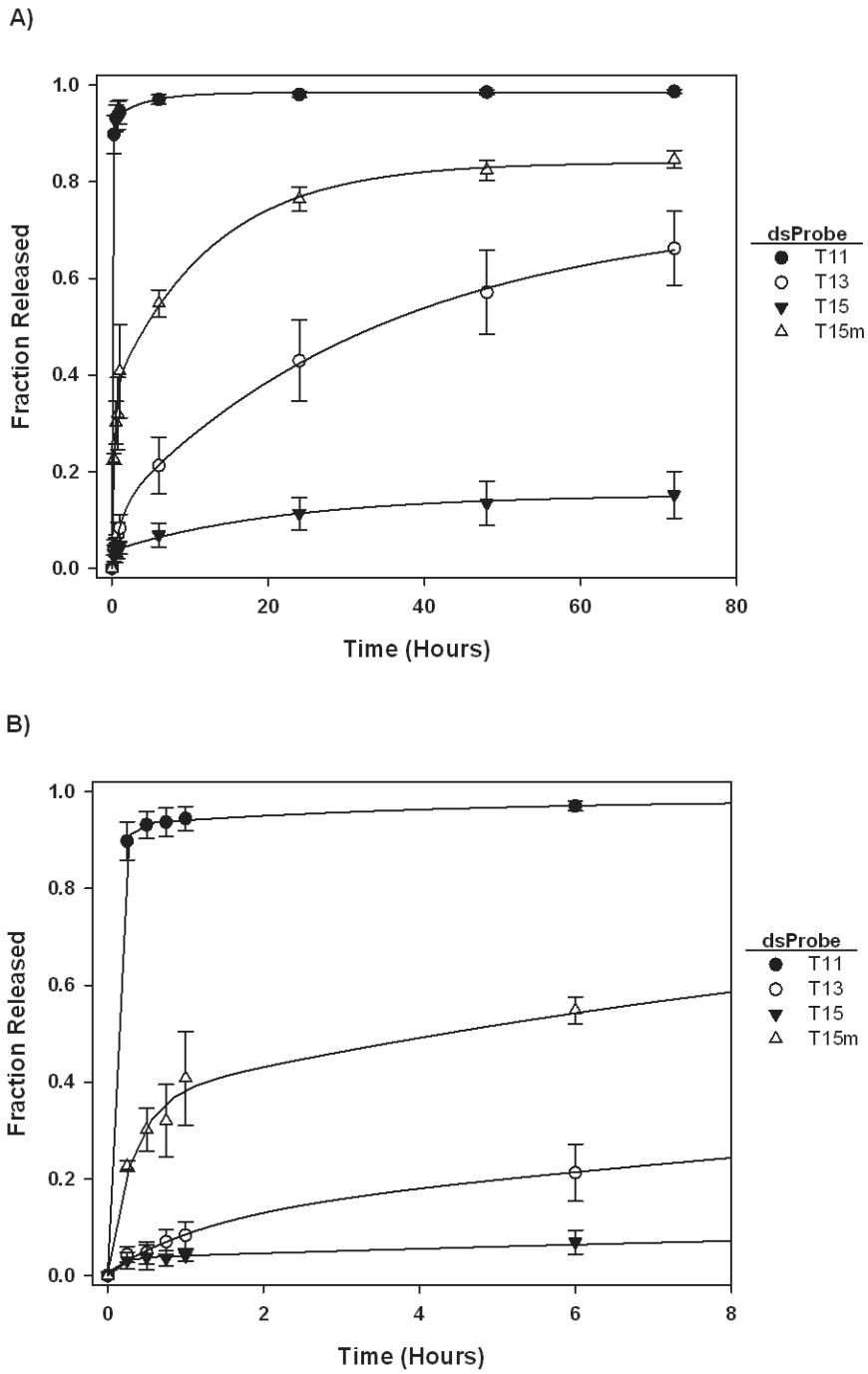

Figure 4.4.2. Fraction released as a function of incubation time with **T15** competitive targets for **P21:T11**, **P21:T13**, **P21:T15** and **P21:T15m** dsProbes following A) 72 h of incubation with an expanded view of B) the first 6 h of incubation.

4.4.2 Incubation of dsProbes with Embedded Targets

As most nucleic acids *in vivo* exist as sequences measure in hundreds to thousand of kilobases, examining the kinetics of competitive hybridization for a target of interest embedded within a long DNA strand is a meaningful extension of our previous studies. An experimental series was designed to characterize the kinetics of competitive displacement of the dsProbes by a 15 base recognition sequence embedded within a 100 base model DNA target strand. The 15 base recognition sequence is the same sequence that has been previously characterized. The remaining 85 bases in the target were selected as thymine bases not intended to participate in hybridization. The variable of interest in this study was the location of the recognition sequence, embedded at either the 3' end, the 5' end, or within the middle of the target, relative to the 3' to 5' backbone orientation of DNA. These target sequences along with a 100 base thymine non-complementary control are shown in Table 4.4.2.

Table 4.4.2. List of sequences of the embedded competitive targets in which the 15 base-long complementary segment is placed at various locations within the 100 base-long competitive target. The bases highlighted in blue correspond to the 15 base recognition sequence complementary to the chemically immobilized strand of the dsProbe. The **T15** competitive target (short target) is also listed as a reference.

Target Name	Sequence
T15	5' – TGA TAG TGT GAC GAG – 3'
NC	5' – (TTT TTT TTT TTT TTT TTT TT)$_5$ – 3'
3' End	5' – T (TTT TTT)$_{14}$ TGA TAG TGT GAC GAG – 3'
5' End	5' – TGA TAG TGT GAC GAG (TTT TTT)$_{14}$ T – 3'
Middle	5' – (TTT TTT)$_7$ TGA TAG TGT GAC GAG (TTT TTT)$_7$ T – 3'

Due to the anti-parallel orientation of two complementary strands in a DNA duplex, an observable difference in the kinetics of competitive displacement was expected for the three embedded targets listed in Table 4.4.2 based on their orientation with the chemically immobilized strand of the dsProbe. Figure 4.4.3 illustrates the differences in orientation of the competitive target after hybridization with the immobilized strand relative to the microsphere surface. The **3' End** target is expected to be the most effective competitor as its orientation with the microsphere surface after hybridization allows for the unhybridized bases to extend away into solution without approaching the microsphere surface. The **5' End**, however, may need to bend at least once in order for the unhybridized bases of the target strand to extend out into the solution after hybridization by the recognition segment. Thus, the **5' End** is expected to be a poor competitor and generate minimal displacement of the original hybridization partner in the dsProbes. Finally, the **Middle** target was expected to result in less competitive displacement that the **3' End** target though its comparison with the **5' End** target was uncertain. While one half of the **Middle** target might have to bend similarly to the **5' End** at the microsphere surface, this unhybridized region would be half as long as the **5´ End**. The other half of the **Middle** target was expected to resemble the **3' End** target as its orientation to the microsphere surface would allow for unhindered extension into the solution.

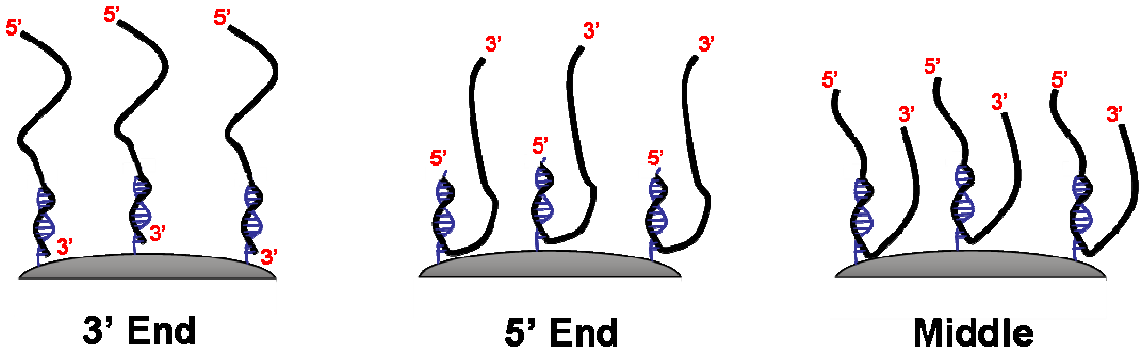

Figure 4.4.3. Schematic illustrating possible orientations of the embedded competitive targets relative to the microsphere surface represented following successful competitive hybridization events. Shown are the **3' End**, **5' End**, and **Middle** long competitive targets with the recognition sequence embedded at different locations to form the duplexes shown.

Figure 4.4.4 shows the fraction of dsProbe released after incubation of the **P21:T11** dsProbe with the embedded targets. For these studies, the incubation time is reported in seconds in order to facilitate direct comparisons with results from the literature. The total time as well as the time intervals studied remained consistent with our previous experiments. In addition to the **NC** target of 100 thymine bases, a sample in which no competitive target was present (**Dissociation**) was also included as a negative control. These two separate controls were used to assess (1) the effect of adding non-complementary DNA target strands as well as (2) the thermal stability of the dsProbes throughout the experimental timeframe of the competition studies. Both the **NC** and **Dissociation** controls showed similar release of the original hybridization partner of the dsProbe, indicating DNA release occurs by the thermal dissociative pathway. The fraction released for these negative controls was significant (~45%) and points to the comparatively weak stability of the **P21:T11** dsProbe. However, in the presence of the competitive target the total fraction of released DNA is even greater than in the two

control experiments. This significant difference in the extent of release points to competitive hybridization events by the embedded targets.

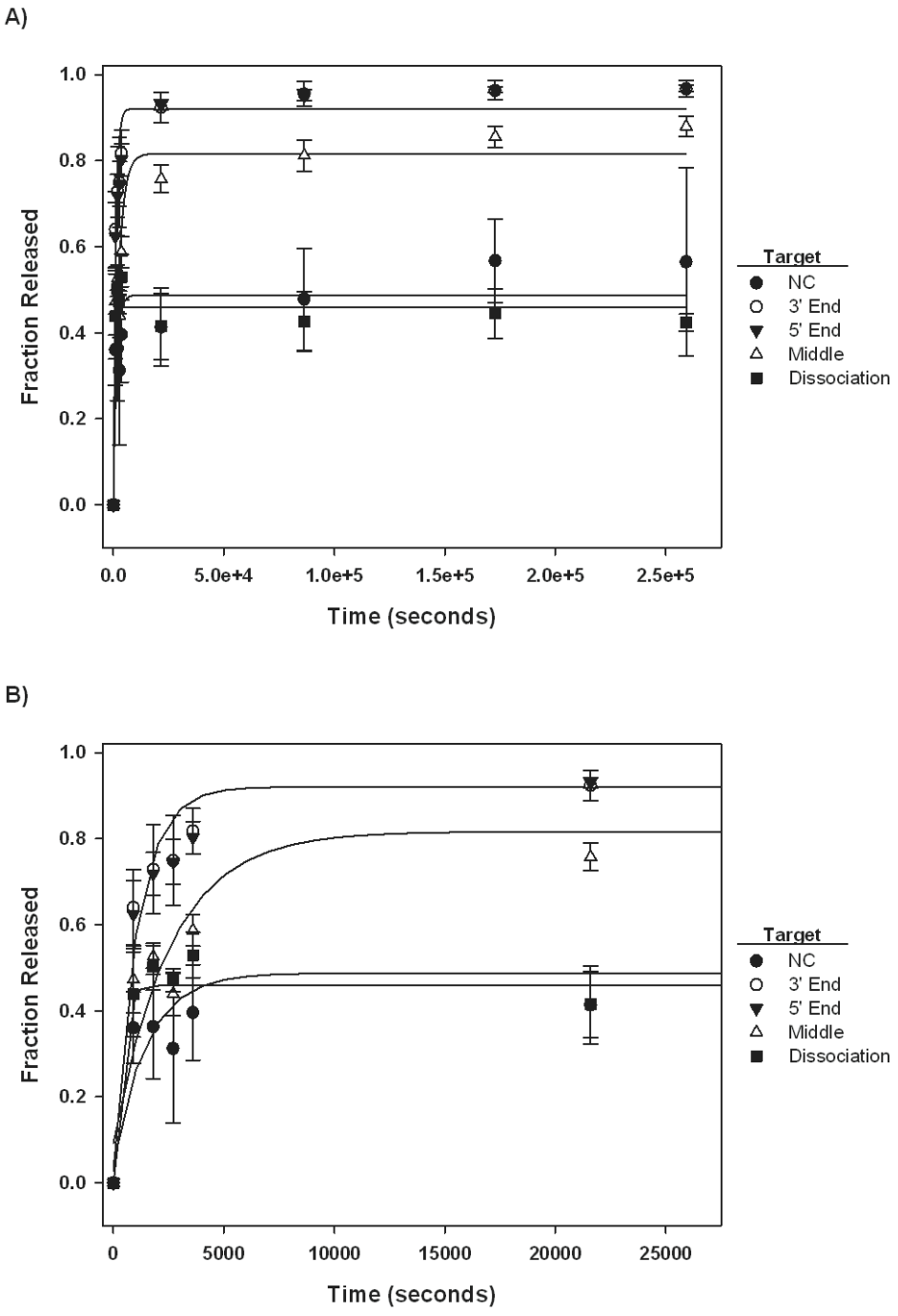

Figure 4.4.4. Fraction released of **T11** from dsProbe as a function of incubation time with **NC**, **3' End**, **5' End**, and **Middle** targets for A) 72 h (259,200 s) with a expanded view of B) the first 6 h (21,600 s). The **Dissociation** sample is included as a dsProbe control in the absence of a competitive target. **NC** is a noncomplementary target and thus represents a second control.

As expected the **3' End** target was an effective competitor resulting in the release of 90% of the **T11** dsProbe at the 6 h point (21,600 s). The kinetics of displacement were, however, slower than that of the short **T15** target in which 90% release was achieved in only ~15 minutes (Figure 4.4.2). What is surprising is how similar the release profiles are for the **5' End** and the **3' End** targets. This similarity in behavior indicates no significant preference for the orientation of the embedded target sequence for either end of the strand. The unhybridized bases of the **5' End** target are either able to orient themselves sufficiently away from the microsphere surface so as not to hinder competitive hybridization, or this orientation is unnecessary. In any case, a distinction cannot be made between the two targets. The final embedded target labeled **Middle** did show a difference in both the timing of release as well as in the total fraction released when compared to the two other embedded targets with the recognition segment at either end locations. The final fraction released is 88% for the **Middle** target versus 97% for the **3' End** and **5' End**. These results suggest that the two segments of unhybridized bases (**Middle**) pose a greater hindrance to hybridization than one longer section of unhybridized bases (**5' End** or **3´ End**).

In order to more directly assess DNA release arising from competitive displacement (as opposed to dissociation), the results presented in Figure 4.4.4 were normalized by subtracting the fraction released observed with the **Dissociation** sample from the fraction released observed from incubation with the complementary embedded targets. The results of this normalization are presented in Figure 4.4.5. At short times (less than 1 h), the **NC** sample shows negative values for the normalized fraction released. These negative values are attributed to minor differences in the fraction

released for the **Dissociation** sample and **NC** sample occurring at early times. Overall, however, the overall normalized data indicates that competitive displacement for the **NC** sample is minimal, ~ 14% displacement by the end of the experiment. The **3´ End**, **5´ End**, and **Middle** targets show similar displacement trends as described previously with good agreement between the two end locations and an approximately 10% difference in normalized fraction displaced by the **Middle** target. As the dsProbe loss due to thermal dissociation has been subtracted, the total normalized fraction displaced plateaus below 60% displacement by the competitive embedded targets, **3´ End** and **5´ End**.

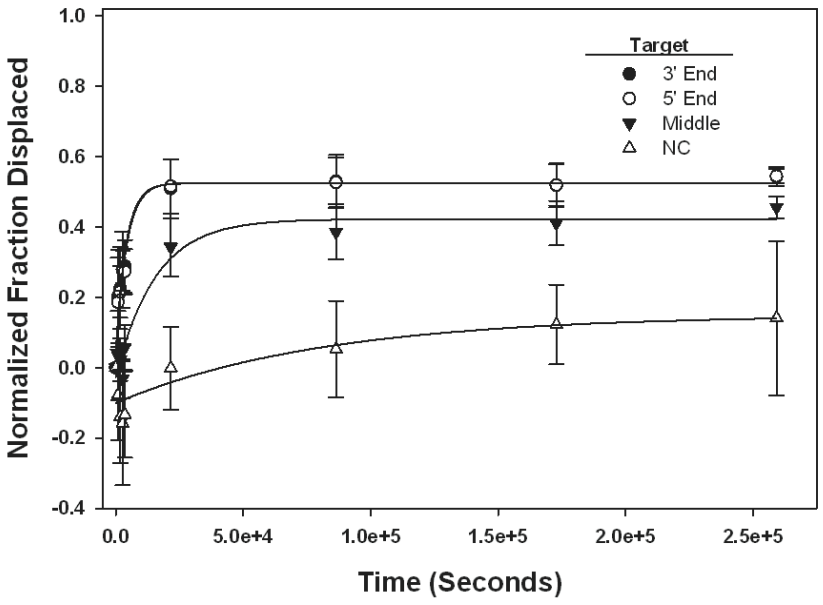

Figure 4.4.5. Normalized fraction of **T11** displaced from dsProbe after incubation with **3´ End**, **5´ End**, **Middle**, and **NC** competitive targets. To normalize the data presented in Figure 4.4.4 and account solely for competitive displacement, the fraction released due to thermal dissociation has been subtracted from the total fraction released.

The results for fraction released of the **T13** from dsProbes after incubation with the competitive targets are shown in Figure 4.4.6. Of note, the fraction released does not approach equilibrium, unlike the **P21:T11** dsProbe. The negative controls for the **P21:T13** dsProbe have different release kinetics in contrast to the behavior observed for the **P21:T11** dsProbe. The **Dissociation** control shows a slight release of **T13** (less than 5%) and quickly reaching a plateau value within the first hour. The **NC** control, however, shows a negative fraction released corresponding to an increase in the fluorescence intensity over the course of the experiment. This seems unlikely given the protocol that includes washing steps to remove any unhybridized fluorescently labeled strands. At most, however, this negative fraction has a magnitude of only 5%. Why one control (**NC**) shows a negative fraction released while the other (**Dissociation**) does not is largely unclear. Experimental errors due to handling or sensitivity changes of the measurement technique are possible explanations. Also, there could in fact be some fluctuation in hybridization of fluorescently labeled strands throughout the time course of the experiment particularly if these hybridization partners are weak. Possible explanations for the measured negative fraction released are provided in more detail in Chapter 5.

For the **P21:T13** dsProbes, the modest displacement activity indicates that the longer competitive targets did undergo significant hindrance in the ability of the recognition segment to displace the dsProbe. After 6 h of incubation with the short **T15** competitive target, 21% of the **T13** dsProbe was released versus only 3% with the embedded competitive targets. At later time points, 24 h and beyond, incubation with the embedded competitive targets did result in moderate **T13** release from **P21:T13**. After

72 h incubation with the **3' End** target yielded 31% release, the **5' End** target 24%, and the **Middle** target only 13%. Of these three embedded targets, the **Middle** target again resulted in minimum fraction released, but unlike the **P21:T11** dsProbe system there is a moderate stratification in fraction release profiles by the end location targets with the **3' End** target releasing 7% more than the **5' End** target. While the higher affinity of the **P21:T13** dsProbe does not allow the system to reach equilibrium displacement over the course of the experiment, this condition may result in the slightly higher sensitivity to the orientation of the **3' End** target.

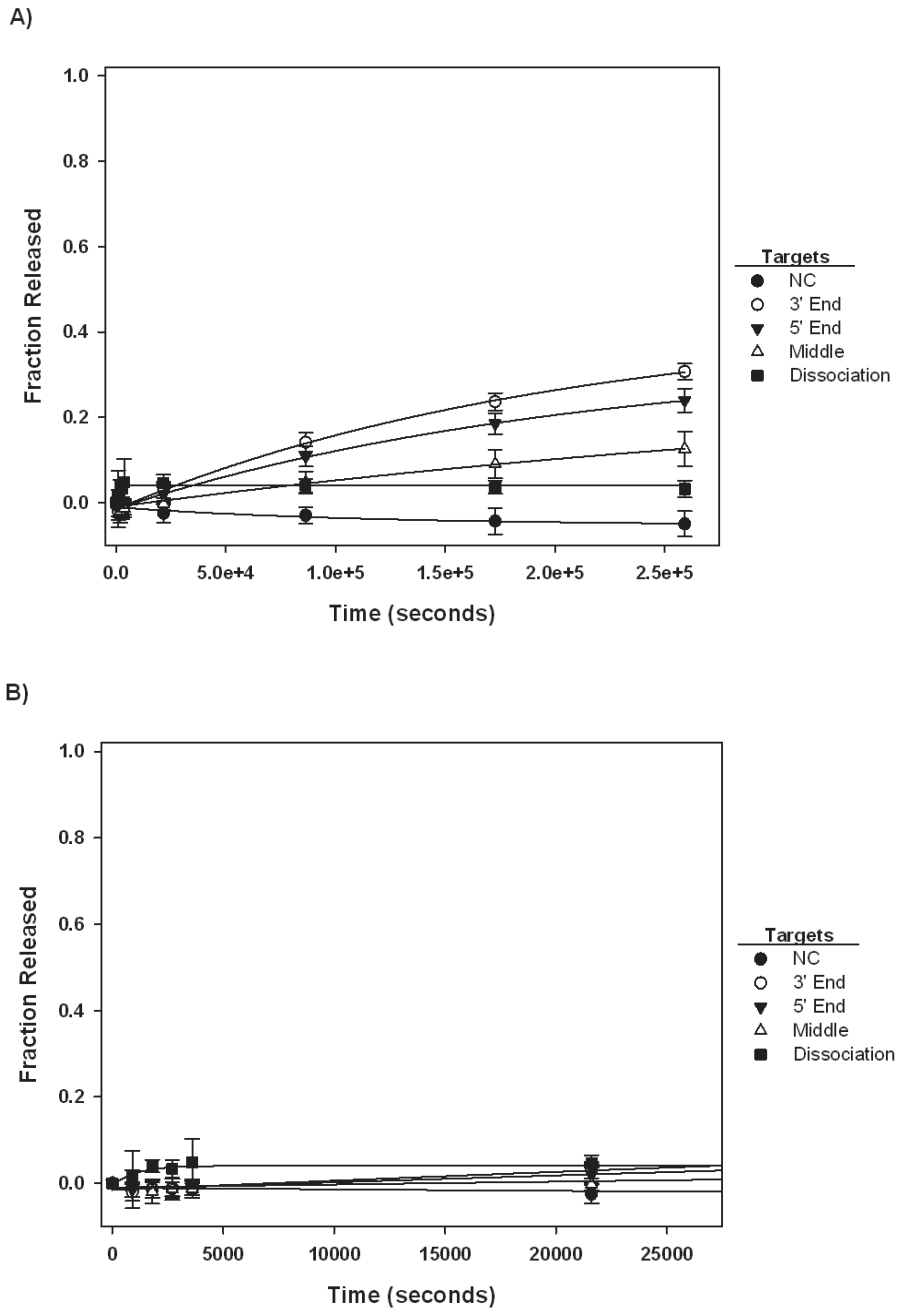

Figure 4.4.6. Fraction released of **T13** from dsProbes as a function of incubation time with **NC**, **3' End**, **5' End**, and **Middle** targets for A) 72 h (259,200 s) with a expanded view of B) the first 6 h (21,600 s). The **Dissociation** sample is included as a dsProbe control in the absence of competitive target. **NC** is a noncomplementary target and thus represents a second control.

Similar to before, the fraction released was normalized for thermal dissociation to yield the fraction displaced due to competitive hybridization shown in Figure 4.4.7. Due to the negative fraction released observed for the **Dissociation** sample, the fraction displaced at early times involves slightly negative values (<10%). These negative values illustrate an important consideration of normalizing the data using dissociation. As negative fraction displaced would physically mean an increase in fluorescence, it is difficult to argue that at early times, the normalized fraction displaced clearly represents the sole contributions of competitive hybridization since all the competitive targets are unlabeled. However, at later times (i.e. beyond 6 h) this discrepancy is resolved as displacement due to competitive hybridization dominates. At these later times, the trends in displacement behavior are similar to those in Figure 4.4.6 with moderate divergence in displacement between the **3´ End** and **5´ End** targets and a more noticeable divergence between the **Middle** target and the end location targets. Due to the complication on the competitive hybridization analysis any subsequent cases involving negative values for thermal dissociation would not be normalized according to the above description. This criterion is applied throughout the remainder of the thesis.

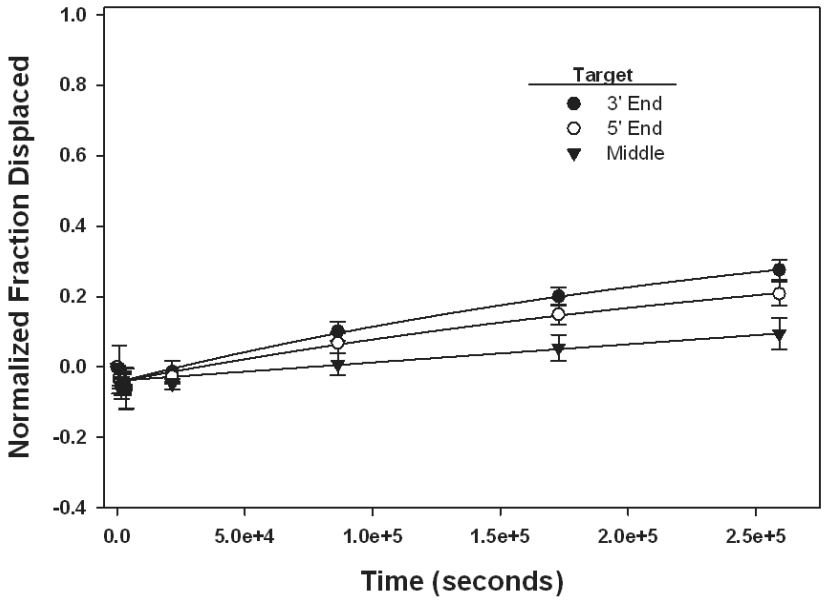

Figure 4.4.7. Normalized fraction of **T13** displaced from dsProbe after incubation with **3´ End**, **5´ End**, **Middle**, and **NC** competitive targets.

Release of **T15m** from dsProbes is shown in Figure 4.4.8. The kinetics of displacement for this dsProbe are moderate in comparison to its **P21:T11** and **P21:T13** dsProbe counterparts and demonstrate the tuned kinetic response as a result of incorporating of a center mismatch within the hybridization segment. The fraction released for the controls, **NC** and **Dissociation**, trace one another with a total fraction released of 26%. The large difference in total fraction released between the embedded targets and the two controls again suggests competitive hybridization as the driving force for the release of the **T15m** from dsProbe. Fraction released as a result of incubation with the **3' End** and **5' End** targets compare very closely with one another and both result in a total fraction released of 86% at the conclusion of the experiment. The **Middle** target is again lower in total fraction released (79%) but more closely resembles the

kinetic trends of the **3' End** and **5' End** targets at early times followed by divergence in the displacement curves after 6 h (21,600 s) of target incubation.

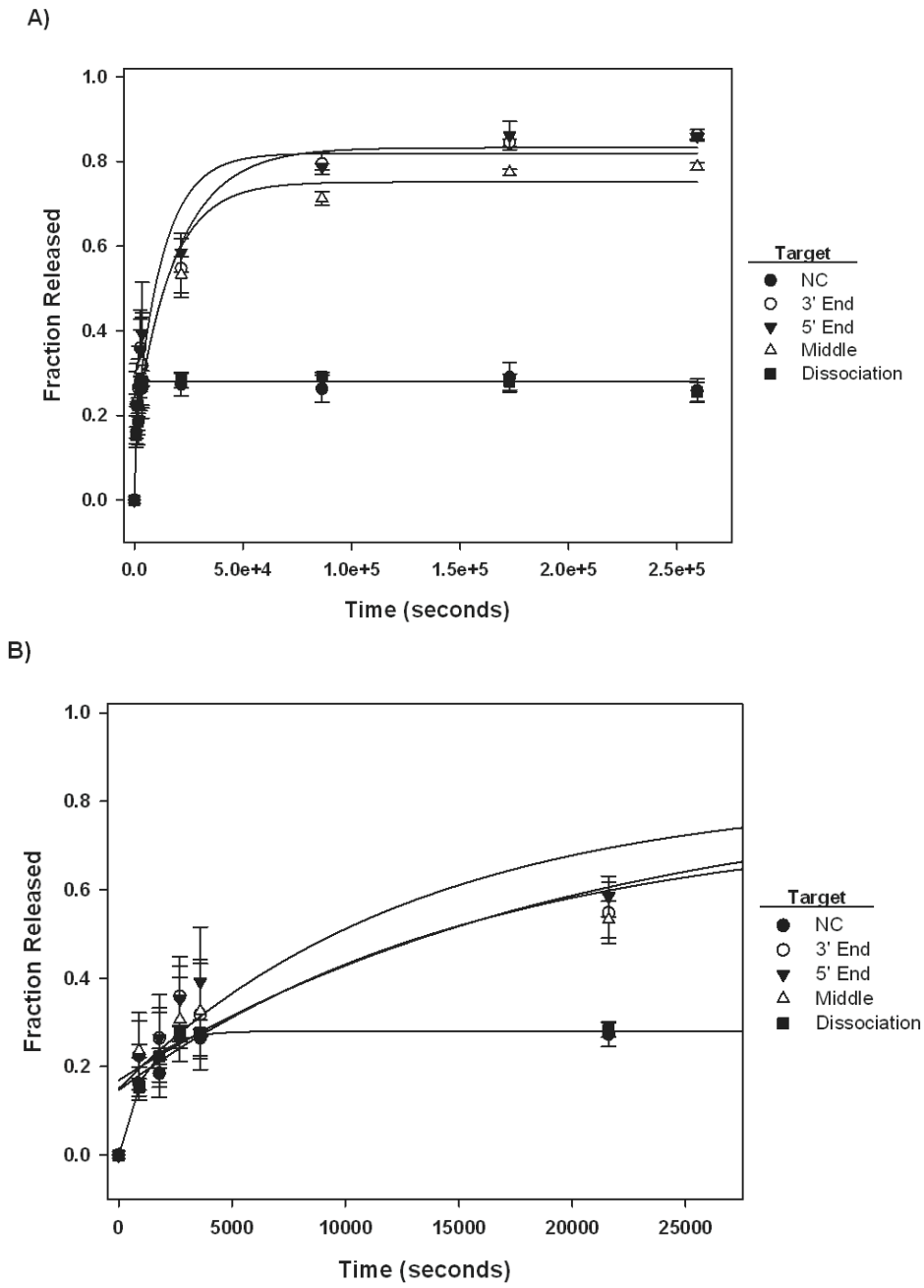

Figure 4.4.8. Fraction released of **T15m** from dsProbe as a function of incubation time with **NC**, **3' End**, **5' End**, and **Middle** targets for A) 72 h (259,200 s) with a expanded view of B) the first 6 h (21,600 s). The **Dissociation** sample is included as a control in the absence of a competitive target.

The fraction displaced due to competitive hybridization could be accurately determined for this dsProbe as there was no negative fraction value in the thermal dissociation data shown in Figure 4.4.8. Figure 4.4.9 shows essentially zero displacement of **T15m** following incubation with the **NC** target while there is significant competitive displacement for the embedded targets. Again, a modest preference for displacing **T15m** in terms of fraction displaced is observed for targets with the recognition sequence embedded at end locations compared to the middle location.

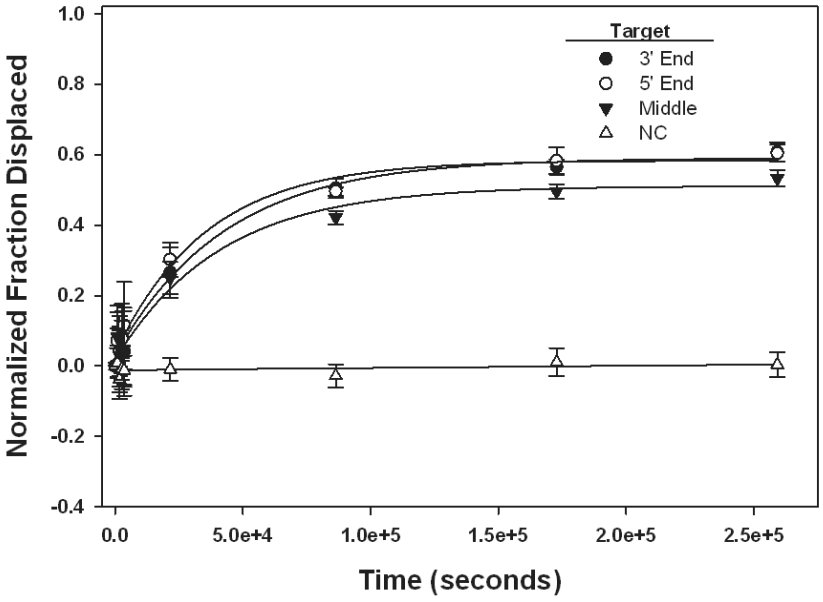

Figure 4.4.9. Normalized fraction of **T15m** displaced from dsProbes as a function of incubation time with **3´ End**, **5´ End**, **Middle**, and **NC** targets.

For dsProbes in which significant thermal dissociation was observed, a closer assessment of dsProbe stability was considered. In this study the stability of the dsProbes was considered as a function of the number of washing steps. For these studies, primary

hybridization to form labeled dsProbes was performed as previously described. At the conclusion of the incubation period, a 40 μL sample was removed from the particle suspension and diluted by the addition of 60 μL of PBS/Tween to a final volume of 100 μL. The sample was set aside until flow cytometry and served as the reference sample in which no washing steps had been performed. The remainder of the particle suspension was centrifuged and resuspended to the volume prior to centrifugation. Another 40 μL was removed and stored as previously described at a final volume of 100 μL. This sample corresponds to 1 washing step. This process was repeated for a total of 6 washing steps for the **T11**, **T13**, and **T15m** dsProbes. Figure 4.4.10 shows the fraction of dsProbe displaced as a function of number of washing steps.

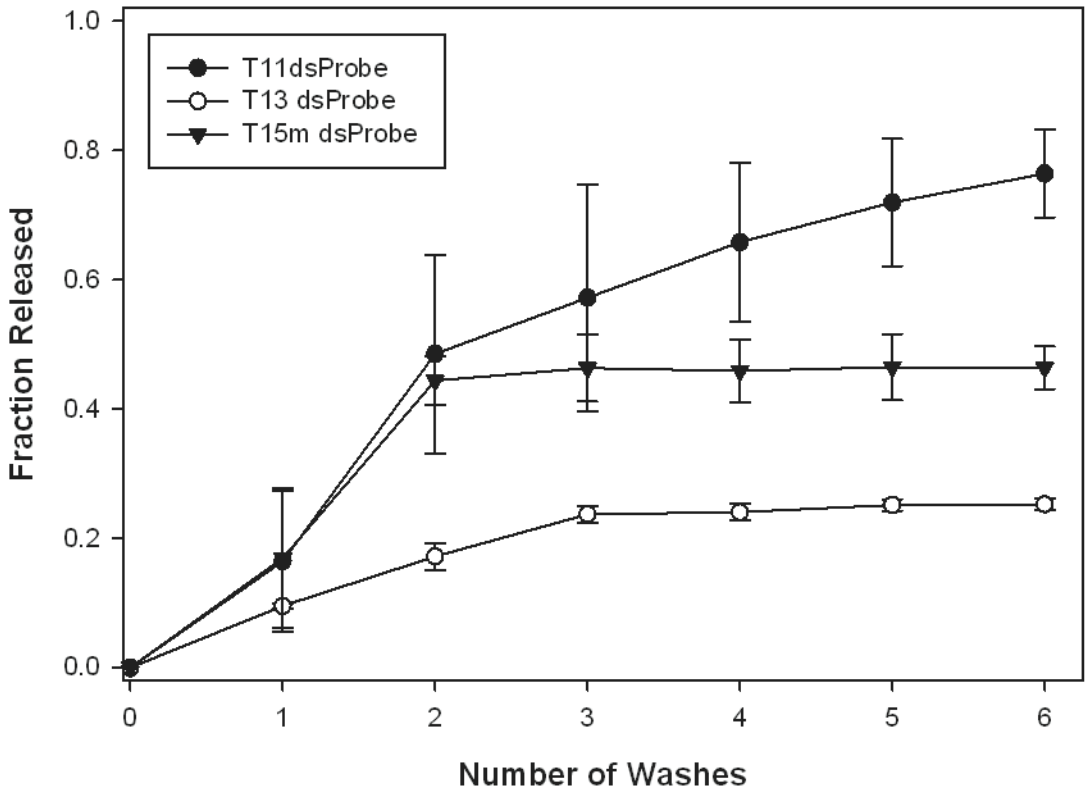

Figure 4.4.10. Fraction released as a function of the number of washing steps for **P21:T11**, **P21:T13** and **P21:T15m** dsProbes. No competitive targets were added for this study.

All dsProbes exhibit a significant fraction released between the zero point (no washes) and two washes. This loss is certainly expected as the purpose of the washing steps is to remove excess or weakly associated fluorescently labeled strands from the suspension. The important comparison occurs between the second and fourth wash step. These points correspond to the number of washes experience by the zero time point and time points incubated with the competitive target, respectively. The loss due to washing

for the **P21:T15m** dsProbe essentially plateaus in this region with only a 2% release of labeled DNA occurring between two and four washes. For the **P21:T13** dsProbe, the fraction released plateaus between the second and third washing step with only a total of 7% loss between step two and step four. In both of these cases the loss in duplex density of dsProbes as represented by fraction released is considered to be minimal. The **P21:T11** dsProbe, however, shows a steady increase in fraction released as the number of washes increases from 2 to 6 washing steps. The fraction released between the second and fourth wash corresponds to a difference of roughly 17%. Although this is a nontrivial loss from washing alone, it does not account for the 80% – 90% release observed in the presence of competitive targets as shown in Figure 4.4.4. Additionally, the total fraction of the **T11** strand released from dsProbes in controls was 42% and 56% for the **Dissociation** and **NC** samples, respectively. These values are significantly higher than the 17% loss as a function of washing alone. Thus, it appears reasonable to conclude that the fraction of labeled hybridization partners released from dsProbes is dominated by either competition or dissociation and is only moderately affected by the number of washing steps in the current protocol in the case of the **P21:T11** dsProbe. However, in order to limit the dsProbe release that may occur as a result in differences between number of washes, the protocol was altered for subsequent studies so that the reference sample (in which no competitive targets were introduced) would undergo the same total number of washes as any and all samples analyzed at later time points (following competitive target incubation).

4.4.3. Determining an Observed Displacement Rate

In order to compare the kinetics of competitive hybridization with results obtained in the literature, we have adapted the approach used by Reynaldo and co-workers[7]. In their analysis, kinetic data was interpreted by curve fitting time-dependent DNA release profiles and an observed displacement rate was obtained. Similarly, we used Sigma Plot 11 to analyze our kinetic data after normalizing to obtain fraction displaced due to competitive hybridization. With this analysis, a value of the experimentally determined observed displacement rate is obtained from the following first order equation:

$$f = f_0 + (f_\infty - f_0)(1 - \exp(-k_{obs} \cdot t)) \quad (1)$$

where f is the fraction displaced at a given time point, f_∞ is the fraction displaced at equilibrium, f_0 is the fraction displaced initially (which is zero at $t = 0$), t corresponds to the time in seconds and k_{obs} is the observed displacement rate expressed in units of (s^{-1}). In order for the successful application of this analysis, the fraction displaced must approach a plateau value where equilibrium conditions appear reasonable. This restriction disqualifies the **P21:T13** dsProbe from consideration. Only k_{obs} values corresponding to a fit of greater than 0.9 R-squared value and passing the constant variance test were reported. The results of this analysis are listed in Table 4.4.3 for both the **P21:T11** and **P21:T15m** dsProbes.

Table 4.4.3. Observed displacement rate k_{obs} (s^{-1}) for **P21:T11** and **P21:T15m** dsProbes for competitive targets using time-dependent fraction displaced data from Figures 4.4.5 and 4.4.9. The values reported corresponds to >0.9 R-squared values and passed the constant variance test.

Target	P21:T11 dsProbe	P21:T15m dsProbe
3' End	2.0×10^{-4}	2.3×10^{-5}
5' End	2.0×10^{-4}	2.8×10^{-5}
Middle	6.4×10^{-5}	2.4×10^{-5}

The observed displacement rate for both **T11** and **T15m** from their respective dsProbes is one to two orders of magnitude greater than those reported by Reynaldo and coworkers[7] thus our system favors faster displacement kinetics. To understand the reasons for these differences in competitive hybridization behavior, it is important to point out key differences between the current system and that of Reynaldo. In the study by Reynaldo and coworkers, the competitive strand and the initial duplex partner were identical in sequence. Subsequently, there was no affinity difference between the initial hybridization duplex and the secondary hybridization duplex to act as a driving force for displacement. Our approach involves incorporating an affinity difference between the dsProbe and the competitive target in order to promote competition-based displacement. Thus with these affinity differences, it is not unexpected that our kinetic studies would generally yield faster observed displacement.

Comparing the values of the observed displacement rate for the **P21:T11** dsProbe, incubation with the **5' End** and **3' End** competitive targets results in identical k_{obs} values which are distinct from observed displacement rate of **P21:T11** dsProbes incubated with

the **Middle** target. The observed displacement values for the **P21:T15m** dsProbes are more similar for all targets and correspond to a k_{obs} of ~ 10^{-5} s^{-1}. A comparison between the **P21:T11** and **P21:T15m** dsProbes reveals that the **P21:T11** dsProbe generally resulted in a faster observed displacement rate than the **P21:T15m** dsProbe. While the **P21:T15m** dsProbe has a similar affinity to the **P21:T11** dsProbe as indicated in initial duplex density, the duplex segment of the **P21:T15m** dsProbe leaves no unhybridized bases on either end of the duplex with which a competitor may initiate hybridization. While the center mismatch of **P21:T15m** may provide enough instability to encourage the ultimate displacement of the labeled strand of the dsProbe, the data indicates that displacement requires longer times of incubation with a competitor.

4.4 Conclusions

In this chapter, the kinetics of competitive hybridization were examined for multiple dsProbes with varying affinities based on sequence design. The first competitive target considered was a short 15 base-long perfectly matched target (**T15**) with a high affinity for the chemically immobilized strand on the particle surface. The change in duplex density as a function of incubation time with **T15** demonstrated a range of kinetic responses with longer and perfectly matched dsProbes being displaced more slowly than their shorter and mismatched counterparts.

Four unhybridized bases near the particle surface generate the affinity difference between the **P21:T11** dsProbe and target of interest (**T15**). For the **P21:T15m** dsProbe the affinity difference stems from a center mismatch in the fluorescently labeled strand.

While these two dsProbes utilize different strategies to promote competition with the perfectly complementary target, their initial duplex densities (6,303 for **T11** and 6,392 for **T15m**) as well as their calculated melting temperatures (62.4 °C for **T11** and 59.5 °C for **T15m** as listed in Chapter 2) are similar. However, their kinetic responses are significantly different. After the first hour of incubation with the competitive target approximately 95% of the **P21:T11** dsProbe had been released compared with only 41% of the **P21:T15m** dsProbe. Similarly, a comparison of the displacement kinetics of the **P21:T13** and **P21:T15** dsProbe provide another illustration with both dsProbes having similar initial duplex densities (11,815 and 12,923 duplexes per μm^2, respectively) but distinct displacement trends. Two possibilities may explain these differences: 1) initial duplex density and duplex melting temperature for oligonucleotide solutions are inaccurate indicators of affinity or 2) competitive displacement is not entirely determined by affinity or the thermodynamic stability of the dsProbe.

In the above comparisons, the longer dsProbe exhibits slower displacement kinetics and a lower total fraction released (99% for **P21:T11**, 85% for **P21:T15m**, 66% for **P21:T13** and 15% for **P21:T15**). Previous studies by Porschke and Eigen have suggested that at least three bases are necessary to form a critical hybridization nucleus for duplex propagation[8]. The four unhybridized bases of the **T11** dsProbe may thus provide a kinetic advantage for displacement by allowing the formation of a hybridization nucleus with the competitive target, an option not available in the **T15m** dsProbe case. Other studies with soluble (not immobilized to a microsphere or flat substrate) double-stranded DNA probes have demonstrated an increase in displacement rate as the length

difference between strands increases[9], though this effect became less pronounced for length differences of 7 bases or more.

Three dsProbes representing slow (**P21:T13**), moderate (**P21:T15m**), or fast (**P21:T11**) displacement kinetics were chosen for studies in which the 15 base target was embedded within a 100 base DNA strand at different locations relative to the 3' to 5' orientation of the sugar-phosphate backbone. These studies demonstrated that location of a recognition sequence within a longer strand context has a moderate effect on the displacement kinetics of the dsProbes, particularly if the sequence of interest is embedded within the middle (**Middle**) of the longer strand versus the ends (**3' End** and **5' End**). This disparity is attributed to the electrosteric hindrance of two chains of unhybridized bases for the **Middle** competitive target as opposed to just one chain of unhybridized bases for the **3' End** and **5' End** competitive targets.

In order to more fully quantify the kinetics of displacement, techniques for determining an observed displacement rate from the literature were applied to those dsProbe systems that reached an equilibrium displacement. The observed displacement rates were generally faster for the **P21:T11** dsProbe than for the **P21:T15m** dsProbe. The role of unhybridized bases in dsProbe bases in forming a stable hybridization nucleus with the competitive target is yet to be clarified from these results. In order to more fully assess this possibility, a series of experiments is performed in which the affinity of the competitive target is varied by incorporating mismatches at various locations within the target strand. These experiments are discussed and the results analyzed in Chapter 5.

4.5 References

1. Dunbar, S.A., et al., *Quantitative, multiplexed detection of bacterial pathogens: DNA and protein applications of the Luminex LabMAP^{TM} system.* Journal of Microbiological Methods, 2003. **53**: p. 245-252.

2. Lu, J., et al., *MicroRNA expression profiles classify human cancers.* Nature, 2005. **435**(9): p. 834-838.

3. Dunbar, S.A., *Applications of Luminex^{R} xMAP^{TM} technology for rapid, high-throughput multiplexed nucleic acid detection.* Clinica Chimica Acta, 2006. **363**: p. 71-82.

4. Dunbar, S. and J.W. Jacobsen, *Quantitative, Multiplexed Detection of Salmonella and Other Pathogens by Luminex^{R} xMAP^{TM} Suspension Arrays*, in *Salmonella: Methods and Protocols*, H. Schatten and A. Eisenstark, Editors, Humana Press, Inc.: Totowa, NJ. p. 1 - 19.

5. Urakawa, H., et al., *Optimization of Single-Base-Pair Mismatch Discrimination in Oligonucleotide Microarrays.* Applied and Environmental Microbiology, 2003. 69(5): p. 2848 - 2856.

6. Fish, D.J., et al., *DNA multiplex hybridization on microarrays and thermodynamic stability in solution: a direct comparison.* Nucleic Acids Research, 2007. 35(21): p. 7197 - 7208.

7. Porschke, D. and M. Eigen, *Co-operative Non-enzymic Base Recognition III. Kinetics of the Helix-Coil Transition of the Oligoribouridylic Oligoriboadenylic Acid System and of Oligoriboadenylic Acid alone at Acidic pH.* Journal of Molecular Biology, 1971. **62**: p. 361-381.

8. Li, Q., et al., *A new class of homogeneous nucleic acid probes based on specific displacement hybridization.* Nucleic Acids Research, 2002. **30**: p. 2e5.

9. Reynaldo, L.P., et al., *The Kinetics of Oligonucleotide Replacements.* Journal of Molecular Biology, 2000. **297**: p. 511-520.

CHAPTER 5

Competitive Hybridization of dsProbes with Mismatched Targets

5.1 Introduction

In Chapter 4, the kinetics of competitive hybridization were analyzed for dsProbes of varying affinity due to base length differences and the incorporation of a center mismatch within the original duplex segment. Here, we consider the effects of incorporating mismatches into the competitive target itself on the kinetics of competitive hybridization. The competitive targets were designed to more fully assess the ability to form a stable hybridization nucleus between the target and chemically immobilized probe strand by varying the availability of unhybridized bases within the dsProbe. A similar kinetic analysis is performed for displacement of the original hybridization partner by the various targets as seen in Chapter 4. In the absence of competitive targets, the dissociation behavior of the dsProbes at early times is also discussed in detail.

5.2 Experimental Methods

Primary and Secondary/Competitive Hybridization. The protocol for competitive hybridization follows the same procedure outlined in Chapter 4 with the exception of the washing steps. After the 6 h incubation at room temperature for primary hybridization to form the dsProbes, the 400 μL particle suspension was centrifuged a total of three times at 9.1 x 1000 g. After each centrifugation the bead pellet was resuspended in 400 μL of PBS/Tween. At the conclusion of this process, 20 μL of the suspension was removed and

diluted in 80 μL of PBS/Tween. In order for the reference sample, at time point zero, to undergo the same number of total washes as the latter time point samples, the reference sample was centrifuged and resuspended a total of three more times. After these additional washing steps, the reference sample was stored at 4 – 8 °C conditions until preparation for flow cytometry. For the remaining suspension, 20 μL of the competitive target was added at 100 μM. The final concentration of the competitive target in the suspension was 5 μM, consistent our with previous studies from earlier chapters. Aliquots were removed at specified time points and washed as previously described. Including all washes, a total of four complete washing steps were performed for each time point taken in the series, including the reference sample. Samples were stored at 4 – 8 °C conditions until preparation for flow cytometry.

5.3 Results and Discussion

In order to generate competitive targets of varying affinity, a single mismatch was incorporated in the **T15** competitive target at one of two locations: the center and three bases from the 3' end. The center mismatch location is the equivalent sequence as the fluorescently labeled strand in the **P21:T15m** dsProbe. Subsequently, this target is labeled **T15m**. The second mismatch target is labeled **T15x3**, referring to the mismatch in the third base from the 3' end. Table 5.3.1 shows the competitive target sequences used in this study along with the chemically immobilized strand of the dsProbe to facilitate identification of the mismatch location. Each of these competitive targets was incubated with the **P21:T11**, **P21:T13** and **P21:T15m** dsProbes to characterize the kinetics of competitive hybridization.

Table 5.3.1. List of sequences of the immobilized ssProbe (**P21**) and three competitive targets used in this study. The competitive targets are highlighted in blue with mismatches underlined and highlighted in red. If present, the mismatches were selected to involve the identical cytosine base for both the original hybridization partner (i.e. **T15m**) and the competitive target (i.e. **T15m** and **T15x3**) as on the immobilized probe strand.

Nomenclature	Sequence
P21	5' – Amine-(carbon12) CTC GTC ACA CTA TCA – 3'
T15	3' – GAG CAG TGT GAT AGT – 5'
T15m	3' – GAG CAG TCT GAT AGT – 5'
T15x3	3' – GAC CAG TGT GAT AGT – 5'

The placement of the mismatch location within the competitive target strand was selected to investigate the role of a "toehold" region (unhybridized bases within the dsProbe) on the possible formation of a stable hybridization nucleus between the competitive target and immobilized probe strand. **T15** was again chosen as one of the competitive targets for these studies and expected to be the most successful competitor in terms of both faster displacement kinetics as well as higher total fraction of DNA displaced. The **T15x3** competitive target was designed with a mismatch at the third base position of a potential hybridization nucleus corresponding to the toehold of **P21:T11**. The presence of this mismatch was expected to interrupt hybridization in the toehold region between the competitive target and the immobilized single-strand of the dsProbe and result in less successful competitive displacement than the **T15** competitive target. The **T15m** competitive target, incorporating a mismatch in the center of the strand, was also chosen to investigate whether or not the ability of hybridization to occur in the

toehold region could overcome a thermodynamically less stable center mismatch during competitive hybridization. Figure 5.3.1 is given for easy reference and in order to illustrate the mismatch location relative to the initial dsProbe duplex.

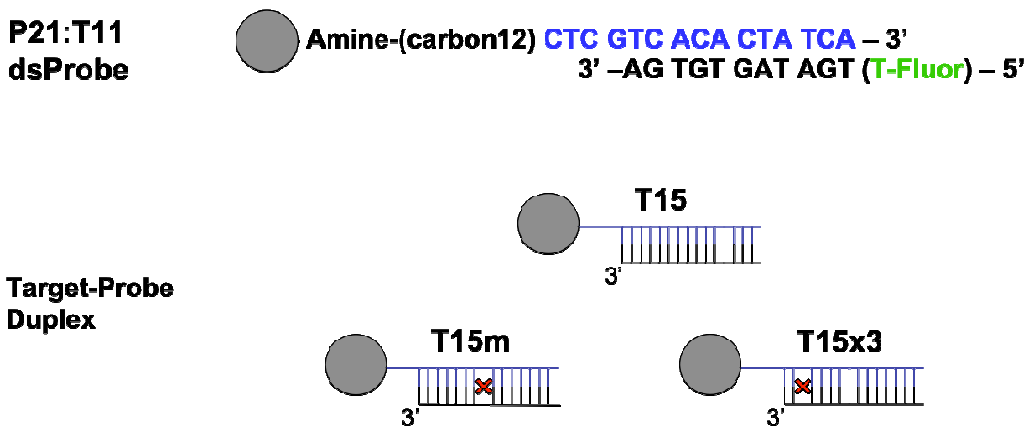

Figure 5.3.1. Schematic illustrating the initial dsProbe duplex (**P21:T11** dsProbe is shown) and the resulting target-probe duplexes after competitive hybridization. The chemically immobilized probe strand is highlighted in blue with target strands illustrated in black. The fluorescein label on the original hybridization partner is represented in green and the mismatched base pairs in the secondary duplex are indicated in red.

The results of incubation of the **P21:T11** dsProbe with various competitive targets are shown in Figure 5.3.2. The control sample, **Dissociation** demonstrates an unexpected trend in fraction released. At early times the fraction released is negative which experimentally corresponds to an *increase* in the average fluorescence intensity for a population of particles functionalized with labeled dsProbes. At later times, 6 h (21,600 s) and beyond, however, the fraction released is positive correlating to a loss in the average fluorescence intensity. By one hour the **Dissociation** sample showed -30% fraction released, but concluded the 72 h incubation with a total fraction released of 45%. Incubation with the **T15** competitive target resulted in a fraction release of 92% after one hour of incubation (3,600 s). At the conclusion of the 72 h of the incubation period (259,200 s), the total fraction released after incubation with the **T15** target was 99%. The results of incubation with **T15x3** were fractions released of 87% and 98% after 1 h and 72 h, respectively. Incubation with the last of the competitive targets, **T15m**, displaced

65% after 1 h of incubation and 78% at the conclusion of the 72 h time course of the experiment. In all cases, the fraction released of the **P21:T11** dsProbe was at or nearly at equilibrium by the conclusion of the experiment.

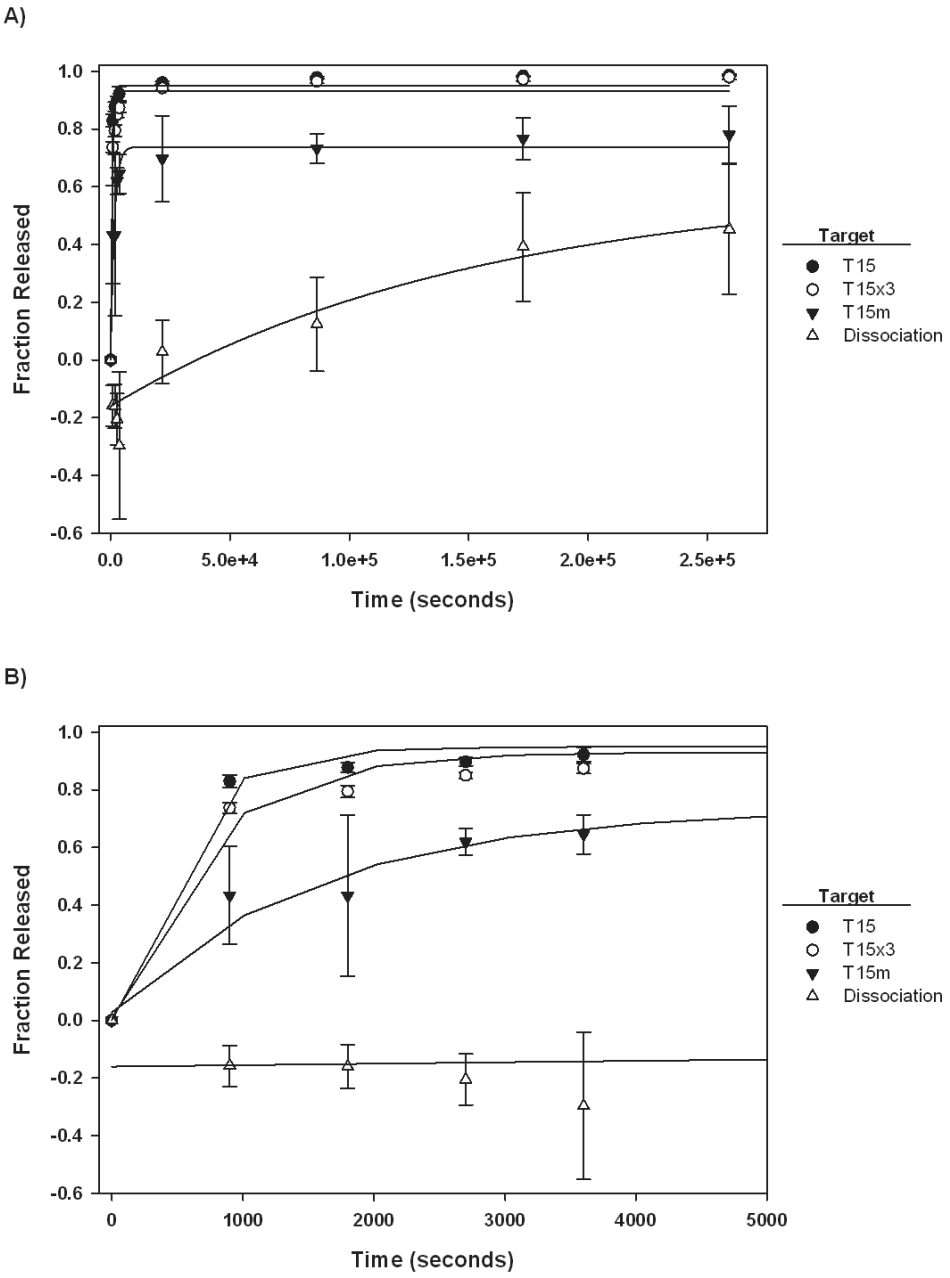

Figure 5.3.2. Fraction released of **T11** from dsProbes as a function of incubation time with **T15**, **T15x3**, and **T15m** competitive targets over A) 72 h (259,200 s) and B) 1 h (3,600 s). The **Dissociation** sample is included as a control in the absence of competitive target.

For the **P21:T11** dsProbe, the similar displacement kinetics and total fraction released after incubation with the **T15** and **T15x3** competitive targets do not indicate a preference for a perfectly-matched toehold region of available bases within the dsProbe. If this 4 base-long toehold serves as a nucleation site for the secondary duplex to form, then incubation with the **T15x3** target should have resulted in less release of **T11** since it is likely that as the mismatch in the third base would disrupt the formation of this nucleus. However, the observed trends in dsProbe release indicate the length of consecutive complementary bases in the competitive targets has significant impact in observed fraction released. Incubation with the **T15m** target, which should be able to form a stable hybridization nucleus in the toehold region with the unhybridized bases of the **P21:T11** dsProbe, results in slower kinetics and lower total fraction released. The presence of the center mismatch means that there are 7 consecutive complementary bases on either side of the mismatch versus the 12 and 15 consecutive complementary bases in the **T15x3** and **T15** competitive target, respectively. These results point to the length of consecutively matched bases in the competitive target as a dominant factor over mismatch location within the competitive target.

The release kinetics of the **P21:T11** dsProbe due to dissociation in the absence of a competitive target (**Dissociation)** is unexpected. At early times the fraction released is negative which, as previously stated, corresponds to an increase in fluorescence intensity on the particle surface. As there is no new fluorescently labeled DNA added at this stage in the experiment, this "increase" in fluorescence intensity must have another explanation for occurring only during the early time points following incubation with the competitive target. It is important to note that the washing protocols were altered for this study in

comparison to studies presented in Chapter 4. In the updated protocol, the zero time point is washed two additional steps immediately after separation from the remaining suspension equaling the total number of washes received by the later time points. We believe that this difference in washing protocol accounts for the observed difference in labeled **T11** release due to dissociation observed in these studies compared to earlier studies in Chapter 4 for this same dsProbe system. At the conclusion of dsProbe preparation, the entire suspension of particles undergoes two complete washing steps followed by the removal of a portion of the suspension that will serve as the zero time point. It is possible that during the formation of dsProbes, imperfect base pairings between the fluorescently labeled hybridization partner probe strand may occur, particularly since the single-stranded probe is immobilized prior to duplex formation. The first set of two washes that all particles undergo may remove some of these imperfect duplexes, but not necessarily all. Since the reference sample undergoes another two washes immediately after removal from the suspension, more of the fluorescent strands imperfectly hybridized are removed than for samples at latter time points. Unlike the zero time point sample, the remaining samples taken from the **Dissociation** series at later times have an opportunity for fluorescently labeled strands to assume more perfectly complementary duplex structures prior to separation and further washing steps. Sometime between 1 h - 6 h dissociation dominates the behavior of the dsProbe duplexes and results in positive fraction released throughout the remainder of the experiment as shown in Figure 5.3.3. This increase in fluorescence or negative fraction released is not observed for samples in which a competitive target is present because weakly associated fluorescent **T11** strands are quickly displaced by the higher affinity competitive targets

within short times as evidenced by the fast release kinetics generally observed for the **P21:T11** dsProbe.

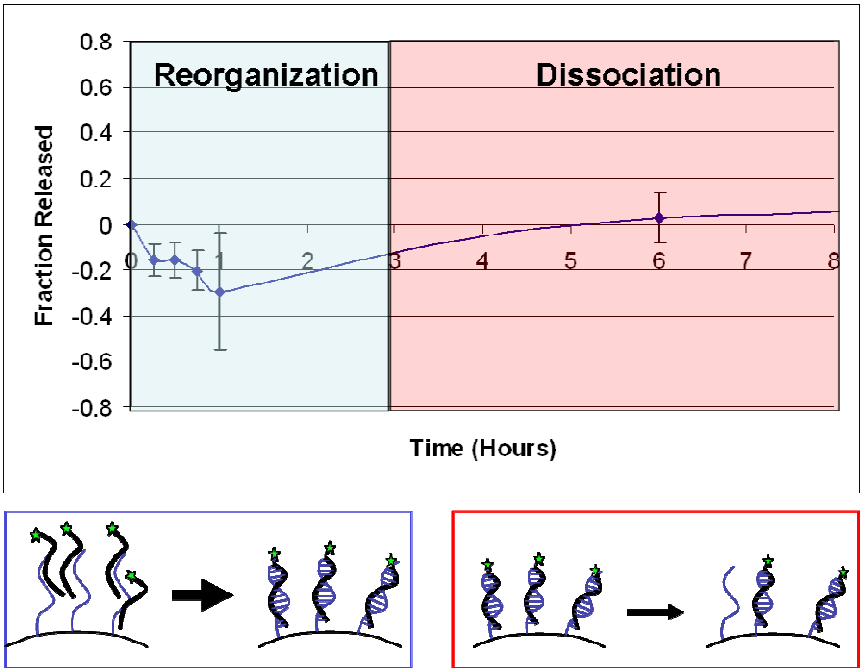

Figure 5.3.3. Fraction of **T11** strand released from dsProbes as a function of incubation time in the absence of competitive targets at early time points up to 6 h. The illustrations at the bottom represent possible imperfect hybridization events at early times followed by dissociation dominating at later times.

This type of imperfect duplex formation has been suggested by Glazer et al. for hybridization of fluorescent targets to probes immobilized on a 2D substrate[1]. In these studies a peak in the absorbed target density, interpreted as imperfect hybridization of targets to immobilized probe strands, was observed to occur at high target concentrations (100 nM) and at early times before later reaching equilibrium within 30 minutes. In our system, we are observing this overshoot at the transition from the 6 h incubation time with the fluorescently labeled DNA strand to initial incubation time with the competitive target strand. Why do we observe a peak in fluorescence at longer times (1 h) in our system if such a peak was resolved more quickly in the Glazer et al. system? We believe this time discrepancy results from the experimental design used in Glazer et al.'s work which involved a 2D substrate in a flow cell at relatively high flow rates[1]. Subsequently, the solution was continually refreshed.

In our case, we performed primary hybridization in a closed reaction vessel, a centrifuge tube, where the excess primary target could freely diffuse throughout the solution surrounding the particle. Since the initial target concentration was 5 μM, the concentration gradient of target was unfavorable for dissociation of imperfectly hybridized targets. As suggested by models of hybridization activity on microparticle surfaces[2], high soluble target concentrations hinder imperfectly hybridized strands from being released into the solution and adopting more favorable hybridization conformations that may otherwise occur in conditions of low soluble target concentration. In our system, high concentrations of soluble target are present only during initial preparation steps to form dsProbes but not during the later incubation period for the **Dissociation** sample in which no competitive target is present. In this time imperfect hybridization

may result with more than one fluorescently labeled strand binding to a given immobilized probe strand. Thus, during the second incubation step, in which the absence of DNA in the surrounding solution yields a favorable concentration profile for dissociation of imperfectly hybridized fluorescent strands. As these strands are better able to dissociate, they may then re-hybridize in a more favorable or stable duplex conformation. The samples removed at early time points of the kinetic study may thus reflect the ability of the imperfectly hybridized fluorescent strands to reorganize on the microsphere surface unlike the reference sample in which the imperfectly hybridized strands may dissociate are removed by the four consecutive washing steps.

Results of incubating the **P21:T13** dsProbe with competitive targets are shown in Figure 5.3.4. Due to the higher affinity of the **P21:T13** dsProbe (compared to **P21:T11**), the observed fraction released did not approach equilibrium during the time course of the experiment except for **P21:T13** dsProbes incubated with the **T15m** competitive target. Similar to the release of **T13** from dsProbes after incubation with the embedded targets discussed in Chapter 4, there is a greater stratification in fraction released for the competitive targets. This stratification may result from the higher affinity of **P21:T13** allowing for better discrimination between the various targets, depending on their affinity for the immobilized DNA strand. Unlike previous cases, the **Dissociation** sample here exhibits negative values of fraction released at early times (-10% at 3,600 s) and does not reach a positive value by the conclusion of the study (-4% at 259, 200 s). Incubation with the **T15** competitive target also shows a negative fraction released after 1 h corresponding to -6% fraction released. Compared to the **P21:T11** case, the negative fraction released at early times after incubation with the **T15** competitive target is

anomalous, given the high affinity of **T15**, even taking into consideration possible reorganization of fluorescently labeled strands on the microsphere surface. However, this negative fraction released is only temporary with a fraction released of 55% by the end of the experiment. Incubation with **T15x3** and **T15m** follow with a total fraction released of 38% and 17%, respectively.

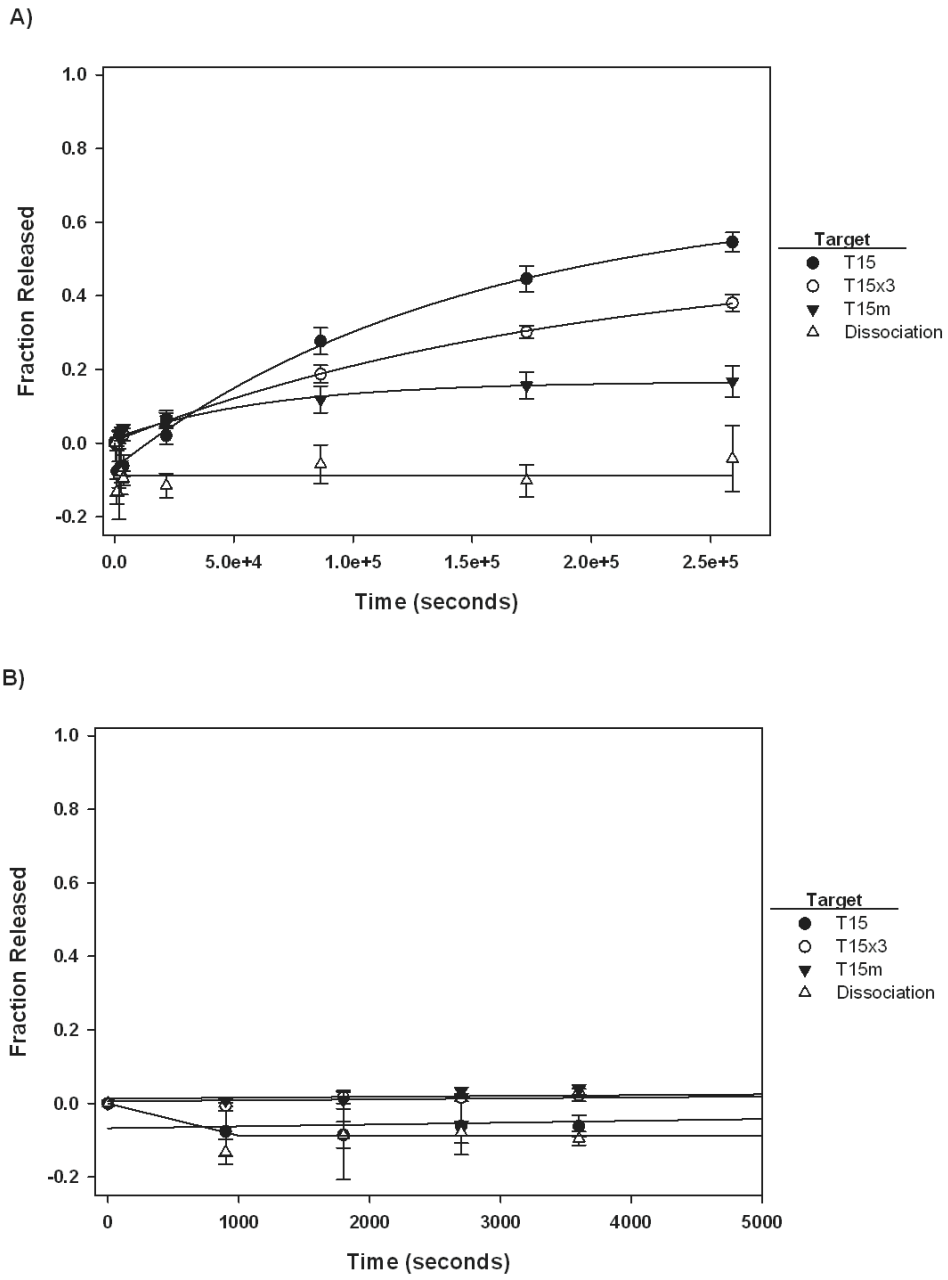

Figure 5.3.4. Fraction released of **T13** from dsProbes as a function of incubation time with **T15**, **T15x3**, and **T15m** competitive targets over A) 72 h (259,200 s) and B) 1 h (3,600 s). The **Dissociation** sample is included as a control in the absence of competitive targets.

The third dsProbe system considered in this study is the **P21:T15m** dsProbe. The **Dissociation** sample resulted in a fraction released of 6% after 1 h and 33% after 72 h of room temperature incubation in the absence of a competitive target. The fraction released after incubation with the **T15** competitive target corresponded to 25% after 1 h and 84% after the 72 h incubation period. Initial results indicate a low fraction of **T15m** is released at early times in the presence of **T15**, which is inconsistent with previous results for this competitor. Subsequently, this competitive target was tested a total of five times as opposed to the normal three. The average values at each time point of the five competitive hybridizations are reflected in the data of Figure 5.3.5. Incubation with the **T15x3** competitive target resulted in 42% fraction released at 1 h and 89% fraction released at the 72 h point. Similarly, the fraction released in the presence of the **T15m** competitive target was 41% and 88% after 1 h and 72 h, respectively. Finally, the **P21:T15m** dsProbe does not exhibit a negative fraction released for the **Dissociation** sample. In light of the observed negative fraction released for both the **P21:T11** and **P21:T13** dsProbes, the most plausible explanation consistent with the reorganization of imperfectly hybridized fluorescent strands is that the presence of the center mismatch destabilizes any imperfect duplexes sufficiently such that only the "most complete" **P21:T15m** duplexes remain after the initial series of washing steps. Thus, the process of reorganization may not occur at all or may occur too quickly to be detected in the allotted experimental time interval.

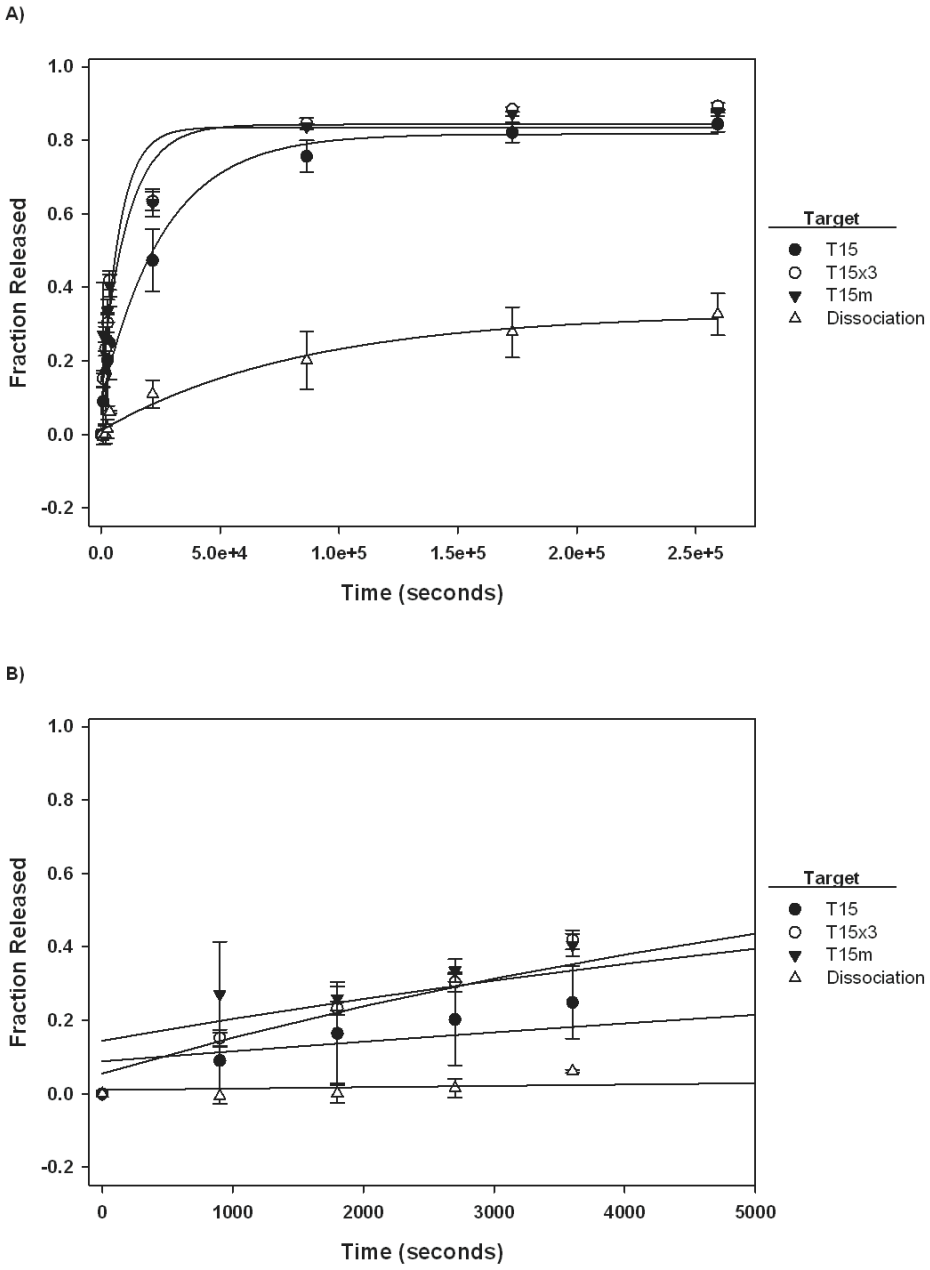

Figure 5.3.5. Fraction released of **T15m** from dsProbes as a function of incubation time with **T15**, **T15x3**, and **T15m** competitive targets over A) 72 h (259,200 s) and B) 1 h (3,600 s). The **Dissociation** sample is included as a control in the absence of competitive targets. Each data point represents the average of three separate measurements except for the **T15** competitive target, which represents the average of five separate measurements.

As done previously, a normalized fraction displaced was determined for the **P21:T15m** dsProbe. Since there was no observed negative fraction released and equilibrium was reached, this method of analysis is straightforward. While all targets result in a significant amount of competitive displacement, there is little difference in normalized fraction displaced for the three different targets explored, namely the perfectly matched **T15** and the single mismatch targets **T15x3** and **T15m**. This similarity in the total fraction displaced implies that the presence of a center mismatch within a dsProbe with no toehold comprise of unhybridized bases may not be able to discriminate between perfectly matched targets and targets with a single base mismatch.

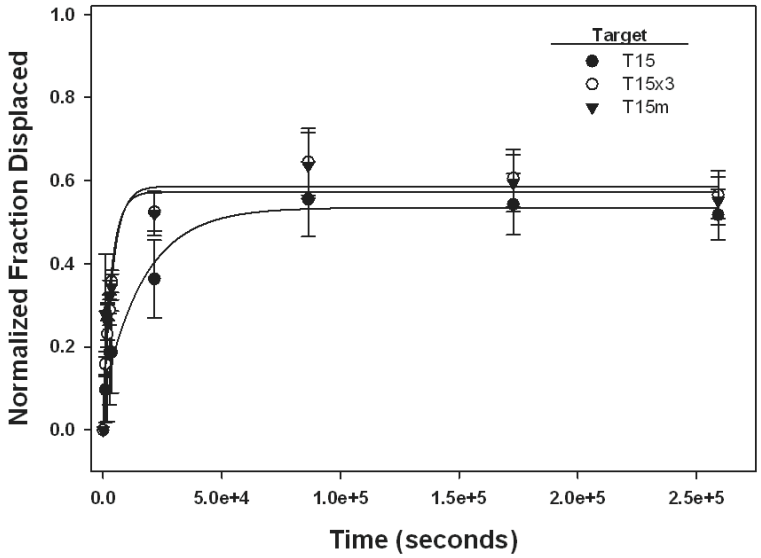

Figure 5.3.6. Normalized fraction of **T15m** displaced from dsProbes after incubation with **T15**, **T15x3**, and **T15m** competitive targets.

Similar to the analysis approach presented in Chapter 4, an observed displacement rate, k_{obs}, was determined from the kinetic data for the normalized fraction displaced of

T15m. Table 5.3.2 lists these values and the corresponding competitive targets. The observed displacement rate for **T15m** is approximately $10^{-4} – 10^{-5}$ s^{-1}. Despite the lack of a toehold region in this 15 base-long dsProbe, these values for k_{obs} are again greater than those reported by Reynaldo and coworkers and reflect the influence of the center mismatch weakening the dsProbe sufficiently to allow a better hybridization partner, even those with a near end mismatch (i.e. **T15x3**), to displace **P21:T15m**.

Table 5.3.2. Observed displacement rate k_{obs} (s^{-1}) for the **P21:T15m** dsProbe for all competitive targets normalized for dissociation. The values reported corresponds to >0.9 R-squared values.

Target	T15m dsProbe
T15	5.8×10^{-5}
T15x3	3.0×10^{-4}
T15m	3.0×10^{-4}

5.4 Conclusions

This study investigated the effect of incorporating a mismatch within the competitive target strand on the kinetics of competitive displacement. Two mismatch locations were considered: at the center position of a 15 base-long target or at the third base position from the 3' end. The latter mismatch was chosen to interrupt any stable nucleus of hybridization that may occur between the unhybridized bases of the **T11** dsProbe and competitive target strand. The kinetics of competitive hybridization for

these mismatch targets were compared to that of a perfectly complementary target as well as the kinetics of release in the absence of a competitive target. Release of the **P21:T11** dsProbe by **T15x3** did not indicate an appreciable disadvantage resulting from the third base-position mismatch. The similar trends in release after incubation with of **T15** and **T15x3** coupled with the lower fraction released of **P21:T11** by the **T15m** competitive target indicated that targets with longer regions of consecutively matched bases were more effective competitors than targets with the ability to access the exposed bases of the toehold region within the dsProbe. This result does not support the theory that a stable hybridization nucleus within this toehold region facilitates fast release of the **P21:T11** dsProbe.

The release observed for both the **P21:T11** and **P21:T13** dsProbes in the **Dissociation** sample showed a region of negative fraction released corresponding to a relative increase in fluorescence between the zero time point and later time points. This negative fraction released transitioned over time to a significant positive fraction released for the **P21:T11** dsProbe but remained negative for the **P21:T13** dsProbe. A physical model describing this behavior was developed accounting for the changes made in the washing protocol. The four consecutive washing steps for the reference sample is thought to remove imperfectly hybridized fluorescent strands while the samples taken at later times have the opportunity for imperfectly hybridized dsProbes to reorganization upon the particle surface and assume more favorable duplex arrangements that are not removed by washing steps at later times. As the time of incubation increases, the process of dissociation dominates the **P21:T11** dsProbe but not the higher affinity **P21:T13** dsProbe. In light of the proposed reorganization model for imperfectly hybridized

fluorescent strands, we reason that an initial stage of negative fraction released is not observed for the **Dissociation** sample of the **P21:T15m** dsProbe because the center mismatch prevents the formation and duration of imperfect hybridization events that can withstand the multiple washing steps.

While the **P21:T11** and **P21:T15m** dsProbes should have a similar affinity based on similar calculated melting temperature values and measured initial duplex densities, as discussed previously in Chapter 2, they differ greatly in responsiveness to the presence of a competitive target. While the **P21:T11** dsProbe is more responsive than the **P21:T15m** dsProbe, neither successfully distinguishes between a perfectly complementary target and a target with a single mismatch. Following this analysis, the **T13** dsProbe is the most successful dsProbe in terms of distinguishing between targets with and without mismatches. The release observed for the **P21:T13** dsProbe, similar to the results presented in Chapter 4, indicates that the higher affinity dsProbe enhances the advantages of some competitive targets over others. This is observed in the greater stratification of fraction released as time of competition increases. However, the limitation of this dsProbe is that these differences are not significant until later incubation times. For detection applications, it would be advantageous if this stratification in response occurred at earlier times, or stated differently, the dsProbe was more responsive to perfectly complementary targets. Considering the design of the **P21:T13** dsProbe, the two unhybridized bases are located adjacent to the particle surface. While the carbon spacer is thought to limit interaction between the particle surface and dsProbe, any target seeking to access these two bases would still have to penetrate into the electosteric layer of chemically immobilized DNA strands and then orient in order to begin hybridization at

this region of the dsProbe. If the design the dsProbe were altered such that the unhybridized bases were oriented away from the particle surface and into the solution, then incubation with competitive targets may result in an affinity-based response at earlier incubation times. This hypothesis is tested and results discussed in Chapter 6.

5.5 References

1. Glazer, M., et al., *Kinetics of oligonucleotide hybridization to photolithographically patterned DNA arrays.* Analytical Biochemistry, 2006. **358**: p. 225 - 238.

2. Stevens, P.W., M.R. Henry, and D.M. Kelso, *DNA hybridization on microparticles: determining capture-probe density and equilibrium dissociation constants.* Nucleic Acids Research, 1999. **27**(7): p. 1719 - 1727.

CHAPTER 6

Effect of Duplex Orientation on Competitive Hybridization of dsProbes

6.1 Introduction

The divergence in the fraction released as a function of target specificity seen with the **T13** dsProbe shows promise for discrimination between not only a perfectly matched and mismatched target but also discrimination based on the locations of the mismatch within the target strand. The limitation, however, of this dsProbe system is that the divergence of fraction released, which distinguishes between the mismatch and perfectly matched targets, was not clear until later times. In order to enhance the responsiveness of this dsProbe to the competitive targets so that discrimination between targets is evident at earlier times, re-orienting the dsProbe in relation to the particle surface is considered in the current chapter. By exposing the unhybridized bases of the **P21:T13** dsProbe to the free end of the duplex, it is hypothesized that electrosteric repulsion experienced by the soluble target strands from the immobilized DNA layer may be reduced. The following chapter reviews the design of this new dsProbe and discusses the kinetics of release by several competitive targets in comparison to releases due to dissociation, or the absence of a competitive target.

6.2 Experimental Methods

Due to unforeseen aging effects in the original Invitrogen 5.1 μm microspheres previously used for competitive hybridization studies, the particle substrate used for this study was a 1 μm carboxylate modified polystyrene microsphere also purchased from Invitrogen (Eugene, OR). The DNA strands used were again purchased from Integrated DNA Technologies (Coralville, IA) and HPLC purified by the supplier. Compared to our previous experiments, the sequence of the immobilized single-stranded probe was reversed for these "flip" studies so that the amine functional group was located on the 3' end along with the 12 carbon spacer instead of the 5´ End. The 13 base-long fluorescein-labeled target strand was designed with the fluorophore attached to the 3' end via a modified thymine base that is not intended to participate in the duplex segment. Probe coupling to the microsphere surface and hybridization protocols were consistent with those used in Chapter 5.

6.3 Results and Discussion

In order to clarify the new orientation of the dsProbe, Figure 6.3.1 illustrates the position of the unhybridized bases and competitive target-probe duplexes that are formed as a result of competitive hybridization. The new dsProbe is labeled as **Flip T13** as it corresponds to the same sequence as the previous **P21:T13** dsProbe but is now conjugated via the 3' end of the immobilized strand to the particle surface. Unlike the other dsProbes from earlier chapters, this orientation results in the two unhybridized bases extending into the solution away from the particle surface. The fluorescently labeled hybridization partner may partially obscure these bases during competitive

hybridization events, however, as the fluorophore is attached on the 3' end. This arrangement was necessary in order to maintain the same sequence complementary to the perfectly matched competitive target.

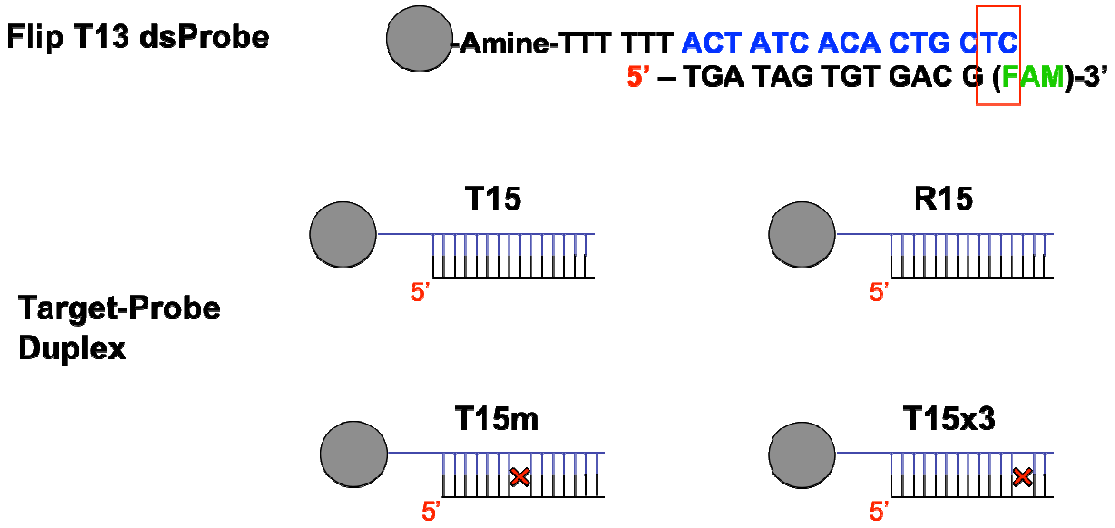

Figure 6.3.1. Schematic illustrating the **Flip T13** dsProbe to highlight the two unhybridized bases near the free end of the duplex. The resulting target-probe duplexes formed between the immobilized strand and the competitive targets **T15**, **T15x3**, **T15m**, and **R15** are shown. The chemically immobilized probe strand is highlighted in blue with target strands illustrated in black. The fluorescein label is green and the mismatched base pairs in the secondary duplex are indicated in red.

The competitive targets selected for this study included the previously studied **T15**, **T15x3**, and **T15m** with the addition and **R15**, a perfectly complementary RNA analog of **T15**. The **R15** strand was selected to evaluate the differences between displacement by a DNA and RNA target of the same sequence (except for the substitution of each thymine with a uracil in RNA). As many nucleic acid targets of interest are RNA species in physiological environments, this competitor is important in assessing the

efficacy of using dsProbes in nucleic acid assays for RNA species. The result of incubating **Flip T13** with these competitive targets as well as in the absence of a competitive target (**Dissociation**) is presented in Figure 6.3.2.

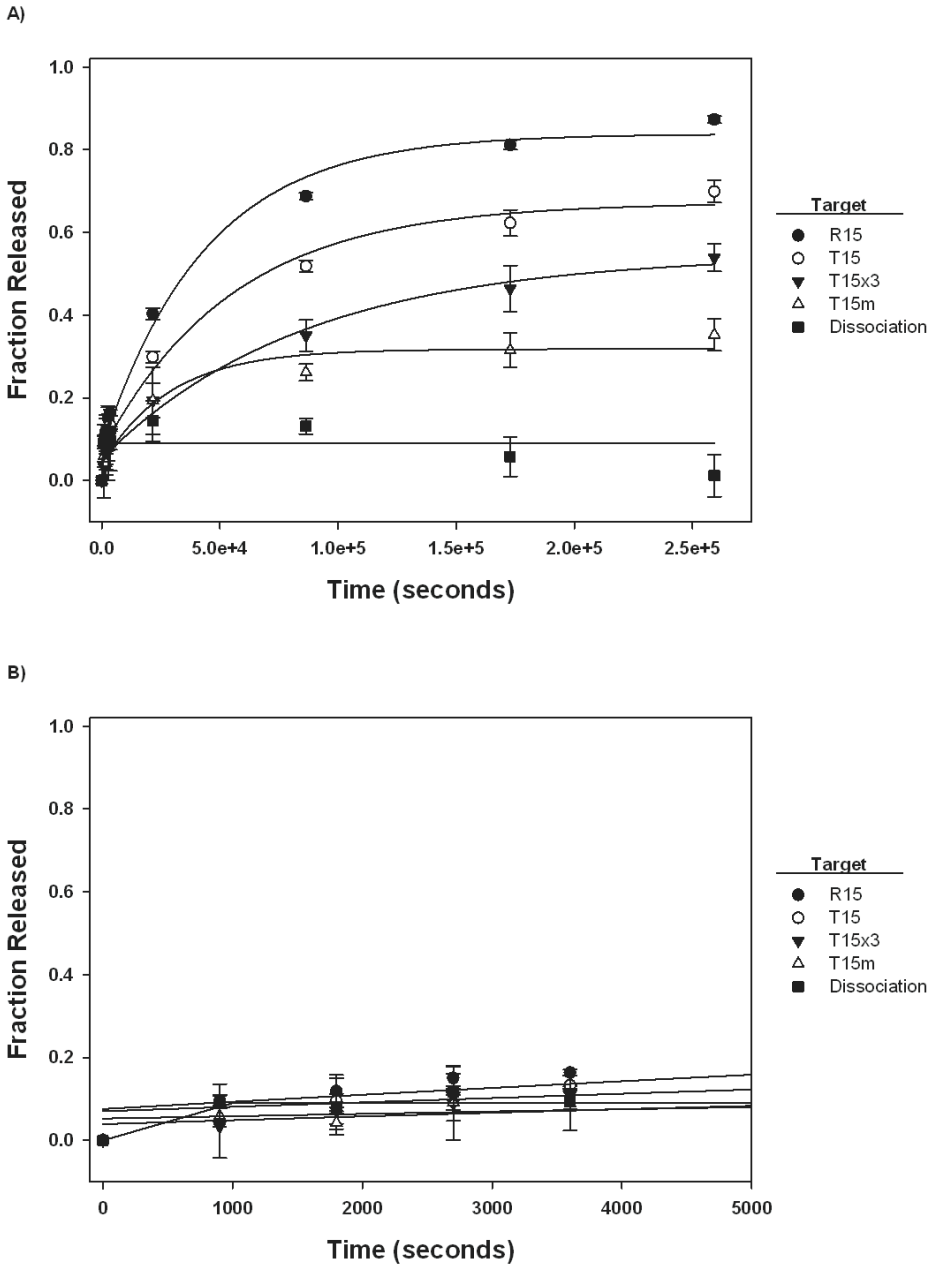

Figure 6.3.2. Fraction of original hybridization partner released from **Flip T13** dsProbe as a function of incubation time with competitive targets for A) the total time duration of 72 h (259,200 s) and B) a blow-up of 1 h (3,600 s). In addition to the competitive targets **T15m**, **T15x3**, **T15** and **R15**, a control in the absence of competitive target labeled as **Dissociation** was also included.

In comparing the release of the original hybridization partner from **Flip T13** dsProbe to the release of the **P21:T13** dsProbe in Figure 5.3.4, one notices that there is generally a larger fraction released with the **Flip T13** dsProbe system after incubation with the competitive targets. The release observed by the **Dissociation** sample peaks at a value of 14%. This result indicates that the **Flip T13** dsProbe exhibits limited loss due to thermal dissociation under the conditions of incubation at room temperature. For the competitive targets, there is a clear distinction in fraction released between targets with a mismatch compared to perfectly complementary targets, between targets with a near end mismatch as opposed to a center mismatch, and between DNA and RNA targets. Distinction between a perfectly complementary DNA target and targets containing a single mismatch can be observed within 24 h. Incubation with the two mismatched targets **T15m** and **T15x3** both result in 19% fraction released whereas incubation with the **T15** competitive target results in a fraction released of 30% after only 6 h (21,600 s). Divergence between the fractions released of the two mismatch targets begins at 24 h (86,400 s) at which time there is 26% partner strand of the **Flip T13** released for dsProbes incubated with **T15m** compared to 35% release for dsProbes incubated with **T15x3**. By the end of the experiment the differences in fraction released continued to increase with 35% release observed for dsProbes incubated with **T15m**, 54% displacement of dsProbes incubated with **T15x3,** and 70% release of dsProbes incubated with **T15**. Lastly, the comparison between fractions released of dsProbes incubated with either the perfectly complementary DNA target, **T15**, or RNA target, **R15**, reveals a consistently higher fraction released for the **R15** system than the **T15** system starting as early as 1 h (3,600 s). By the conclusion of the experiment, the dsProbes incubated in the

presence of the **R15** target had a total fraction released of 87%. An analysis of the normalized fraction displaced and subsequently the observed displacement rate was then performed using the approach previously described in Chapters 4 and 5. It should be noted that the normalized fraction displaced shown in Figure 6.3.3 does not reach equilibrium.

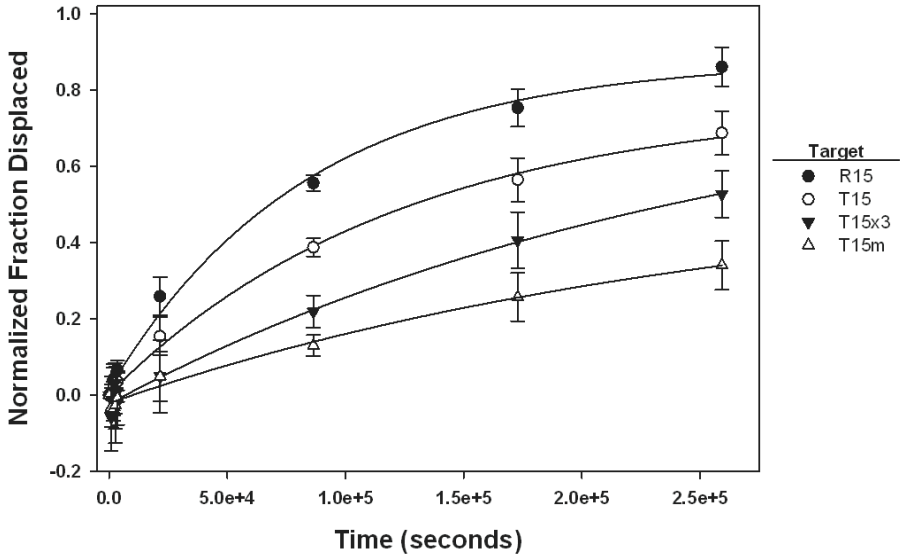

Figure 6.3.3. Normalized fraction displaced for the **Flip T13** dsProbe after incubation with **T15**, **T15x3**, and **T15m** competitive targets.

As this study represents a change from the 5.1 µm microsphere substrate to the 1 µm microsphere substrate, a separate experiment was performed with the **P21:T13** dsProbe in order to assess whether or not the observed fraction displaced is a result of the orientation of the **Flip T13** dsProbe, with unhybridized bases extending out into solution, or the change from a 5.1 µm particle substrate to a 1 µm particle substrate. Figure 6.3.4 shows the release profiles for the **P21:T13** dsProbe immobilized to the 1 µm particle

substrate. The fraction released of the **P21:T13** dsProbe is significantly higher than observed for dsProbes immobilized to the 5.1 μm microsphere shown in Figures 4.4.6 and 5.3.4. This difference indicates that the substrate particle plays a significant role in the observed dsProbe release. While incubation with competitive targets **T15x3** and **T15** show similar fractions of released DNA for both **Flip T13** and **P21:T13**, there is a higher fraction released of the **Flip T13** dsProbe after incubation with the **T15m** and **R15** competitive targets than observed for the **P21:T13** dsProbe (35% versus 23% for the **T15m** target and 87% versus 76% for the **R15** target). Additionally, there is a greater stratification in the observed release between dsProbes incubated with the **T15** and **R15** competitive targets in the **Flip T13** dsProbe system. The most probable explanation for the discrepancy in the fraction released for the **P21:T13** dsProbe on 5.1 μm particle substrates versus 1 μm substrates is the related difference in the observed duplex density of the **P21:T13** dsProbe on each. Generally, the duplex density of **P21:T13** on the 1 μm particle substrate (3,552 duplexes per μm^2) was 33% to 50% of the value of the duplex density observed on the 5.1 μm particle substrate. This decreased density on the smaller microspheres suggests more facile access by the competitive target to the dsProbe and subsequently greater fraction of labeled hybridization partner released from the dsProbes. As the **Flip T13** dsProbe also has a lower duplex density (1,759 duplexes per μm^2) than other dsProbes on the 5.1 μm particle substrate, dsProbe density most likely is a significant factor in the amount of displacement observed for this system as well.

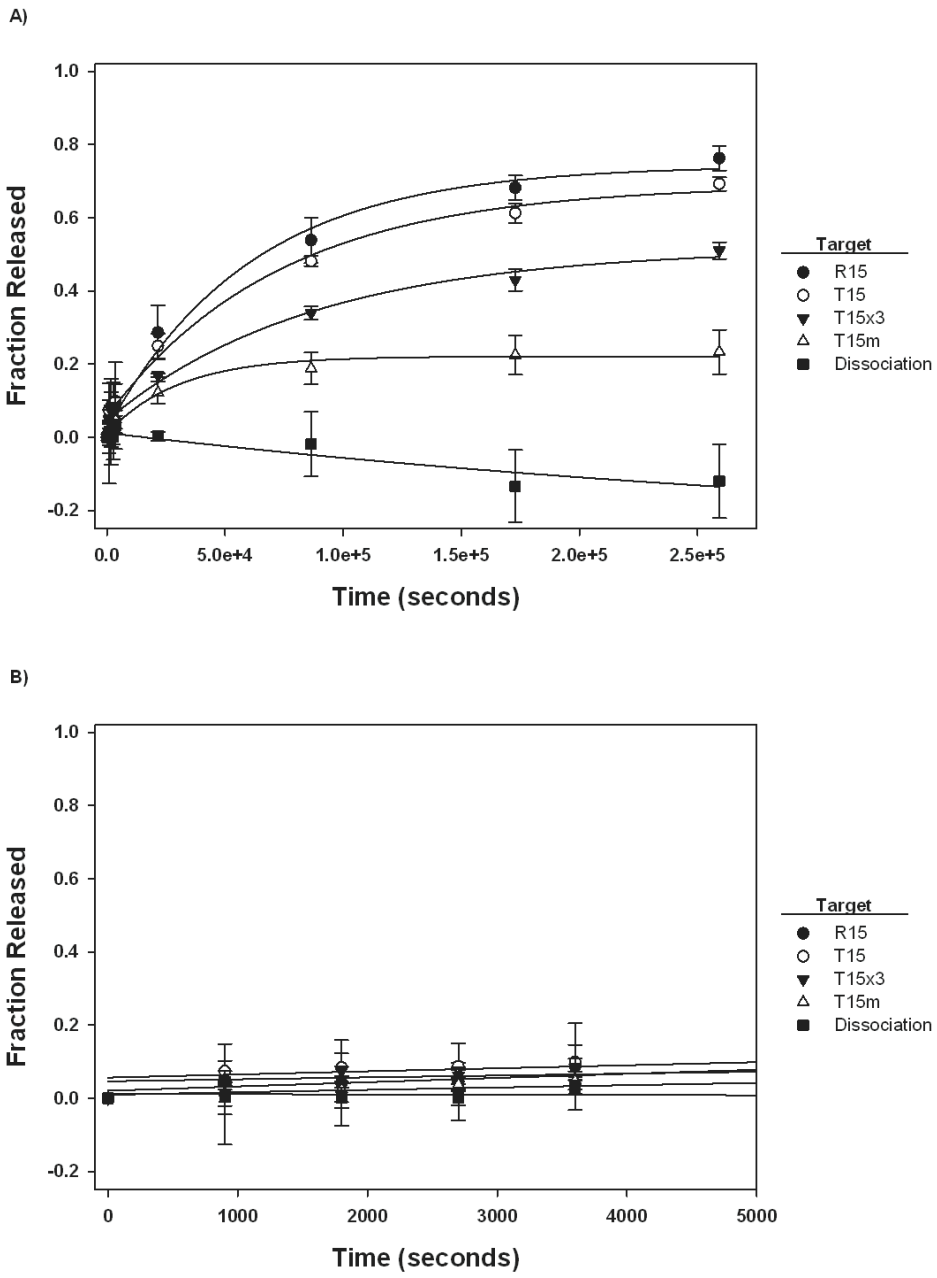

Figure 6.3.4. Fraction released of **T13** from dsProbe as a function of incubation time with competitive targets for A) 72 h (259,200 s) and B) 1 h (3,600 s). In addition to the competitive targets **T15m**, **T15x3**, **T15** and **R15** a control in the absence of any competitive target labeled as **Dissociation** was also included.

6.4 Conclusions

The results of competitive hybridization with the **Flip T13** dsProbe system highlight several features for competitive hybridization events in nucleic acid detection. First, the higher affinity of the **P21:T13** dsProbe is an advantage over **P21:T11** and **P21:T15m** for increasing the discrimination between competitive targets. Reorienting this dsProbe to form the **Flip T13** in conjunction with reducing the size of the particle substrate resulted in a more noticeable distinction in competitive target displacement. However, because the change to a 1 μm particle substrate also resulted in a lower initial duplex density for both the **Flip T13** and **P21:T13** dsProbes, the relative contributions to release kinetics due to dsProbe orientation and initial duplex density is unclear. The **Flip T13** dsProbe did demonstrated a clear difference in fraction released between perfectly complementary targets and targets with a single mismatch. Additionally, there is a clear distinction between the displacement of a target with an end mismatch and target with a center mismatch. Finally, the preferential displacement of RNA competitive targets versus DNA targets with an analogous sequence is also shown. Comparing the fraction displaced after incubation with the **T15** DNA competitive target versus the **R15** RNA competitive target suggests a preference for the RNA/DNA duplex over the DNA/DNA secondary duplex. As early as 1960, studies motivated by inquiry into the mechanism of transcription have indicated the hybrid formation of DNA and RNA duplexes[1] with some results pointing to a stability preference for hybrid duplex formation over pure DNA duplexes[2]. Later, x-ray diffraction studies of crystallized RNA-DNA hybrids revealed the influence of the RNA strand on the conformation of the DNA strand of the duplex, as the ironically more flexible DNA strand may adopt either a C2´ or C3´ *endo*

sugar pucker conformation whereas the RNA strand more commonly retains the C3´ *endo* of the A-form structure[3]. Molecular Dynamics simulations have supported this conclusion and, based largely on DNA's ability to interconvert between the C2´ and C3´ *endo* conformations compared to RNA's rigidity of the C3´ *endo* conformation, revealed that the hybrid duplex structure is closer to the RNA A-form conformation than the traditional B-form conformation found in DNA duplexes[4, 5]. These conformational variations are perhaps exploited by enzymes such as RNase H in selecting specifically the RNA strand of the RNA-DNA hybrid in intracellular cleavage events, an important structural consideration for antisense-based therapeutics[5].

These results help to explain and support the competitive hybridization behavior of the RNA target relative to its DNA counterpart. Both strands should have similar affinity based on sequence design, but the RNA competitive target consistently shows greater fraction released at all time points one hour and beyond. This difference in behavior can be explained by the enhanced stability of the RNA-DNA hybrid compared to an analogous DNA-DNA duplex. The conformational influence of the RNA strand on the dsProbe, assuming the formation of some tertiary intermediate complex, would induce an unfavorable change in the immobilized probe strand which would facilitate the displacement of the initial hybridization partner of the dsProbe. Furthermore, the relative stability of the resulting RNA-DNA hybrid duplex is greater than the DNA-DNA duplex. Work by Lesnik and Freier specifically demonstrates that for RNA-DNA duplexes of 70-80% deoxypyrimidine base content and moderate A-T/U content the hybrid duplex is more stable than the DNA-DNA duplex[6]. The RNA-DNA hybrid resulting from competitive hybridization in the **Flip T13** study would have 66% deoxypyrimidine

content, a value consistent with the deoxypyrimidine content proposed by Lesnik and Freier. These factors contribute to and explain that while absent base mismatches or different duplex lengths, the induced conformational differences between an RNA and DNA competitive target are sufficient to result in a distinct competitive hybridization behavior as observed with the **Flip T13** dsProbe.

6.5 References

1. Rich, A., *A Hybrid Helix Containing Both Deoxyribose and Ribose Polynucleotides and Its Relation to the Transfer of Information Between the Nucleic Acid.* Proceedings of the National Academy of Sciences of the United States of America 1960. **46**: p. 1044 - 1053.

2. Schildkraut, C.L., et al., *Formation and Properties of Polyribonucleotide-Polydeoxyribonucleotide Helical Complexes.* The Journal of Biological Chemistry, 1960. **236**(1): p. PC2 - PC4.

3. Wang, A.H.-J., et al., *Molecular structure of r(GCG)d(TATACGC): a DNA-RNA hybrid helix joined to double helical DNA.* Nature, 1982. **299**: p. 601 - 604.

4. Cheatham, T.E. and P.A. Kollman, *Molecular Dynamics Simulations Highlight the Structural Differences among DNA:DNA, RNA:RNA, and DNA:RNA Hybrid Duplexes.* Journal of the American Chemical Society, 1997. **119**: p. 4805 - 4825.

5. Noy, A., et al., *Structure, Recognition Properties, and Flexibility of the DNA-RNA Hybrid.* Journal of the American Chemical Society, 2005. **127**: p. 4910 - 4920.

6. Lesnik, E.A. and S.M. Freier, *Relative Thermodynamic Stability of DNA, RNA, and DNA:RNA Hybrid Duplexes: Relationship with Base Composition and Structure.* Biochemistry, 1995. **34**: p. 10807 - 10815.

CHAPTER 7

Relating the Nearest Neighbor Model to Experimental Trends in Competitive Hybridization

7.1 Introduction

Thermodynamic analysis of DNA hybridization at the molecular level is based on determining the free energy changes between single-stranded and double-stranded states. There has been a significant effort to model these free energy changes as nearest neighbor (NN) interactions. The following chapter will apply and extend key principles of NN models to compare the stability of primary and secondary duplexes as they apply to our system. The published results of SantaLucia's group and those of Sugimoto and colleagues describing the energetic contributions of DNA/DNA base pairs, RNA/DNA base pairs, mismatched base pairs, and dangling ends are applied to the current research. The calculated thermodynamic parameters are determined for the dsProbes as well as the resulting duplexes after competitive hybridization. Comparisons between the hybridization behaviors predicted by NN modeling and the observed trends in competitive hybridization are discussed. As past studies in this area have focused on soluble oligonucleotides, suggestions for comparing and extending this type of sequence-dependent modeling to immobilized strands as well as competitive hybridization events are also provided.

7.2 Calculation of Free Energy

One of the most widely applied models to analyzing the free energy of DNA hybridization events is the nearest neighbor model developed in large part by the efforts of SantaLucia's group. The nearest neighbor model, or NN model, is based on the assumption that the stability of a base pair is dependent not only on its composition but also the composition of neighboring base pairs[1]. This assumption means that the stability of a given duplex can be predicted based on the knowledge of its sequence, the salt concentration and temperature of the solution. Generally, the thermodynamic parameters for sets of short duplexes are obtained from melting studies. Analysis of these results provides the NN parameters ($\Delta G^\circ, \Delta H^\circ, \Delta S^\circ$) for sets of two base pairs[2-4]. The values for the change in free energy is commonly given at the temperature of 37 °C because of its relevance to physiological conditions, but ideally the modeling is most consistent for temperatures at or near 50 °C[5]. As both primary and competitive hybridization for our studies occurred at room temperature (~ 22° C) the change in free energy was adjusted for this temperature regime.

To begin modeling the free energy change due to hybridization for the sequences used in our studies, NN parameters were selected from reported results. The ΔG° values for DNA/DNA nearest neighbor pairs were taken from Sugimoto et al. 1996[3]. The ΔG° values for RNA/DNA nearest neighbor pairs were taken from Sugimoto et al. 1995[2]. The ΔG° values for NN pairs of DNA containing C-C mismatches were obtained from Peyret et al[4]. The free energy contribution from 5´ dangling ends, which occurs for the **P21:T13** and **P21:T11** dsProbes, were obtained for the first dangling base

pair from Bommarito et al[6]. The free energy contribution to hybridization of the one remaining unhybridized base in **T13** duplexes and three remaining unhybridized bases in **T11** duplexes are not considered in the stability calculation. Finally, the free energy contribution of duplex initiation was taken for RNA/DNA duplexes from Sugimoto et al. 1995[2] and for DNA/DNA duplexes from Sugimoto et al. 1996[3]. All values taken from the literature were corrected for room temperature and 154 mM salt conditions.

Temperature corrections to convert the reported ΔG° values from the literature at 37° C to 22° C were completed as follows. The enthalpic and entropic contributions from literature were substituted into the standard Gibbs free energy statement with T = 295 K.

$$\Delta G^\circ_{22^\circ C} = \Delta H^\circ - (295K)\cdot\Delta S^\circ \qquad (1)$$

This value of free energy change was then corrected for the salt concentration of the PBS buffer used for hybridization (154 mM Na^+). The salt concentration correction taken from SantaLucia and Hicks[5] is as follows:

$$\Delta G^\circ_{22^\circ C}[0.154M]_{Na^+} = \Delta G^\circ_{22^\circ C}[1M]_{Na^+} - 0.114\cdot\frac{N}{2}\cdot\ln[0.154M]_{Na^+} \qquad (2)$$

where $\Delta G^\circ_{22^\circ C}[1M]_{Na^+}$ corresponds to the free energy contribution calculated for 1M Na^+ concentration after the temperature correction and where N corresponds to the number of phosphates in the duplex. For the case of applying the salt concentration correction to the

NN parameters themselves $N = 1$[5]. Applying these corrections for the free energy changes reported in the literature gives the NN parameters listed in Table 7.2.1 for RNA/DNA and DNA/DNA duplexes.

Table 7.2.1. RNA/DNA and DNA/DNA Nearest Neighbor parameters corrected for temperature and salt concentration. The NN parameters are listed as 5´ to 3´ / 3´ to 5´. The notation "r" refers to an RNA sequence and "d" refers to a DNA sequence. The salt concentration used was 0.154 M Na^+ and the temperature was 22° C. Values were corrected from reported values in literature[2, 3, 5].

RNA/DNA	$\Delta G°_{22°C}$ (kcal/mol)	DNA/DNA	$\Delta G°_{22°C}$ (kcal/mol)
rAA/dTT	-1.23286	AA/TT	-1.43286
rAC/dTG	-2.16486	AT/TA	-1.00936
rAG/dTC	-2.06086	TA/AT	-1.06536
rAU/dTA	-1.14286	CA/GT	-1.89836
rCA/dGT	-1.19386	CT/GA	-1.65536
rCC/dGG	-2.34936	GA/CT	-1.76086
rCG/dGC	-2.29886	GT/CA	-1.77086
rCU/dGA	-1.08186	CG/GC	-3.13836
rGA/dCT	-1.41086	GC/CG	-2.60536
rGC/dCG	-2.84886	GG/CC	-2.41536
rGG/dCC	-3.28286		
rGU/dCA	-1.32136		
rUA/dAT	-0.84936		
rUC/dAG	-1.73786		
rUG/dAC	-1.91536		
rUU/dAA	-0.65536		

The NN parameters for the mismatches and dangling ends are listed in Table 7.2.2 along with the initiation parameters of duplex formation for both RNA/DNA and DNA/DNA duplexes. As with the NN parameters, the same temperature and salt correction methodologies were used to obtain values corresponding to the conditions of our primary and competitive hybridization reaction conditions.

Table 7.2.2. Nearest Neighbor parameters for C-C mismatch, dangling ends and the duplex initiation parameters corrected for temperature and salt concentration. The NN parameters are listed as 5´ to 3´ / 3´ to 5´. Both C-C mismatches and Dangling Ends correspond to DNA sequences. The salt concentration used was 0.154 M Na^+ and the temperature was 22° C. Values were corrected from reported values in literature[4-6].

C-C Mismatch	$\Delta G°_{22°C}$ (kcal/mol)
AC/TC	1.372186
CA/CT	1.401086
CG/CC	0.701136

Dangling Ends	$\Delta G°_{22°C}$ (kcal/mol)
GT/_A	0.331636
TC/_G	-0.67786

Duplex Initiation	$\Delta G°_{22°C}$ (kcal/mol)
DNA	3.361636
RNA	3.157136

The total free energy for duplex formation can be determined by summing the nearest neighbors and adding the contribution due to duplex initiation and symmetry terms as follows:

$$\Delta G^{\circ}_{duplex} = \Delta G^{\circ}_{initiation} + \Delta G^{\circ}_{symmetry} + \sum \Delta G^{\circ}_{NN} \qquad (3)$$

The free energy contribution due to the symmetry terms arises from the duplex formation of same sequence duplexes hybridized in anti-parallel orientation and involving perfectly complementary bases[5]. The duplexes in these studies have no same-sequence hybridization but rather hybridization between two distinct sequences resulting in a zero free energy contribution due to symmetry.

In order to illustrate the determination of the free energy of duplex formation used in this chapter, Figure 7.2.1 illustrates the **T11** duplex and the component NN interactions that comprise the total free energy.

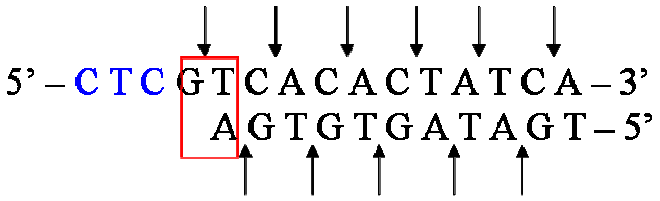

Figure 7.2.1. Schematic illustration of the **T11** duplex NN terms indicated by an arrow between the bases of the NN units. For clarity, the red box denotes the NN parameter for the dangling end contribution. The bases highlighted in blue correspond to bases that were not considered in the free energy calculations for the duplex.

The free energy is then determined by summing the NN contributions as follows:

$$\Delta G^{\circ}_{duplex} = \Delta G^{\circ}_{initiation} + 0 + (\Delta G^{\circ}_{GT/\_A} + \Delta G^{\circ}_{TC/AG} + \Delta G^{\circ}_{CA/GT} + \Delta G^{\circ}_{AC/TG} + \Delta G^{\circ}_{CA/GT} + \Delta G^{\circ}_{AC/TG} + \Delta G^{\circ}_{CT/GA} + \Delta G^{\circ}_{TA/AT} + \Delta G^{\circ}_{AT/TA} + \Delta G^{\circ}_{TC/AG} + \Delta G^{\circ}_{CA/GT})$$

Substituting the values from Table 7.2.1 and 7.2.2 yields

$$\Delta G^{\circ}_{duplex} = 3.36 + 0 + (0.33 - 1.76 - 1.90 - 1.77 - 1.9 - 1.77 - 1.66 - 1.07 - 1.01 - 1.76 - 1.9)$$

$$\Delta G^{\circ}_{duplex} \approx -12.81$$

where the values above have been rounded to two decimal places for convenience. The graphical data, in subsequent figures, however, represent values of ΔG° carried out to at least six significant figures. All the duplexes formed by either primary hybridization or competitive hybridization in Chapter 5 and 6 are similarly analyzed in terms of NN pairs as well as the RNA/DNA duplex formed via competitive hybridization. Figure 7.2.2 presents the resulting free energy of duplex formation (-ΔG) for each of these duplex pairs. The negative sign is merely a convention applied to present the free energy change above the x-axis to facilitate easier comparison.

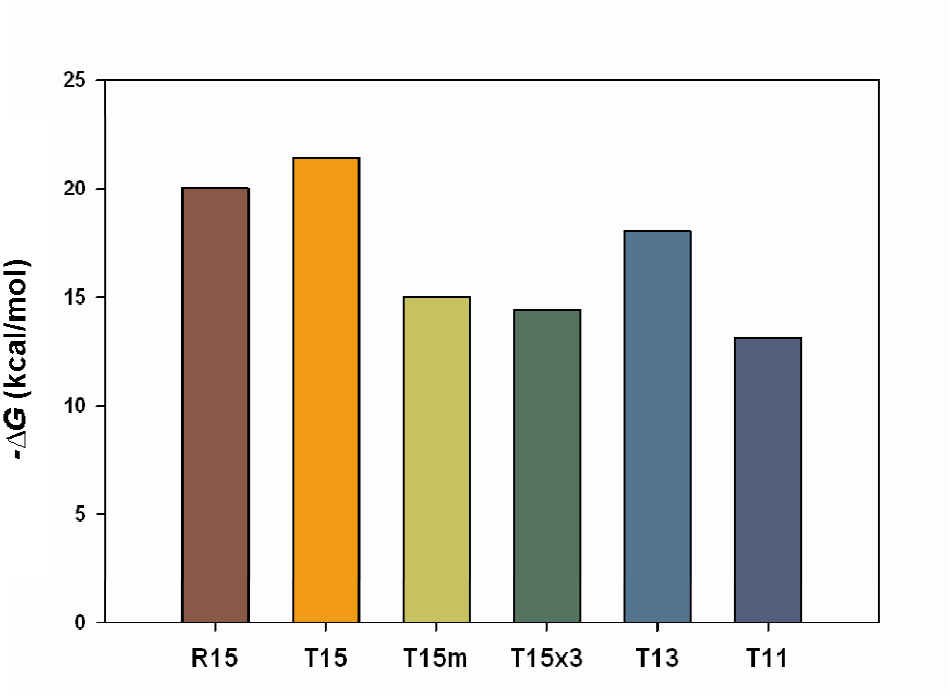

Figure 7.2.2. Calculated change in free energy of duplex formation based on NN analysis for the duplexes formed from both primary and competitive hybridization. The change in free energy is reported as the negative free energy to aid interpretation. The **P21:T13** dsProbe is considered equivalent to the **Flip T13** dsProbe.

The thermodynamic preference of one duplex over another is a driving force in the process of competitive hybridization. The difference between the free energy of duplex formation of one duplex compared to another provides a means to asses this thermodynamic driving force. Figure 7.2.3 presents the negative change in the change of free energy ($-\Delta\Delta G$) between a given dsProbe and target-probe pair resulting from competitive hybridization with the target. The sign convention for this presentation is such that a positive value indicates that competitive displacement of the original hybridization partner in the dsProbe by the target is favorable whereas a negative value indicates that competitive displacement is unfavorable.

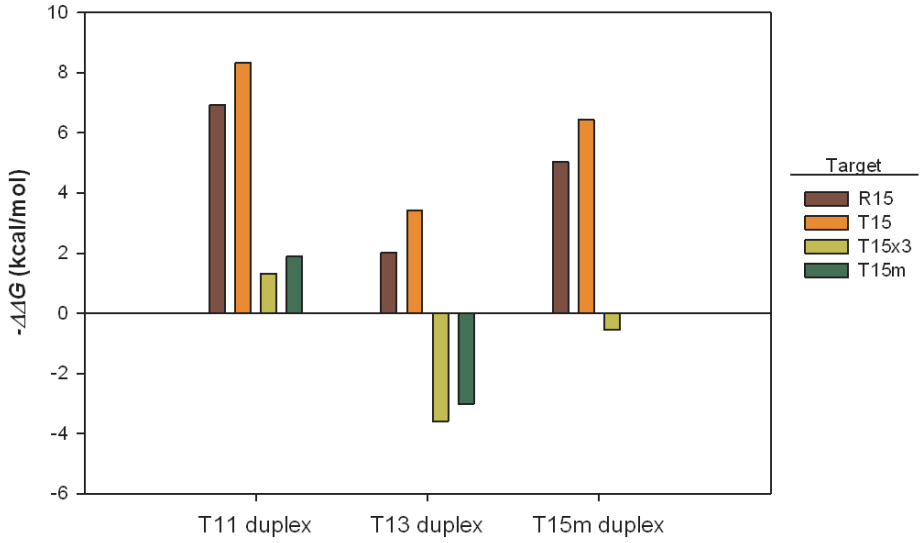

Figure 7.2.3. Change in the change in free energy *(-ΔΔG)* for formation of a secondary duplex due to a hybridization event between the competitive target with a given dsProbe. The values were obtained by subtracting the difference in free energy change between the original dsProbe duplex and secondary probe-competitive target duplex. Negative values indicate an unfavorable competitive hybridization event. The **P21:T13** dsProbe is considered equivalent to the **Flip T13** dsProbe.

The formation of the **T15** duplex results in the greatest change in free energy, which suggests that, this duplex is the most favorable of all the competitive targets considered. Comparing the differences in free energy between dsProbes and the **T15** duplex indicates that this competitive target is predicted by NN methods to be the most effective competitor, followed by **R15**. Experimental data from the **Flip T13** dsProbe study in which the **T15** and **R15** competitive targets are compared side by side, however, do not support this conclusion. In fact incubation with the **R15** competitive target resulted in a total fraction displaced of 87% compared to the 70% observed for dsProbes incubated with **T15**. Additionally, duplex formation with the competitive target **T15x3** is not predicted to facilitate a large thermodynamic driving force for displacement by the

analysis in Figure 7.2.3. The NN method predicts that the **T15m** target is equally if not more likely to result in duplex formation. However, for all dsProbes analyzed, incubation with the **T15x3** competitive target resulted in a higher fraction displaced than for the dsProbes incubated with **T15m**. Thus, while the NN approximation considers a single mismatch to be equivalent regardless of location, the result of competitive hybridization studies indicate preferential displacement occurs by the target with the longer segment of consecutive complementary bases.

These discrepancies between what the NN stability model predicts and what is experimentally observed in competitive hybridization studies may be accounted for by differences in the systems considered. The model represents the predicted change in free energy due to primary hybridization event, not a competitive or secondary hybridization event. Also, the NN model was developed from melting studies of duplexes freely diffusing in solution. In our case we have chemically immobilized the duplex to the surface of a particle substrate. The spontaneous process of hybridization correlates to a negative change in free energy, depending on temperature. The interplay of entropy and enthalpy is such that the loss of entropy as a result of hybridization, which restricts the conformations of the single DNA strands, acts to oppose duplex formation whereas the enthaplic contribution of hydrogen bonding between the bases acts to promote hybridization. Additionally, the structure of the resulting duplex favors a hybridization event in so much as the duplex localizes the hydrophobic bases in the interior of the duplex away from the solvent water molecules. The transition of duplex formation results in hydrophobic bases surrounded by loosely associated water molecules into a centralized hydrophobic region. Both stacking of the hydrophobic bases and hydrogen

bond formation contribute to a net negative change in free energy that drives the hybridization of complementary DNA strands in solution. In the case of the immobilized probe, the DNA probe strand has been restricted in the number of available conformations by covalently linking one end to the microsphere. This restriction results in a smaller entropic penalty for hybridization. Entropy, *S*, can be defined as

$$S = k \ln \Omega_i \tag{4}$$

where *k* is the Boltzmann's constant and Ω_i corresponds to the number of allowable energy states of a system. Subsequently, by comparing the change in entropy between two states of a system, i.e. immobilizing a soluble strand to a solid support, we can say

$$\Delta S = k \ln\left(\frac{\Omega_2}{\Omega_1}\right) \tag{5}$$

If the number of states or conformations of the single strand of DNA has been reduced via immobilization onto the particle surface, or $\Omega_2 < \Omega_1$, then $S_2 < S_1$. If we consider the entropy of the duplex to be described by S_3, then the transition from either an immobilized or soluble single strand to a duplex would result in a restriction in the number of conformation such that $S_3 < S_2 < S_1$. Comparing the change in entropy from an immobilized probe to duplex versus a soluble probe to duplex results in $\Delta S_{2\to 3} < \Delta S_{1\to 3}$, or a reduced entropic barrier to hybridization for the immobilized probe case.

Based on free energy considerations alone, it would seem that the immobilization of one strand would promote duplex formation. However, by immobilizing DNA to a surface, the steric effects and electrostatic repulsions between probe and target strands become more significant factors especially as probe density increases. Modeling of hybridization to immobilized DNA strands has demonstrated that these effects may result from Coulombic interaction between strands[7]. In both immobilized arrays[8] and particle platforms[9], high DNA probe densities have been observed to limit hybridization.

7.3 Conclusions

In this chapter, a discussion of the Nearest Neighbor thermodynamic modeling of DNA stability was applied to the dsProbes and competitive targets investigated in the competitive hybridization studies. A comparison between the likelihood of duplex formation indicated by the NN modeling and what was observed in competition studies revealed two examples of inconsistency. The **R15** and **T15x3** competitive targets were both underestimated by the free energy calculations in comparison to **T15** and **T15m**, respectively. The NN model also considered the presence of a single mismatch to be nearly equivalent regardless of whether the mismatch was located in the middle or near the end of the duplex. In the experimental competitive hybridization studies presented in Chapters 4-6, however, preferential displacement was observed for the competitive target with the longer sequence of consecutively matched base pairs, **T15x3**. It is important to note that thermodynamic calculations based on the Nearest Neighbor Model do not

currently consider the effect of strand immobilization on duplex formation free energy. Also, while suggestive of the likelihood of one duplex forming over another, the current thermodynamic models do not include an initiation term corresponding to a competitive event but rather only a primary hybridization event. The addition of this term could provide meaningful input to the free energy comparisons between probe and target pairings in hybridization-based assays that employ a competitive method rather than primary hybridization. A similar approach used in developing NN parameters could be extended to account for immobilized duplexes. By performing a series of melting studies with various sequences of immobilized duplexes, similar NN parameters may be developed. Understanding how immobilization affects the stability of DNA duplexes could aid in the development of nucleic acid-based detection methodologies immobilized to a solid support.

7.4 References

1. SantaLucia, J., *A unified view of polymer, dumbbell, and oligonucleotide DNA nearest-neighbor thermodynamics.* Proceedings of the National Academy of Sciences of the United States of America 1998. **95**: p. 1460 - 1465.

2. Sugimoto, N., et al., *Thermodynamic Parameters To Predict Stability of RNA/DNA Hybrid Duplexes.* Biochemistry, 1995. **34**: p. 11211 - 11216.

3. Sugimoto, N., et al., *Improved thermodynamic parameters and helix initiation factor to predict stability of DNA duplexes.* Nucleic Acids Research, 1996. **24**(22): p. 4501 - 4505.

4. Peyret, N., et al., *Nearest-Neighbor Thermodynamics and NMR of DNA Sequences with Internal A-A, C-C, G-G and T-T Mismatches.* Biochemistry, 1999. **38**: p. 3468 - 3477.

5. SantaLucia, J. and D. Hicks, *The Thermodynamics of DNA Structural Motiffs.* Annual Review of Biophysics and Biomolecular Structure, 2004. **33**: p. 415 - 440.

6. Bommarito, S., N. Peyret, and J.S. Jr., *Thermodynamic parameters for DNA sequences with dangling ends.* Nucleic Acids Research, 2000. **28**(9): p. 1929 - 1934.

7. Vainrub, A. and B.M. Pettit, *Coulomb blockage of hybridization in two-dimensional DNA arrays.* Physical Review E, 2002. **66**: p. 041905.

8. Peterson, A.W., R.J. Heaton, and R.M. Georgiadis, *The effect of surface probe density on DNA hybridization.* Nucleic Acids Research, 2001. **29**(24): p. 5163 - 5168.

9. Henry, M.R., et al., *Real-Time Measurements of DNA Hybridization on Microparticles with Fluorescence Resonance Energy Transfer.* Analytical Biochemistry, 1999. **276**: p. 204 - 214.

CHAPTER 8

Conclusions

8.1 Comparisons with Modern Approaches to Nucleic Acid Detection

The current research highlighted in this thesis involved in-depth studies of hybridization between DNA duplexes and competitive targets. The original duplexes were presented in two contexts: 1) DNA linkages forming fluorescent colloidal satellite assemblies and 2) fluorescently labeled dsProbes immobilized on a microsphere substrate. In both cases variations in sequence length and presence of mismatches were used to generate an affinity difference between the initial dsProbe and the competitive target of interest. Successful competitive hybridization events in the satellite assembly studies resulted in disassembly of the colloidal satellites. We found that disassembly required the presence of perfectly matched competitive targets. In studies involving fluorescent dsProbe immobilized on microspheres, successful competitive hybridization events resulted in a measurable loss of fluorescence intensity associated with the microsphere population. The kinetics of competitive hybridization varied greatly depending on the sequence characteristics of both the dsProbes and the competitive targets. Given the overall success of these studies, our approach employing competitive hybridization interactions offers promise as an alternative to current methods for detecting soluble nucleic acid targets of interest.

Using colloidal particles to form fluorescent satellite assemblies that only disassembly in the presence of the target of interest provides an advantage in its

simplicity since disassembly events can be observed with light microscopy. The advantage of this approach is a simple binary result: an assembled state if the specific target is lacking; a disassembled state if the target is present. While both results were observed in the current experimental system, it is important to note that the competitive target concentration used for these studies was intentionally high to drive competition forward. Thus, the 48 and 72 h time points typically necessary to observe disassembly (where favorable) do not correspond to a fast detection protocol. Additionally, the heterogeneity in fluorescent particle coverage for a given sample does not provide a uniform detection platform. Similar DNA-linked colloidal aggregate systems, however, also involve heterogeneity in terms of different cluster sizes. These aggregate systems also use DNA linkages responsive to environmental stimuli, such as target strands or temperature. In particular, aggregate systems comprised of gold nanoparticles provide a unique opportunity, based on plasmon resonance effects, to both visibly observe a "response" as well as spectroscopically characterize it. These systems have been able to provide concentration-dependent responses to the presence of desired analytes in more dilute amounts and in faster time periods relative to the current system.

While these particular optical properties and low target sensitivities are not presently available with our system, the current research does consider several features pertinent to nucleic acid detection. First, the colloidal particles are of a sufficient size to facilitate observation of individual assemblies or particles (if disassembled) with light microscopy. Second, the DNA duplexes used to form linkages between the constituents of the satellite structures were selected based on the *Salmonella* genome, a relevant target of interest in pathogen detection. Third, variations of the DNA duplex linkages were

successfully incorporated as length differences and mismatches to weaken linkages enough to allow competitive displacement to occur in the presence of specific target sequences. Fourth, the initial formation of the satellite structures was found to be more dependent on DNA density than duplex affinity. Varying DNA density may provide an avenue to further tune the behavior of these colloid-based systems.

As opposed to using dsProbes immobilized on both ends between multiple particle surfaces in satellite assemblies, competitive hybridization was also evaluated in the context of fluorescently labeled dsProbes immobilized only on one end to a microsphere surface. The majority of modern nucleic acid-based detection platforms utilize a single-stranded DNA probe to capture a target of interest and involves a separate labeling step to detect or report the capture event. This secondary step is likely to require chemical modification of the target of interest. In order to ensure specific hybridization of the target of interest, the capture step is commonly performed in an elevated temperature environment or at long incubation times to approach equilibrium. The author suggests that our competitive hybridization approach adapted for fluorescence assays may address these two limitations in current detection technologies. In all competitive hybridization studies with the fluorescent dsProbes, incubation with the target of interest occurred at room temperature without the chemical modification of the target sequence needed to tag the target with a dye or other "reporter" molecule. The observed dsProbe release as a result of either dissociation or competition was measured as loss in fluorescence intensity with significant difference between release observed for the dissociation pathway compared to the competitive hybridization pathway. Because the dsProbe methodology incorporates the fluorescent label on the dsProbes themselves

(not the targets), the capture and signaling events in the presence of targets are directly linked and can be evaluated simultaneously.

In addition to elevated temperature conditions, the specificity of target detection is also evaluated by accounting for false signals from negative or nonspecific controls. A well-known example of these modern detection systems is the mismatch probe in the DNA microarray format. In order to access the specificity of a microarray probe for its target, a mismatch probe for each perfectly matched probe is also patterned onto the array[1, 2] as seen in the Affymetrix GeneChip™ system. The signals are compared from each probe and the mismatched probe signal is subtracted from the matched probe signal. This difference is reported as "Average Difference" (AD) and is given by the relationship

$$AD = \frac{\sum (PM - MM)}{\#\,\mathrm{Pr}\,obes} \tag{1}$$

where *PM* is the fluorescence associated with the perfectly matched probe for a given labeled target sequence, *MM* is the fluorescence associated with the mismatched probe for a given labeled target sequence, and *# Probes* is the total number of probe pairs making up the microarray. The value of *AD* corresponds to the signal of each target that is due to complementary base pairing.

Generally, this approach is sufficient to normalize the results against nonspecific hybridization and limit the number of false positives. What this approach may not be successful in screening out of analysis is the fluorescence contributions of hybridized targets with an end or near end location mismatch. In the scenario of a center mismatch

the resulting duplex would be interrupted in such a way as to typically reduce the number of consecutive perfectly matched base pairs by approximately 50%. Probe affinity models have demonstrated this disruptive influence of the center mismatch on the stability of the resulting target-probe duplex[3]. Though a center mismatch has a profound effect on duplex stability, an end or near end mismatch may not be as disruptive. Studies of hybridization in a spotted array format of tandem or consecutive mismatched base pairings has revealed that some mismatch targets with end located mismatches can have comparable signal intensities to their perfectly matched analogs[4]. In fact for gel spotted arrays, a mismatch located near the 5' termini, the free end of the probe, in the ultimate or penultimate position[5] is not readily distinguishable. Moving that mismatch to the 3rd to 5th position, however, results in a significant affect on the T_d or duplex retention temperature[6]. T_d is not an equilibrium parameter and may be different than the commonly cited duplex melting temperature, T_m, though it may be interpreted as a measure of specificity. Physically, T_d corresponds to the temperature at which 50% of the duplex remains intact for a given washing period[7]. While any resulting discrepancies may be mild in terms of percent signal change for many samples, their effect on fluorescence intensity becomes more important factors if targets exist at low concentrations or as low copy numbers per cell. Targets with mismatches at the penultimate or ultimate base pair position could readily occur and contribute to a false positive signal. Additionally, studies have demonstrated that some microarray probes can consistently express signals that are inaccurate based on cross hybridization with non-complementary targets or a failure to hybridize with target sequences[9]. In these cases the density of probes may influence the level of cross-hybridization observed.

A double-stranded probe approach based upon competitive hybridization addresses these challenges in two ways. First, the issue of cross-hybridization with other probe strands is dependent on available complementary bases and flexibility of the probe strand relative to the substrate to which it is immobilized. By utilizing a double-stranded, or dsProbe, the majority of bases that may be self-complementary on the probe strand would participate in the duplex, thus greatly reducing the likelihood of cross-hybridization. Second, the dsProbe approach addresses end location mismatch specificity by increasing the stringency of the assay and promoting preferential displacement of the original hybridization partner by higher affinity (i.e. perfectly matched) targets. The results of the **Flip T13** study support this conclusion, as there was an observable discrepancy in observed release after incubation with the end mismatch target **T15x3** and the complementary target **T15** (Chapter 6).

While currently unused in clinical and diagnostic applications, dsProbes may offer an alternative to modern single-stranded probe assays. Eliminating the necessity of an elevated temperature protocol to enforce specific hybridization is a meaningful step to extending the usefulness of nucleic acid detection in field test models. As all competitive hybridization studies were performed at room temperature or isothermal conditions, the current research demonstrates this capacity inherent to dsProbes. Similarly, the specificity of a dsProbe for a given target can be tuned by duplex sequence design in order to discriminate between competitive interactions of perfectly matched and mismatched sequences as demonstrated particularly well in the **Flip T13** dsProbe study. Finally, the reduction of target analysis from two distinct steps of capture and signaling found in single-stranded probe approaches to the single step, simultaneous capture and

signaling of a competitive hybridization event is advantageous to simplifying assay protocols as well as limiting the need for chemical modification to the target of interest. For these reasons, the author suggests that competitive hybridization assays with dsProbes may provide meaningful advantages for nucleic acid-based detection.

8.2 Development of General Guidelines for dsProbe Approach

The current research has explored competitive hybridization with dsProbes in several contexts. First, the affinity of the dsProbes was tuned by the sequence design parameters of length and incorporation of mismatches. The kinetics of competitive hybridization for these dsProbes of various affinities with a short perfectly complementary target was assessed. Second, the effect on competitive hybridization of target sequence location within a longer strand context was examined in the embedded target study. Third, the role of specificity of the target strand itself in dsProbe release was studied by comparing the competitive displacement of a short perfectly complementary target, a short target with a mismatch near the end of the strand, and a short target with a center mismatch. Fourth, the effects of dsProbe orientation and 1 μm compared to 5.1 μm particle substrate were considered in the **Flip T13** study in which unhybridized bases were oriented away from a 1 μm particle substrate in contrast to previous design. This study also explored the effect of mismatch location and compared displacement by DNA and RNA strands. Throughout these competitive hybridization studies, care was taken to distinguish between release by either the dissociation or competitive displacement pathways. Based on the results from early studies, changes in the competitive hybridization protocol have been discussed. Finally, the application of

the Nearest Neighbor Model to the present system highlighted discrepancies between NN predictions and observed experimental results. Drawing from the breadth of study represented by these results, it is advantageous to enumerate general considerations for the development of dsProbe approaches in nucleic acid-based detection as well as suggest potential areas of further study. Subsequently, the following section will generalize these findings and suggest direction for future efforts.

A successful dsProbe design must result in a probe that is stable at incubation conditions but responsive to the presence of the desired target. From these studies, 11 bases of a DNA based system is approaching the lower limit of desired stability. With ~45% release due to dissociation the **P21:T11** dsProbe was certainly the weakest of the three primary dsProbes studied. The most significant amount of competitive displacement of this dsProbe was observed within the first hour of incubation, making this probe responsive to high affinity competitive targets. **P21:T11** was only modestly able to distinguish between a perfectly matched target and a target with a center mismatch. However, **P21:T11** dsProbes were not able to distinguish between a perfectly matched target and a target with a mismatch three bases from the end of the strand. On the other hand, the **P21:T15** dsProbe, which has the same length and sequence as the **T15** competitive target, does not allow for significant dissociation but is nonresponsive. By incorporating a center mismatch within this dsProbe a more responsive dsProbe with relatively moderate timing in terms of displacement kinetics was generated. The limitation of the **P21:T15m** dsProbe is its inability to successfully distinguish between perfectly matched targets and targets containing a single mismatch. The author believes that from these results, it is more favorable to design a dsProbe with unhybridized bases

(i.e. a toehold region) rather than a center mismatch to promote competitive hybridization. This conclusion is supported by the success of the **P21:T13** and **Flip T13** dsProbes which exhibited distinct displacement responses depending on the presence or absence of mismatch as well as the mismatch location itself (center location versus end location).

In considering the dsProbe orientation relative to the substrate, positioning the unhybridized bases such that they extend away from the substrate surface (**Flip T13** dsProbe) resulted in both a faster and higher response level (i.e. higher fraction displaced at earlier times) as well as distinct stratification in the data sets dependent on target specificity. Also, comparisons between the 1 μm and 5.1 μm particle substrate for the **P21:T13** dsProbe suggest that the resulting lower DNA density on the 1 μm particle contributes to increased fraction released. Subsequently, the dsProbe density is a variable that should be considered more fully in future work in order to determine if the orientation or initial duplex density is more important to observed release kinetics. The **Flip T13** dsProbe study showed distinct displacement results for perfectly matched versus mismatched targets, center versus end mismatch targets, and DNA versus RNA target strands. The 13 base-long duplex segment in the dsProbe was relatively stable as evidenced by the limited dissociation. Finally, even though the two unhybridized bases are less than the three bases suggested as a critical nucleus size for hybridization to proceed, these two unhybridized bases appear sufficient to facilitate competition.

When targeting a recognition sequence within the context of an embedded target, there is a modest preference for targets to hybridize if the recognition sequence located at either end of the target strand. While the current research only considered competitive

hybridization interactions with recognition sequences embedded in model target strands composed of thymine base segments (as the nonhybridizing segments), future studies should incorporate recognition sequences within target strands of random sequence. Possible secondary structure of the target such as hairpin formation may be a challenge to isothermal assays based at room temperature. The presence of "self-hybridized" regions in the single-stranded target may compromise the ability of the dsProbe to interact with the recognition sequence. These potential challenges should be considered in more detail in future studies. Possible methods to overcome any such secondary structure within the target strand may include a thermal annealing approach as well as changes in the ionic strength of the solution.

Finally, the Nearest Neighbor model, derived from melting analysis of solution duplexes, does not accurately predict if competitive hybridization interactions are favorable. In all fairness, the model was not developed with competitive hybridization in mind. However, duplex stability based on sequence context is an important factor in dsProbe approaches as the affinity difference driving competitive hybridization events is derived largely from sequence variations. While the term ($-\Delta\Delta G$) should represent the difference in stability of one duplex relative to another and potentially assess if competitive hybridization is thermodynamically favorable, the application of the current model does not accurately correlate to the competitive hybridization behavior observed in the current experimental studies. There are two likely sources of this discrepancy: 1) the current system involves hybridization on immobilized probes, not soluble strands freely diffusing in solution (as considered in the NN model) and 2) the initiation term of the NN model is based on hybridization between two single strands, not between a duplex and

single strand as occurs during competitive hybridization in the current system. These two differences provide a needed area of further research focus in order to successfully extend the application of the NN approach to competitive hybridization. In a revised model, the term describing initiation of competition, for example, would depend first of all on the number of available bases relative to critical number of bases necessary for hybridization nuclei formation. Secondly, this new initiation term would need to account for the probability of displacing proximal bases in the initial duplex to further stabilize the hybridization nuclei and propagate formation of the secondary duplex. Considering the effect of immobilizing at least one strand to a substrate is yet another issue that merits attention by a revised model. This additional consideration would not only extend the application of NN modeling to competitive hybridization, but it would also provide additional capability in predicting the hybridization behavior in single-stranded probe systems such as microarrays or particle immobilized systems like xMAP^{TM} from Luminex. Such a model would have to account for the ionic strength of the solution, the length of the spacer, whether the probe is double-stranded or single-stranded, and the density of the probe immobilized. Following the experimental assumption used to derive the current NN model, a series of melting studies of immobilized duplexes of various sequences, solution ionic strength, and immobilized probe density is a recommended starting point to begin compiling the necessary data set to determine the thermodynamic parameters of immobilized duplexes.

These generalizations are offered to assist in further development of nucleic acid-based detection methods. Currently, single-stranded probe mechanisms are dominant in the field of diagnostics and clinical application. With greater understanding and efforts to

optimize the responsiveness of double-stranded probe formats, dsProbe assays may contribute an extended capability to this area of biotechnology. Linking target capture with reporting as presented in this signal loss approach results in a responsive assay that decreases the modifications necessary to the target of interest and subsequently simplifies the process of analysis. Using sequence-based affinity differences to drive competitive hybridization promotes an intrinsic stringency or specificity limitation. Specificity that is dependent on the probe construct and not environmental regulation (i.e. increased temperature) provides a degree of freedom not currently available in single-stranded probe based assays. While useful in a controlled laboratory environment, the current approach has potentially broader impacts since imposing isothermal specificity will be important to development of nucleic acid-based detection in field tests where such environmental control is not easily achieved.

8.3 References

1. Baldi, P. and G.W. Hatfield, *DNA Microarrays and Gene Expression: From Experiments to Data Analysis and Modeling*. 2002: Cambridge University Press. 213.

2. Knudsen, S., *Guide to Analysis of DNA Microarray Data*. 2nd ed. 2004, Hoboken: John Wiley & Sons, Inc.

3. Mei, R., et al., *Probe selection for high-density ologonucleotide arrays.* Proceedings of the National Academy of Sciences of the United States of America, 2003. 100(20): p. 11237 - 11242.

4. Fish, D.J., et al., *DNA multiplex hybridization on microarrays and thermodynamic stability in solution: a direct comparison.* Nucleic Acids Research, 2007. 35(21): p. 7197 - 7208.

5. Urakawa, H., et al., *Optimization of Single-Base-Pair Mismatch Discrimination in Oligonucleotide Microarrays.* Applied and Environmental Microbiology, 2003. 69(5): p. 2848 - 2856.

6. Urakawa, H., et al., *Single-Base-Pair Discrimination of Terminal Mismatches by Using Oligonucleotide Microarrays and Neural Network Analyses.* Applied and Environmental Microbiology, 2002. 68(1): p. 235 - 244.

7. Zheng, D., et al., *Characterization of Universal Small-Subunit rRNA Hybridization Probes for Quantitative Molecular Microbial Ecology Studies.* Applied and Environmental Microbiology, 1996. 62(12): p. 4504 - 4513.

8. Zhang, J., et al., *Detecting false expression signals in high-density oligonucleotide arrays by an in silico approach.* Genomics, 2005. 85: p. 297 - 308.

Appendix A

Calculation of Number of Duplexes between the Template Microsphere and Each Fluorescent Particle

A.1 Calculations

The contact area is a function of the fluorescent particle radius and the length of the DNA duplexes between the template microsphere and a fluorescent particle. The length of the DNA between the particle surfaces is the sum of the 12 carbon spacer group, unhybridized bases and the duplex segment of each double stranded probe. If we assume that the mismatched bases with a center mismatch have the same length duplex segment as their perfectly matched counterpart, then we only need to calculated the DNA lengths for 11,13, or 15 base-long duplexes formed between **T11**, **T13**, or **T15** targets and the probe.

The length of the hybridized duplex segment corresponds to the distance between hybridized bases and is equaled to (number of bases in duplex-1) x (0.34 nm between base pairs in B form DNA)

The length of the unhybridized bases in the dsProbe is equal to (number of unhybridized bases) x (0.59 nm corresponding to the phosphate to phosphate difference along the DNA backbone)

The length of each C-C bond in the 12 carbon spacer (extended conformation) is equal to

$$1.5 \text{ Å} \times \cos(\theta/2) = 1.24 \text{ Å}, \text{ where } \theta = 68°.$$

For 11 C-C bonds this result in a total length contribution of 1.368 nm for each 12 carbon spacer.

Length of 11 base duplex:

$L^{11}_{unstretched}$ = 2 (11 C-C bonds) + 4 unhybridized bases + duplex

$L^{11}_{unstretcehd}$ = 2 (1.368 nm) + 4 (0.59 nm) + 10 (0.34 nm) = 8.496 nm

DNA duplexes can be stretched, however, providing an important consideration for the calculation of the contact area. The calculated stretch length of the DNA segment is based on the work of Bustamante et al[1] and has been experimentally determined to be 1.7 times the unstretched duplex length.

$L^{11}_{stretch}$ = 2 (1.368 nm) + 4 (0.59 nm) + 1.7 x 10 (0.34nm) = 10.876 nm

Define the quantity as

$s = L_{stretch} - L_{unstretch}$

Thus for the 11 base duplex,

s^{11} = 10.876 nm – 8.496 nm = 2.38 nm

Similar calculations are described below for the 13 and 15 base long duplexes.

Length of 13 base duplex:

$L^{13}_{unstretched}$ = 2 (11 C-C bonds) + 2 unhybridized bases + duplex

$L^{13}_{unstretcehd}$ = 2 (1.368 nm) + 2 (0.59 nm) + 12 (0.34 nm) = 7.996 nm

$L^{13}_{stretch}$ = 2 (1.368 nm) + 2 (0.59 nm) + 1.7 x 12 (0.34nm) = 10.852 nm

s^{13} = 10.852 nm – 7.996 nm = 2.856 nm

Length of 15 base duplex:

$L^{15}_{\text{unstretched}}$ = 2 (11 C-C bonds) + duplex

$L^{15}_{\text{unstretcehd}}$ = 2 (1.368 nm) + 14 (0.34 nm) = 7.496 nm

L^{15}_{stretch} = 2 (1.368 nm) + 1.7 x 14 (0.34nm) = 10.828 nm

s^{15} = 10.828 nm – 7.496 nm = 3.332 nm

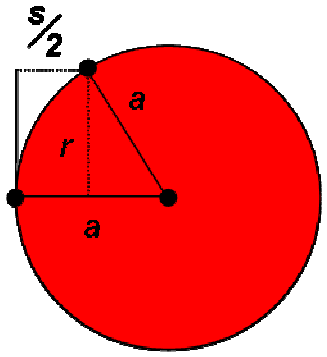

Figure A.1. Geometric parameters of the fluorescent particle that are used to calculate the contact area between the template microsphere and fluorescent particle.

If the radius of the contact area is defined by *r*, the radius of the fluorescent particle is given by *a*, and the length that the duplex segment must stretch on one side of the DNA bridge is $\frac{s}{2}$ then we can calculate *r* as follows:

$$r = \sqrt{a^2 + \left(a - \frac{s}{2}\right)^2}$$

and express the projected contact area as $A_{contact} = \pi \bullet r^2$.

For the 11 base duplexes:

$$r^{11} = \sqrt{100nm^2 + \left(100nm - \frac{2.38nm}{2}\right)^2}$$

$r^{11} = 15.38$ nm

$A^{11}{}_{contact} = \pi \cdot r^2 = 743.13$ nm^2

For the 13 base duplexes:

$$r^{13} = \sqrt{100nm^2 + \left(100nm - \frac{2.856nm}{2}\right)^2}$$

$r^{13} = 16.84$ nm

$A^{13}{}_{contact} = \pi \cdot r^2 = 890.83$ nm^2

For the 15 base duplexes:

$$r^{15} = \sqrt{100nm^2 + \left(100nm - \frac{3.332nm}{2}\right)^2}$$

$r^{15} = 18.18$ nm

$A^{15}{}_{contact} = \pi \cdot r^2 = 1{,}038.1$ nm^2

Multiplying the contact area, $A_{contact}$, with the duplex density obtained from flow cytometry results in the predicted number of duplex linkages between the template microsphere and a fluorescent particle.

Table A.1. Duplex density, contact area, and number of duplexes in contact area for the HODM (5.1μm) for a given target sequence.

Target	Duplex Density (oligos / nm^2)	Contact Area (in nm^2)	# Duplexes in contact area
T11	0.006303	743.13	5
T11m	0.000309	743.13	<1
T13	0.011816	890.83	11
T13m	0.005654	890.83	5
T15	0.012923	1,038.1	13
T15m	0.006392	1,038.1	7

Table A.2. Duplex density, contact area, and number of duplexes in contact area for the LODM (5 μm) for a given target sequence.

Target	Duplex Density (oligos / nm^2)	Contact Area (in nm^2)	# Duplexes in contact area
T11	0.002719	743.13	2
T11m	0.000365	743.13	<1
T13	0.004112	890.83	4
T13m	0.002103	890.83	2
T15	0.004321	1,038.1	4
T15m	0.002879	1,038.1	3

A.2 Reference

1. Smith, S.B., Y. Cui, and C. Bustamante, *Overstretching B-DNA: The Elastic Response of Individual Double-Stranded and Single-Stranded DNA Molecules.* Science, 1996. 271: p. 795-799.

Appendix B

Measuring Single-Stranded DNA Probe Density on Template Microspheres Using UV-vis Spectroscopy

In order to determine the number of single stranded probes on the particle surface after coupling, UV-vis spectroscopy was used to measure the concentration of DNA in solution before and after coupling. The difference between these concentrations corresponds to the amount of DNA coupled to the template microsphere surface. The same protocol was used for coupling though after incubation the sample was centrifuged at 10,000 g for 5 minutes before the supernatant was removed. This supernatant was centrifuged two additional times to facilitate particle removal. In addition to the supernatant post-coupling, a representative pre-coupling solution was made with 175 μL of Coupling Buffer and 200 μL of 10 μM DNA and tested also. A negative control of 175 μL Coupling Buffer and 200 μL Tris/EDTA Buffer without DNA was made to calibrate the spectrometer. Finally, a series of known concentrations of DNA were prepared in order to calibrate the absorbance as a function of DNA concentration in a linear regime correlating to Beer's Law. These calibration samples were also made with 175 μL of Coupling Buffer and 200 μL of DNA at a pre-determined concentration so that for the calibration volume of 375 μL the DNA concentration was 10 μM, 5 μM, 1 μM, or 0.1 μM. All samples were diluted equally by the addition of 600 μL of Tris/EDTA (pH 7.4) buffer in order to bring the total volume to 1 mL for cuvette measurement. The UV-vis absorbance measurement was conducted at a wavelength of 260 nm. Three samples of the pre-coupled solution, the Bangs Laboratories microsphere post-coupled solution, and the Invitrogen microsphere post-coupled solution were tested and an average absorbance value was determined.

Table B.1. Absorbance values at 260 nm after dilution with 600 μL Tris/EDTA for calibration standards, pre-couple, and post-couple solutions for both Bangs Laboratories and Invitrogen microspheres.

Calibration Standards	Absorbance	Samples	Absorbance (average of three separate samples)
10 μM	0.630	Pre-Couple Solution	0.31
5 μM	0.329	Post-Couple Bangs Laboratories	0.202
1 μM	0.113	Post-Couple Invitrogen	0.172
0.1 μM	0.051	--	--

The calibration samples were plotted as shown in Figure B.1 and the linear fit was used to determine a correlation coefficient to convert between the reported absorbance value and concentration of DNA in μM as shown in Table B.2.

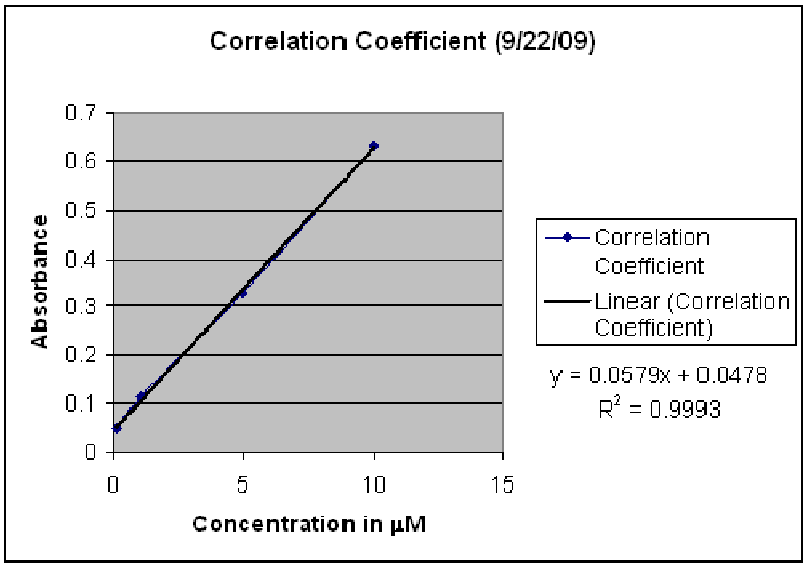

Figure B.1. Absorbance as a function of DNA concentration for the calibration standards. The slope gives the correlation coefficient used to translate absorbance values into DNA concentration.

The resulting relationship between absorbance and DNA concentration is given by

Concentration (μM) = Abs. / 0.0579.

Table B.2. DNA concentration of the pre- and post-coupling solutions for both LODM Bangs Laboratories and Invitrogen microspheres. The difference between the pre- and post-coupling solutions is assigned as the concentration of the DNA coupled to the microsphere surface (assuming no DNA probe loss during preparation or from nonspecific adsorption on the microsphere surface).

	DNA Concentration (μM)
Pre-Coupling Solution	5.35 μM
Post-Coupling Solution Bangs Laboratories	3.5 μM
Post-Coupling Solution Invitrogen	2.97 μM
Δ Bangs	1.85 μM
Δ Invitrogen	2.38 μM

The values for "Δ Bangs" and "Δ Invitrogen" correspond to the concentration of probe strands covalently linked to the template microsphere surface. This concentration was

used to calculate average the number of probe strands coupled to the surface of each template microsphere as outlined below.

For Bangs Laboratories Microspheres (LODM)

Number of Coupled DNA Strands:

1.85 μM coupled DNA = 1.85×10^{-6} mol/L

(1.85×10^{-6} mol/L) x (375 μL coupling solution volume) x (10^{-6} L/μL) = (6.94×10^{-10} mol of coupled DNA)

(6.94×10^{-10} mol of coupled DNA) x (6.02×10^{23} molecules/mol) = (**4.18×10^{14} coupled DNA strands**)

Number of Particles in Coupling Solution:

(0.01 volume fraction of particles) x (100 μL) = (1 μL of particles)

(1 μL of particles) x (375 μL of coupling solution)$^{-1}$ = (0.0027 volume fraction of particles in coupling solution)

(0.0027 volume fraction of particles in coupling solution) x (375 μL of coupling solution) = (1 μL of pure particles)

Volume of one Bangs Microsphere = $(4/3)\pi r^3 = (4/3)\pi (2.5\ \mu m)^3 = 65.45\ \mu m^3$

($65.45\ \mu m^3$) x ($1\ cm^3/10{,}000^3\ \mu m^3$) x (1,000 μL/1 cm^3) = 6.545×10^{-8} μL/particle

(1 μL of particles in coupling solution) / (6.545×10^{-8} μL/particle) = (**1.53×10^7 particles in coupling solution**)

Number of DNA Strands per Particle:

(4.18 x 10^{14} coupled DNA strands) / (1.53 x 10^{7} particles in coupling solution) = (**2.73 x 10^{7} strands/particle**)

Coupled DNA Strand Density:

Surface Area of one Bangs Microsphere = $4\pi r^2 = 4\pi (2.5\ \mu m)^2 = 78.54\ \mu m^2$

(2.73 x 10^{7} strands/particle) / (78.45 μm^2/particle) = (**3.48 x 10^{5} strands/μm^2**)

The parking area is a vendor-supplied value that corresponds to the average area or "footprint" occupied by each available COOH functional groups on the microsphere surface. The vendor reported parking area for the Bangs Laboratories Microspheres is 44.5 $Å^2$/COOH group.

Available COOH Groups per Microsphere:

Particle surface area in $Å^2$: (78.45 μm^2) x (1,000^2 nm^2/1 μm^2) x (10^2 $Å^2$/1 nm^2) = 7.845 x 10^{9} $Å^2$ per particle

(7.845 x 10^{9} $Å^2$ per particle) / (44.5 $Å^2$/group) = (**1.76 x 10^{8} COOH/particle**)

Coupling Efficiency:

Efficiency = (Number of strands/particle) / (Number of COOH groups per particle) x 100

(2.73 x 10^{7} strands/particle) / (1.76 x 10^{8} COOH/particle) x 100 = **15.5%**

For Invitrogen Microspheres (HODM)

Number of Coupled DNA Strands:

2.38 μM coupled DNA = 2.38 x 10^{-6} mol/L

(2.38 x 10^{-6} mol/L) x (375 μL coupling solution volume) x (10^{-6} L/μL) = (8.93 x 10^{-10} mol of coupled DNA)

(8.93 x 10^{-10} mol of coupled DNA) x (6.02 x 10^{23} molecules/mol) = (**5.38 x 10^{14} coupled DNA strands**)

Number of Particles in Coupling Solution:

(0.01 volume fraction of particles) x (100 μL) = (1 μL of particles)

(1 μL of particles) x (375 μL of coupling solution)$^{-1}$ = (0.0027 volume fraction of particles in coupling solution)

(0.0027 volume fraction of particles in coupling solution) x (375 μL of coupling solution) = (1 μL of pure particles)

Volume of one Invitrogen Microsphere = (4/3)π r^3 = (4/3) π (2.55 μm) ^{3} = 69.46 μm^3

(69.46 μm^3/particle) x (1 cm^3/10,000^3 μm^3) x (1,000 μL/1 cm^3) = 6.946 x 10^{-8} μL/particle

(1 μL of particles in coupling solution) / (6.946 x 10^{-8} μL/particle) = (**1.44 x 10^7 particles in coupling solution**)

Number of DNA Strands per Particle:

(5.38 x 10^{14} coupled DNA strands) / (1.44 x 10^7 particles in coupling solution) = (**3.74 x 10^7 strands/particle**)

Coupled DNA Strand Density:

Surface Area of 1 Invitrogen Microsphere = $4\pi r^2 = 4\pi (2.55\ \mu m)^2 = 81.71\ \mu m^2$

$(3.74 \times 10^7$ strands/particle) / ($81.71\ \mu m^2$) = (**4.58×10^5 strands/μm^2**)

The parking area is a vendor-supplied value that corresponds to the average area or "footprint" occupied by each available COOH functional groups on the microsphere surface. The vendor reported parking area for the Invitrogen Microspheres is 50 $Å^2$/COOH group.

Available COOH Groups per Microsphere:

Particle surface area in $Å^2$: ($81.71\ \mu m^2$) x ($1{,}000^2\ nm^2/1\ \mu m^2$) x ($10^2\ Å^2/1\ nm^2$) = $8.17 \times 10^9\ Å^2$ per particle

($8.17 \times 10^9\ Å^2$ per particle) / ($50\ Å^2$/group) = (**1.63×10^8 COOH/particle**)

Coupling Efficiency:

Efficiency = (Number of strands/particle) / (Number of COOH groups per particle) x 100

(3.74×10^7 strands/particle) / (1.68×10^8 COOH/particle) x 100 = **22.3%**

Table B.3. Summation of the important values used in the calculation of the number of single-stranded probes chemically coupled to either the Bangs Laboratories (LODM) or Invitrogen (HODM) microsphere surface.

	Bangs Laboratories Microspheres (LODM)	Invitrogen Microspheres (HODM)
Concentration of Coupled DNA Strands	1.85 μM	2.38 μM
Total Number of Coupled DNA Strands	4.18×10^{14}	5.38×10^{14}
Number of Strands per Particle	2.73×10^{7}	3.74×10^{7}
Coupled Probe Density (per μm^2)	3.48×10^{5}	4.58×10^{5}
Vendor Supplied Parking Area ($Å^2$/COOH group)	44.5	50
COOH Groups per Particle	1.76×10^{8}	1.63×10^{8}
Coupling Efficiency	15.5%	22.3%
Parking Area of ssProbe (nm^2 / Probe strand)	2.87	2.18

Appendix C

Demonstration of Excess Target Concentration in Disassembly Studies

In order to demonstrate an excess competitive target concentration was present in the satellite disassembly studies, a calculation of the concentration of DNA duplex linkages based in the quantitative data from flow cytometry is presented for the highest duplex density primary target, **T15**. Two assumption are made to facilitate calculation: first, the author assumes that the template microsphere concentration is equal to the satellite assembly concentration and second, the duplex density values for **T15** on the LODM taken from flow cytometry are within a reasonable value of the duplex density values for the DNA linkages forming the satellite assemblies.

The final volume fraction of the template microspheres in the assemblies is 0.5% w/v solids in a volume of 100 µL. For the disassembly study, 10 µL are removed and diluted to a final volume of 40 µL.

C_2 (Concentration of LODM in disassembly suspension) = C_1 x V_1 / V_2

C_2 = (0.005) x 10 µL / 40 µL

C_2 = 0.000125 or 0.0125% w/v solids of LODM in disassembly suspension

0.000125 x 40 µL = **0.005 µL of pure particles** in disassembly suspension

Volume of one LODM:

4/3 π (2.5 µm)^3 = 64.45 µm^3 or **6.545 x 10^{-8} µL/particle**

Number of LODM in Disassembly Suspension:

0.005 µL pure particle / 6.545 x 10^{-8} µL/particle = **7.64 x 10^{4} total particles**

Duplex Density of fluorescein-labeled **T15** as determined from flow cytometry:

4,321 duplexes / µm^2

(4,321 duplexes / µm^2) x (78.54 µm^2 surface area of LODM) =

3.39 x 10^{5} duplexes/particle

(3.39 x 10^{5} duplexes/particle) x (7.64 x 10^{4} total particles) =

2.59 x10^{10} total T15 duplexes

(2.59 X 10^{10} duplexes) / (6.02 x 10^{23} duplexes/mole) =

4.31 x 10^{-14} moles of T15

(4.31 x 10^{-14} moles) / (4 x 10^{-5} L total disassembly suspension) =

1.08 x 10^{-9} M or **1.08 x 10^{-3} µM** of **T15** duplexes linkages in disassembly suspension

Since 1.08 x 10^{-3} µM << 5 µM, the competitive target is considered to be in excess.

Appendix D

Representative Flow Cyometry Data from Competitive Hybridization Studies

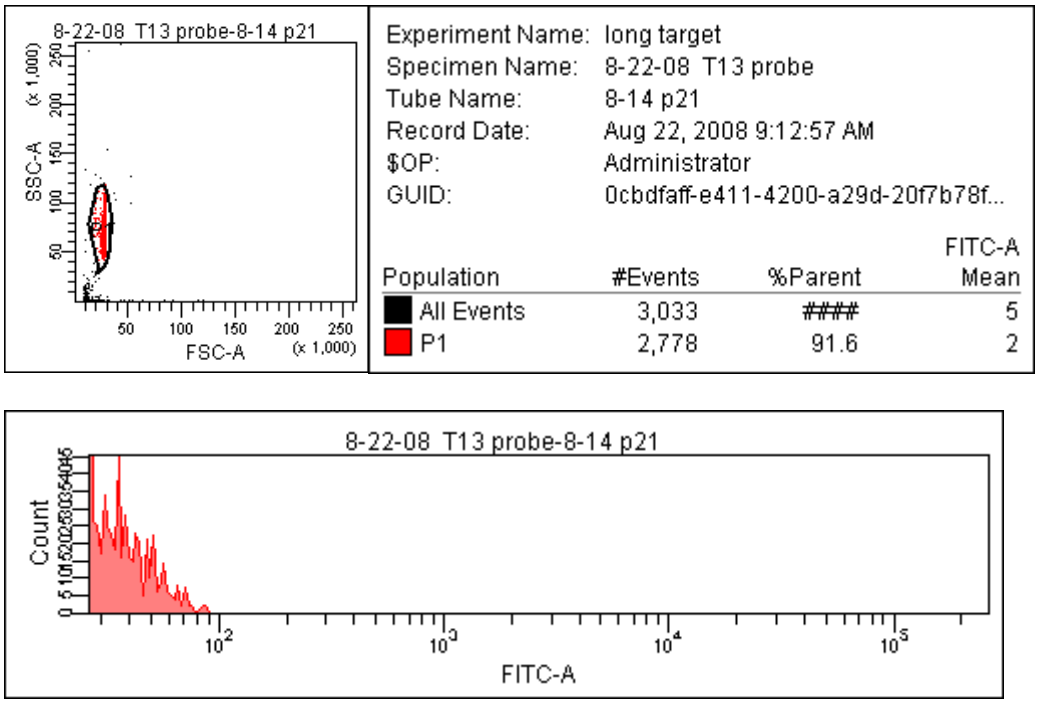

Figure D.1. Representative flow cyometry data for a negative control sample of a 5.1 µm microsphere functionalized with the immobilized probe strand but not incubated with fluorescently labeled strands. The forward scatter-side scatter plot is gated on the singlet particle population. The fluorescence histogram displays the fluorescence contribution from this population.

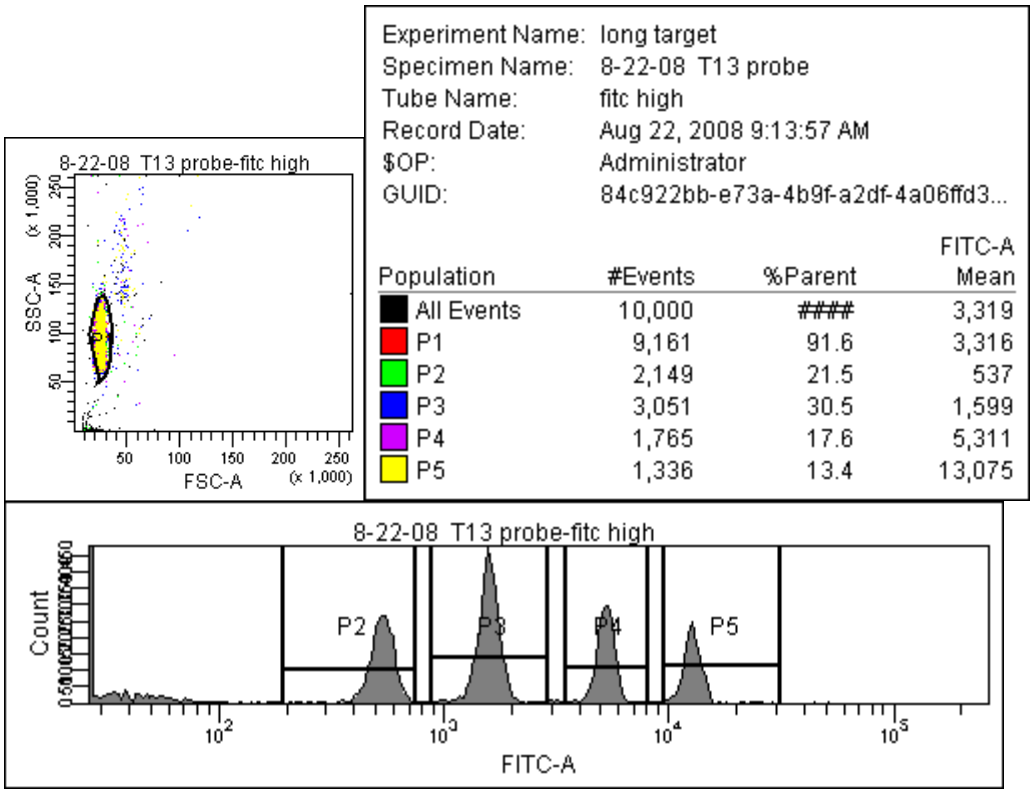

Figure D.2. Representative flow cyometry data for MESF FITC calibration standards (Bangs Laboratories). The forward scatter-side scatter plot is gated on the singlet particle population. The four gated peaks in the fluorescence histogram correspond to known fluorescence amounts, the intensities of which are listed in the table by gate number. These fluorescence values were used to quantify the fluorescence on the microsphere surface from the fluorescently labeled dsProbes.

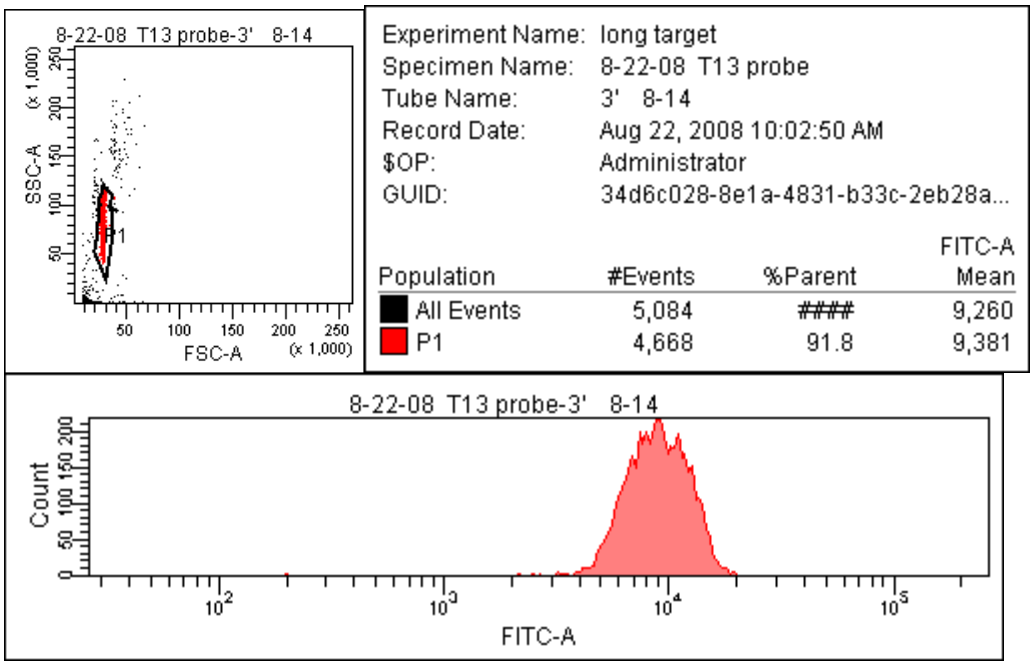

Figure D.3. Representative flow cyometry data for the zero time point (reference point) sample of a 5.1 µm microsphere functionalized with the **P21:T13** dsProbe. The forward scatter-side scatter plot is gated on the singlet particle population. The fluorescence histogram displays the fluorescence contribution from this population.

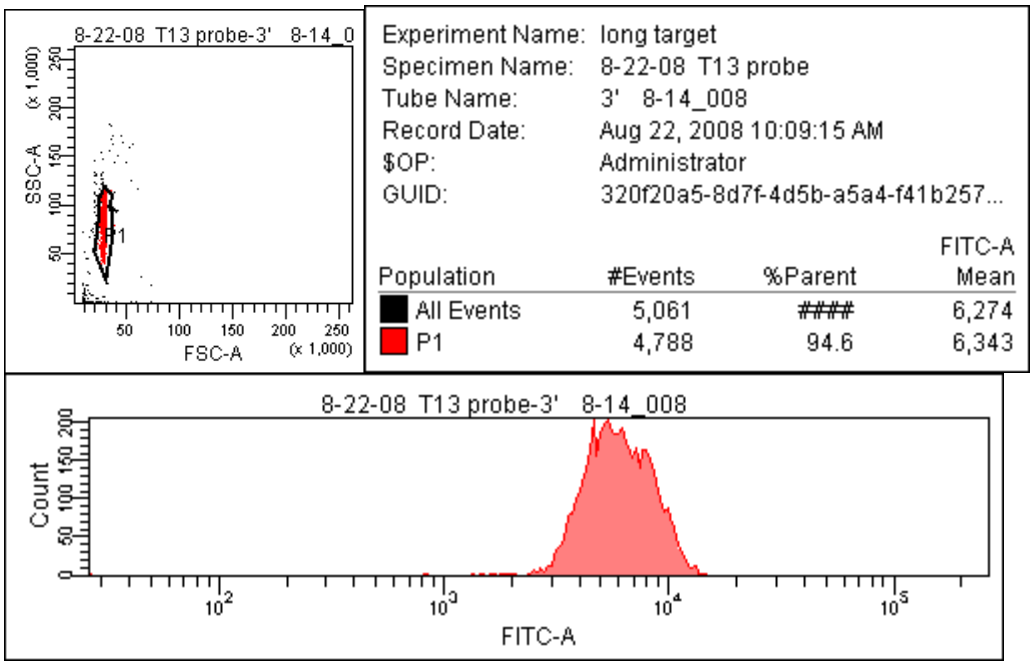

Figure D.4. Representative flow cyometry data for the 72 h time point sample of a 5.1 µm microsphere functionalized with the **P21:T13** dsProbe and incubated with **3' End** target. The forward scatter-side scatter plot is gated on the singlet particle population. The fluorescence histogram displays the fluorescence contribution from this population.

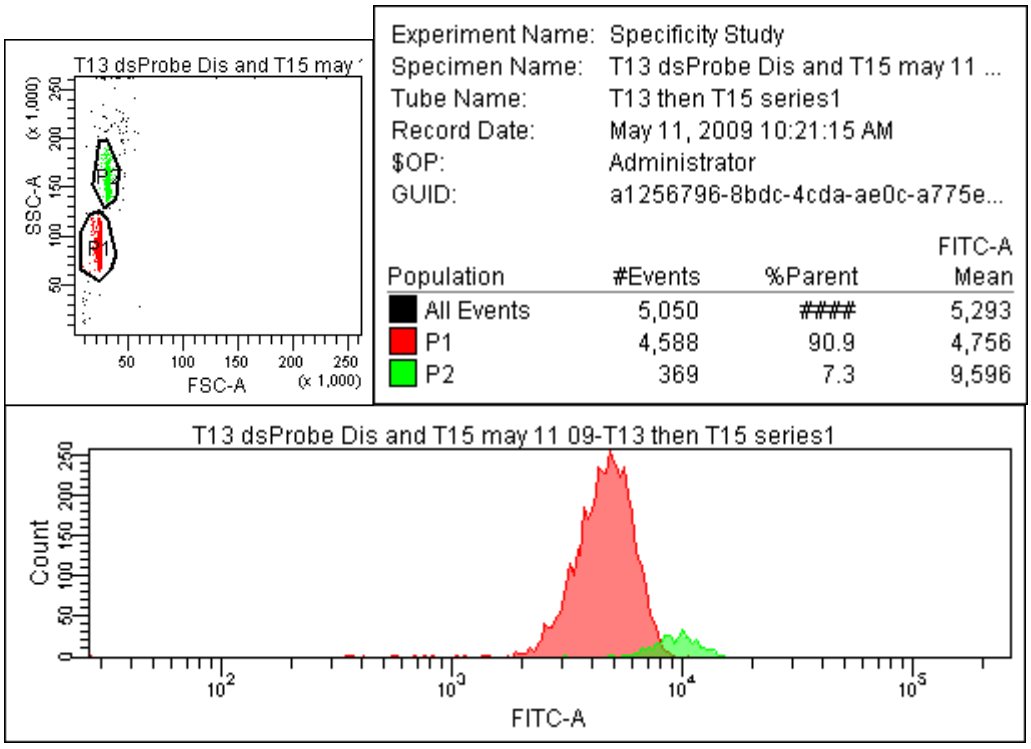

Figure D.5. Representative flow cyometry data for the zero time point (reference point) sample of a 5.1 µm microsphere functionalized with the **P21:T13** dsProbe. The forward scatter-side scatter plot is gated on the singlet particle population in red and an aggregate population in green. The fluorescence histogram displays the fluorescence contribution from these populations as color-coded.

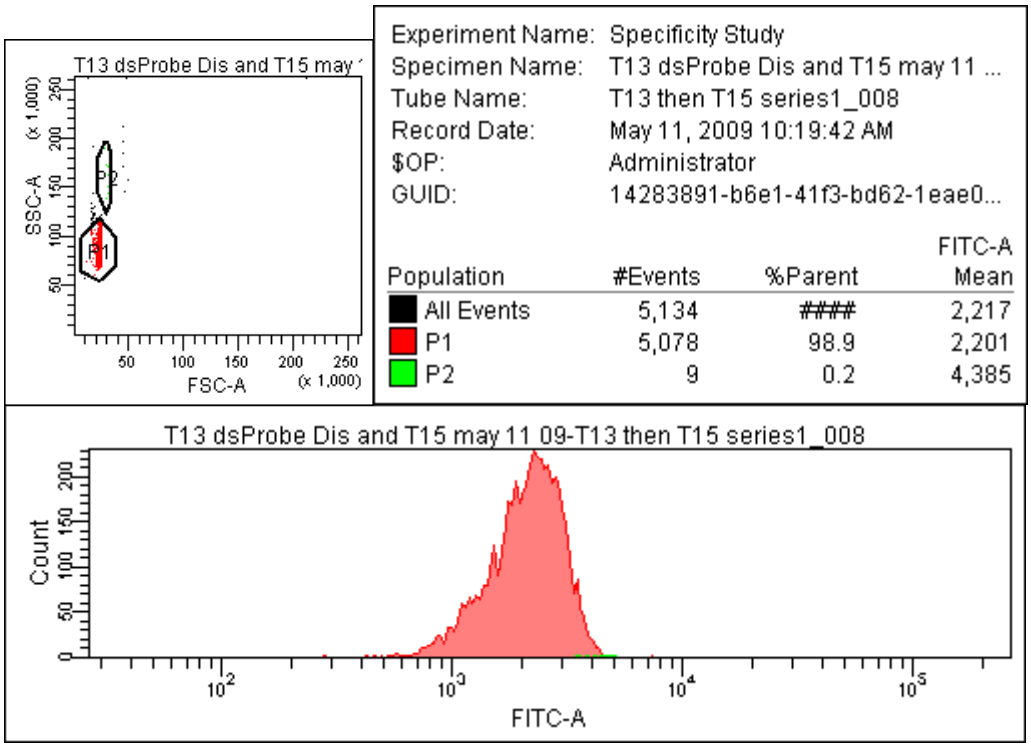

Figure D.6. Representative flow cyometry data for the 72 h time point sample of a 5.1 µm microsphere functionalized with the **P21:T13** dsProbe and incubated with the **T15** target. The forward scatter-side scatter plot is gated on the singlet particle population in red and an aggregate population in green. The fluorescence histogram displays the fluorescence contribution from these populations as color-coded.

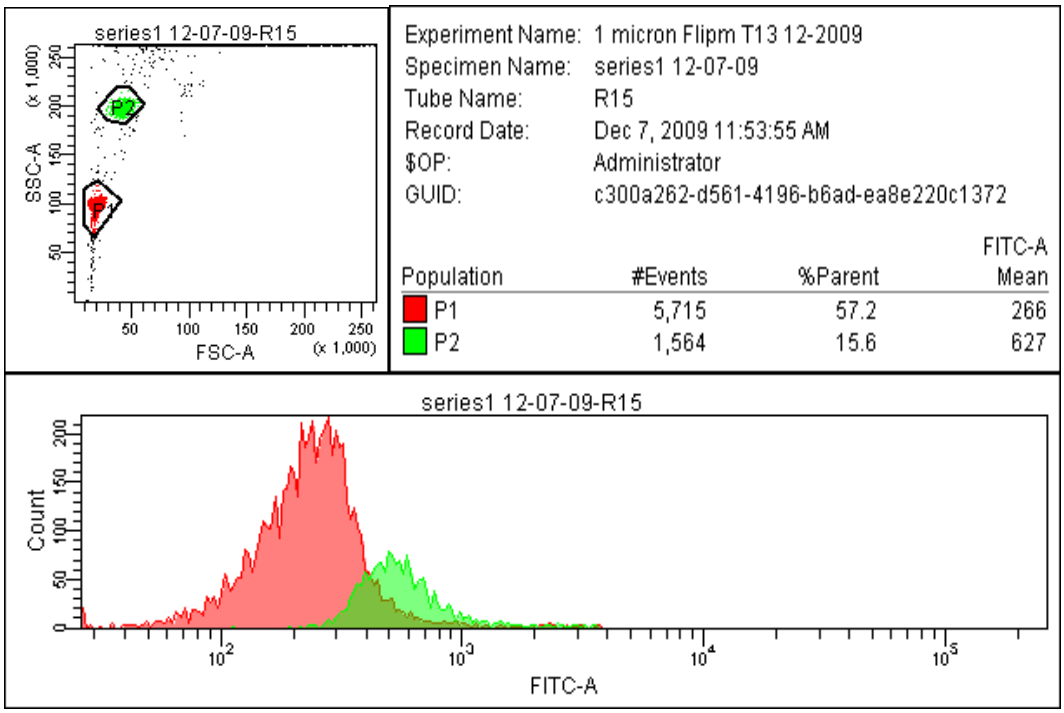

Figure D.7. Representative flow cyometry data for the zero time point (reference point) sample of a 1 μm microsphere functionalized with the **Flip T13** dsProbe. The forward scatter-side scatter plot is gated on the singlet particle population in red and an aggregate population in green. The fluorescence histogram displays the fluorescence contribution from these populations as color-coded.

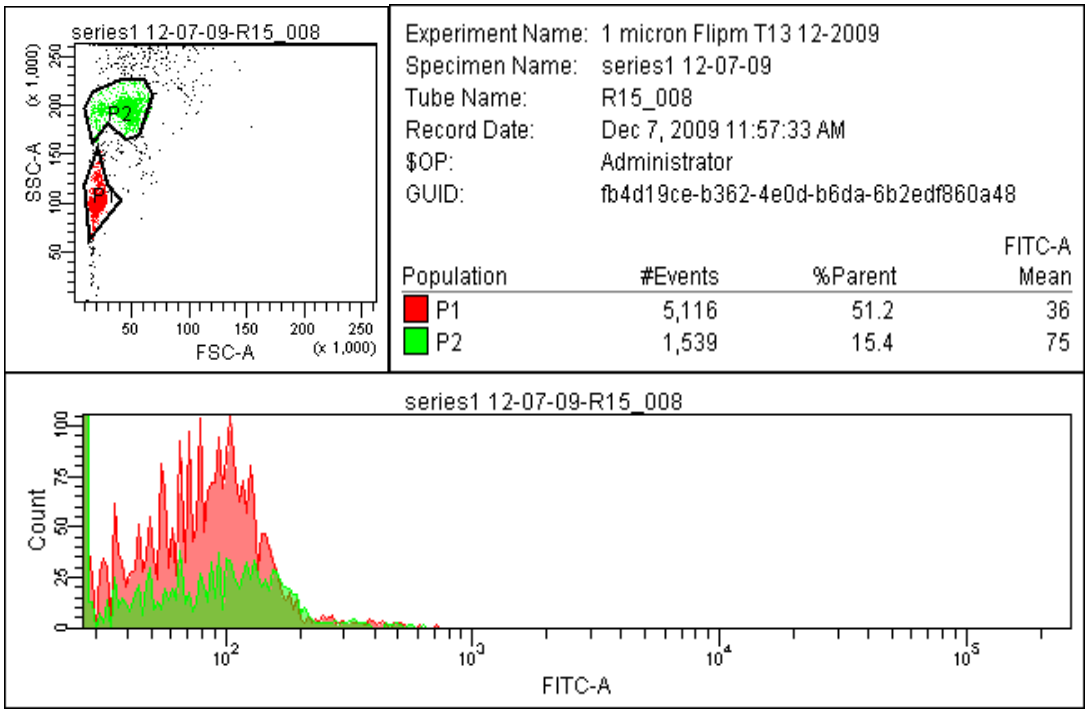

Figure D.8. Representative flow cyometry data for the 72 h time point sample of a 1 µm microsphere functionalized with the **Flip T13** dsProbe and incubated with **R15** target. The forward scatter-side scatter plot is gated on the singlet particle population in red and an aggregate population in green. The fluorescence histogram displays the fluorescence contribution from these populations as color-coded.

VITA

Bryan Alexander Baker was born in the verdant piedmont of Greenville, SC on March 4 1981. He graduated as valedictorian of Wren High School's class of 1999. While attending Furman University in Greenville, SC, Bryan chose to pursue a major in physics. Upon graduating magna cum laude and with honors as a Phi Beta Kappa and Sigma Pi Sigma inductee from Furman University in 2003, the desire for more applied research prompted him to pursue a graduate education at the Georgia Institute of Technology. Upon arriving at the School of Materials Science and Engineering, on time in spite of traffic, he joined the research group of Dr. Valeria Milam. Soon the "study of flow" dominated his interest as Bryan delved into a rigorous characterization of the rheological properties of hydrogel materials. Though many variables were considered, a thesis was not meant to be. In the summer of 2007 he transitioned his studies to competitive DNA hybridization. Fruitful years followed enhanced only by the synergy of his and Dr. Milam's efforts and in the spring of 2010, Bryan defended his dissertation examining the competitive hybridization of double-stranded DNA probes.